

Cooperative Predictive Control to enhance Power System Security

Zur Erlangung des akademischen Grades eines

Doktor-Ingenieurs

von der Fakultät für

Elektrotechnik und Informationstechnik
des Karlsruher Institut für Technologie (KIT)
genehmigte

Dissertation

von

Dipl. Ing. *Matthias Kahl*
aus Recklinghausen

Tag der mündlichen Prüfung: 08. Dezember 2014

Hauptreferent: Prof. Dr.-Ing. Thomas Leibfried

Korreferent: Prof. Dr.-Ing. Christian Rehtanz

Acknowledgements

This thesis has been written during my time at the Institute of Electric Energy Systems and High-Voltage Technology (IEH) of the Karlsruhe Institute of Technology. Foremost, I would like to thank my doctoral supervisor Prof. Dr.-Ing. Thomas Leibfried for the opportunity to write this thesis. Prof. Dr.-Ing. Thomas Leibfried gave me the freedom to explore possible means to enhance Power System Security and helped me with his insight to keep on track. I am in his debt, since he provided the needed stability, the trusting relationship and guidance to make this thesis possible.

My gratitude goes towards my second supervisor Prof. Dr.-Ing. Christian Rehtanz, who mustered the time to welcome me warmly at his institute, and evaluated the presented thesis critically.

I would like to thank my colleges of the Institute of Electric Energy Systems and High-Voltage Technology (IEH) for the great team spirit, the fun we had and for the creative environment.

My deepest gratitude goes towards my supervised students, without their help and countless hours they invested this thesis would not have been possible. Especially, I would like to thank Claudius Freye, Lennart Merkert and Simon Wenig for their excessive commitment.

Last but not least, I would like to thank Dr. Kym Watson for prove reading the entire thesis and for supporting me.

Contents

1	Introduction	3
1.1	Motivation	3
1.1.1	Stationary operation	4
1.1.2	Transient operation	5
1.2	Contributions	5
1.3	Thesis Outline	6
1.4	List of Publications	7
2	Model predictive control	9
2.1	Receding horizon control	10
2.2	Model predictive control without constraints	10
2.3	Model predictive control with constraints	12
3	Cooperative Multi-area Optimization	15
3.1	Introduction	15
3.1.1	Coordination of control areas to ensure operational security	16
3.1.2	Multi-area optimization	17
3.2	Power Node Framework	19
3.2.1	Dispatch Formulation	19
3.2.2	Redispatch Formulation	21
3.2.3	Network mapping	22
3.2.4	Modeling example - Dispatch Problem	23
3.3	Feasible Cooperation MPC	28
3.3.1	Cooperation of control areas	28
3.3.2	Cooperative Dispatch	30
3.3.3	Cooperative Redispatch	32
3.3.4	Initial Values.	34
3.3.5	Complexity	34
3.4	Case Study.	35
3.4.1	General setup	35
3.4.2	IEEE 14 network	36
3.4.3	IEEE 118 network	40

3.5	Conclusion	41
3.5.1	Outlook	42
4	Dynamic Security	43
4.1	Motivation	43
4.1.1	Network Model Overview and Applications	45
4.2	Dynamic network model	46
4.2.1	State Space Formulation	48
4.2.2	dq-Transformation of the model	49
4.3	Model of the Synchronous Generator	51
4.3.1	Nonlinear Model	51
4.3.2	Torque equations	54
4.3.3	Reference Frame Theory	54
4.3.4	Linearized Model	55
4.4	External Loads and Static Var Compensator	58
4.4.1	External Loads	58
4.4.2	Static Var Compensator	58
4.5	Overall model including dynamic network and generators	61
4.6	Interaction of Grid, Generators and SVCs	62
4.6.1	Applications small signal stability	63
4.7	Eigenvalue comparison	64
4.7.1	Evaluation of the dynamic network model	65
5	State Estimation	73
5.1	Observer	73
5.2	Results	75
6	FC-MPC to improve dynamic stability	77
6.1	Motivation	77
6.1.1	Literature Review	78
6.1.2	Controller Structure	79
6.2	Modeling Framework	81
6.3	Feasible Cooperation MPC	82
6.3.1	Model manipulation	82
6.3.2	Objective Function	85
6.3.3	Implementation	86
6.3.4	Simulation Results - 2 Area Network	87
6.3.5	Simulation Results - 5 Area Network	89
6.3.6	Discussion	94
6.3.7	Conclusion	95

7	Conclusion and Outlook	97
7.1	Outlook.	98
A	Control Theory	101
A.1	Linearization of a nonlinear system around an operating point	101
A.2	Discretization of linear state space models	102
B	Multiband PSS	103
C	Network Data	105
C.1	SVC Example.	105
C.2	IEEE 14 Network	106
C.3	IEEE 118 Network	108
C.4	2 Area Network	122
C.5	5 Area Network	123

Kurzfassung

Durch den starken Ausbau erneuerbarer Energiequellen erhöht sich der Anteil von volatiler Einspeisung immer weiter. Folglich sind zu Zeiten von einem hohem Wind bzw. Solarenergie aufkommen auch weniger konventionelle Kraftwerke am Netz. Durch den steigenden Bedarf an Energieübertragung ist die Leitungskapazität häufiger ausgeschöpft, sodass eingreifende Maßnahmen notwendig sind. Ziel der Arbeit ist es die Versorgungssicherheit bei auch bei stark ausgelasteten Netzen zu gewährleisten.

Die Versorgungssicherheit muss zunächst für den stationären Betrieb sichergestellt werden. Hierfür wird überprüft, ob für einen geplanten Kraftwerksfahrplan keine Betriebsmittel überlastet werden. Dieses Problem wird in der Arbeit als Optimierungsproblem aufgefasst, wobei mehrere Regelzonen unter Berücksichtigung von Speichern und regenerativer Energieerzeuger optimiert werden sollen.

Der zweite Teil der Arbeit optimiert das Verhalten nach einem Störfall, hierzu zählen Kurzschluss, Kraftwerksblockausfall und Leitungsausfall. Um das transiente Verhalten des Energieübertragungssystems zu verbessern, wird ein Systemmodell verwendet, welches explizit Regler-Interaktionen berücksichtigt und eine Vielzahl von Dämpfungssystemen koordiniert. Für die Koordination kommt ein Weitbereichsüberwachungssystem zum Einsatz.

In der Dissertation kommen verteilte kooperative Regelstrukturen zum Einsatz um der Komplexität und Größe des Energieübertragungssystems Rechnung zu tragen. Die Arbeit beschäftigt sich mit der Formulierung von kooperativen Gütekriterien, die eine bessere Performance zu ermöglichen als bei der Verwendung von dezentrale Verfahren.

Chapter 1

Introduction

1.1 Motivation

Power systems are under an elementary stress to change. With the rising number of renewable energy sources (RES) the fundamental methods for power system planning, operation and security of supply have to be validated and updated as needed. RES are volatile, leading to several problems. Conventional generation or storage devices need to close the gap between demand and supply. The network needs to support high RES feed-in. If that happens rarely, the produced energy does not justify the costs for network reinforcements. Hence, an economically planned network does include curtailment of RES. On the other hand, optimal operation is attained by using curtailment of RES as little as possible. While conventional power generation was concentrated at well planned connection points, RES are built in areas where environmental conditions (i.e. high wind potential) are most suitable.

Not only the expansion of RES has increased the strain on the grid significantly, but also the growing demand for electrical power and the hesitant expansion of the power grid. Consequently, transfer capacities can reach their limits and corrective actions are needed more frequently. An optimal operation of a stressed network with a high share of volatile RES leads to a high number of redispatch events. Furthermore, the transient performance of a stressed network is in particular challenging. The high number of RES makes the overall behavior difficult to control.

With the unbundling of energy generation, transmission and sales, the transmission system operator (TSO) has the obligation to guarantee safe operation and should exploit all possibilities to comply with physical and normative constraints at minimum costs. Safe operation can be divided into safe stationary operation and safe transient operation.

This thesis presents novel procedures to implement and guarantee safe operation in both stationary and dynamic situations.

1.1.1 Stationary operation

Stationary operation includes the balance of supply and demand, the compliance with thermal lines rating, voltage constraints and maximum power output of power plants. Safe dynamic operation includes the dynamically stable system behavior influenced by the generators in operation and the operation condition of the network. As depicted in Fig. 1.1 fulfilled stationary constraints and dynamic stability need to be guaranteed for a planned schedule. The transmission dispatch system checks if a planned schedule is within operating constraints and guarantees safe operation.

Based on [68] a high level functional representation of a transmission dispatch system is shown in Fig. 1.1. This thesis treats the dispatch and the dynamic operational security modules. The transmission dispatch system is based on the network

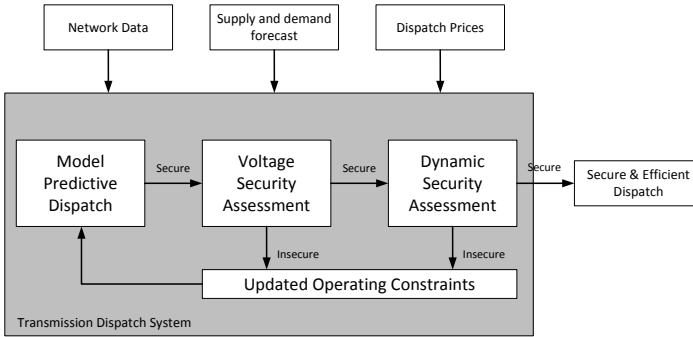


Figure 1.1: Block diagram of transmission dispatch system

data, supply/load predictions and dispatch costs. The model predictive dispatch calculates an optimal trajectory dispatching all available units with minimum costs. The method as presented in Chapter 3 also includes storage devices and RES feed-in predictions. The calculated schedule is evaluated with a security constrained optimal power flow (SC-OPF) ensuring voltage security. If no secure power flow ensuring voltage constraints exists for the planned schedule, the constraints of the dispatch function are updated. In case the planned schedule is within the defined constraints, the schedule is further validated by the dynamic security assessment. A dynamic model of the system as presented in Chapter 4 is used for the dynamic security assessment. Analogously to the voltage security assessment, constraints are adapted, if the proposed operating schedule is dynamically unstable and the model predictive dispatch will be executed again. In case the operating schedule is dynamically secure, appropriate set points are communicated to generation operators.

1.1.2 Transient operation

Although dynamic security is verified during stationary operation, methods to extend the dynamic operating range of power systems are of great importance. They improve operational flexibility and the security of supply. Modes with poor or even negative damping, which limit the operating range, are created by weak interconnections. The performance after line outages, short circuits and generator unit losses is of paramount importance. Outages of long duration cause enormous economic losses. The most economic solutions to damp low frequency oscillations are PSS and dampening strategies for FACTS & HVDC. Alternatives like operating restrictions or transmission extensions, are very costly compared to active damping approaches.

Power systems with several generator units, FACTS, HVDC and transformers with on-load-tap-changer operate with a multitude of control loops which may interact. Multiple-input and multiple-output (MiMo) system description explicitly accounts for the interactions mentioned above. Control methods relying on MiMo models can coordinate all controllable devices effectively and therefore provide dynamic stability and good transient behavior. Coordination of a large number of devices requires a systematic control design approach.

1.2 Contributions

- A distributed problem formulation is introduced to integrate RES and storage devices optimally during stationary operation.
- An advanced model predictive dispatch system is developed within the presented transmission dispatch system of Fig. 1.1. The algorithm dispatches conventional generation, RES and storage devices. Load and generation predictions are considered. Optimal schedules are attained for several control areas through a cooperative approach.
- A system model is presented that describes control interactions and includes network dynamics. The advanced model can be used in the transmission dispatch system to guarantee dynamic security and for controller synthesis explicitly considering control interaction.
- An eigenvalue comparison is carried out, comparing models relying on static network equations and models relying on dynamic network equations.
- A dynamic state estimator is developed, using dynamic network equations. The estimator is able to calculate voltage absolute value and angle of transients with sparse measurements.

- An integral control strategy is presented which applies data from phase measurement units to damp inter-area oscillations. The proposed distributed model predictive control method realizes one control unit for each controllable device (Generators, FACTS, HVDC), and coordinates their behavior after a fault. Each unit is designed by applying a systematic controller synthesis.

1.3 Thesis Outline

Chapter 2 gives an overview of model predictive control, which was applied throughout this thesis as a control and optimization method. This method will be introduced and explained.

Chapter 3 adapts model predictive control to power systems in stationary operation. Both dispatch and redispatch formulations are developed. The approach is further extended to cooperative dispatch and redispatch methods, which can be applied to an interconnected network, optimizing several control areas. Simulation results are presented using benchmark networks with 14 and 118 nodes respectively.

Chapter 4 provides a model formulation valid for dynamical processes in power systems. Models for synchronous generators, Static Var Compensators and the network are introduced. An eigenvalue comparison of models relying on static network equations and models relying on dynamic network equations is conducted.

Chapter 5 develops a state estimator, which is able to track absolute value and angle of voltages during transient events.

Chapter 6 presents a cooperative MPC strategy, which enhances the performance of PSS using the network state as a global signal. Simulation results are obtained using 11 and 59 node benchmark networks respectively.

Chapter 7 concludes with a summary of the presented work and an outlook.

1.4 List of Publications

- M. Kahl, C. Freye, T. Leibfried: "A Cooperative Multi-area Optimization with Renewable Generation and Storage Devices", IEEE Transactions on Power Systems 2014
- M. Kahl, D. Uber, T. Leibfried: "Dynamic State Estimator for voltage stability and low frequency oscillation detection", IEEE Innovative Smart Grid Technologies Conference- Asia, Malaysia 2014
- M. Kahl, S. Wenig, T. Leibfried: "Dezentrale modellprädiktive Optimierungsstrategien zur Einbindung erneuerbarer Erzeugungskapazität und Speichersysteme", Konferenz für Nachhaltige Energieversorgung und Integration von Speichern-NEIS, Hamburg 2013
- M. Kahl, T. Leibfried: "Decentralized Model Predictive Control of Electrical Power Systems", International Conference on Power Systems Transients (IPST2013) in Vancouver, Canada 2013
- M. Kahl, T. Leibfried: "Stabilitätsanalyse von stromrichterbetriebenen Anlagen zur Blindleistungskompensation und deren Auslegung", VDE Kongress, Stuttgart 2012
- M. Kahl, T. Leibfried: "Modellbasierte Regelungsalgorithmen für das Energienetz der Zukunft", IT für die Energiesysteme der Zukunft, Lecture Notes in Informatics (LNI), Berlin 2011
- U. Reiner, M. Kahl, T. Leibfried, F. Allending, H. Schmeck: "MeRegioMobil-Labor - Entwicklungsumgebung für zukünftige Smart-homes", ETG Kongress, Leipzig 2010

Chapter 2

Model predictive control

The used methodology for all security enhancing measures presented in this thesis originates from model predictive control. Model predictive control (MPC) is a control method, which relies on a dynamic model [57]. With the developed model the predicted behavior of the plant is optimized applying an objective function. As depicted in Fig. 2.1 the controller considers predicted plant behavior. The optimal trajectories for all control variables are calculated over a horizon. Furthermore, MPC can explicitly account for constraints like a maximal rate of change or a control variable limit. Hence, an operation close to the operational limits is possible, which increases overall productivity.

MPC is a multiple input multiple output (MiMo) control method, which is able to implement a controller for several control variables and can incorporate several measurement systems, while explicitly account for system coupling.

The number of control variables and measurement variables can be adapted on-line without the necessity of controller reconfiguration. Each power plant can be integrated, seamlessly if it joins or drops out of interconnected operation.

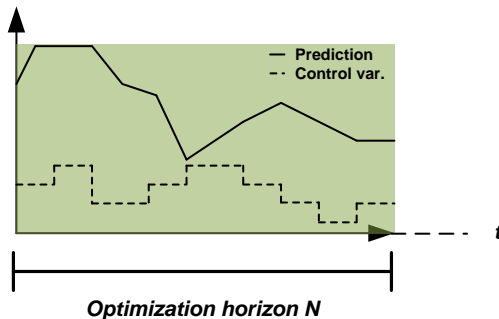


Figure 2.1: Observer structure

2.1 Receding horizon control

Receding horizon control describes the working principle of MPC. MPC is based on a process model, which is used to predict the behavior of the plant. The optimization horizon is the time interval for which the prediction is executed and the influence of the control variables are considered. The optimization horizon has the length N . The optimization takes place over the entire optimization horizon; however only the first steps of the calculated control sequence is applied. The length of the applied control sequence is called optimization frequency. The control method looks continually ahead to optimize current and future decisions, to achieve better performance compared to one step methods without prediction. Depending on the agility of the underlying process the length of the optimization horizon needs to be adapted. Slow evolving chemical systems or quasi-static power systems as in Chapter 3 have for example long prediction horizons, whereas fast evolving transients as discussed in Chapter 6 may only have an optimization horizon of a few steps.

One way to ease the computable burden is to increase the length of the applied control sequence (i.e. optimization frequency). However, due to model and measurement errors the performance of the controller may suffer significantly. In this thesis MPC is used as a superordinate system and will only calculate new set points for fast acting PI-controllers. This fact decreases the vulnerability to communication delays.

2.2 Model predictive control without constraints

In order to compute a model predictive controller, a forecast for the state variable $x(1) \dots x(N)$ is needed. The variable is calculated with the help of the current state variable $x(0)$ and a potential input sequence $u(0) \dots u(N)$.

Power systems can be described with a discrete state space system of the form

$$x(k+1) = Ax(k) + Bu(k), \quad (2.1)$$

where x is the state vector, u is the vector of control variables, A is the time discrete system matrix and B is the time discrete input matrix. With the help of (2.1) the prediction is realized. Moreover, (2.1) is equal to the first prediction step.

The second step with $k \Rightarrow k+1$ is

$$\begin{aligned} x(k+2) &= Ax(k+1) + Bu(k+1) \\ &= A^2x(k) + ABu(k) + Bu(k+1). \end{aligned} \quad (2.2)$$

Consequently, the equation for the N -th prediction step is

$$x(k+N) = A^N x(k) + A^{(N-1)} Bu(k) + \dots + Bu(k+N-1). \quad (2.3)$$

The optimal trajectory $\bar{u}^* = [u(0), u(1), \dots, u(N-1)]^*$ is calculated with the help of a positive definite objective function ϕ over the optimization horizon N . A quadratic cost function, which optimizes both control and state variables is defined with

$$\min_{\bar{u}} \phi(\bar{u}, x(0)) = \sum_{k=1}^N u^T(k-1)Ru(k-1) + x(k)^T Qx(k), \quad (2.4)$$

where R and Q are positive definite weighing matrices. With (2.1 - 2.3) and $k = 0$, a prediction of state variables in dependence of the current and future control variable inputs as well as the initial values $x(0)$ is given through

$$\underbrace{\begin{pmatrix} x(1) \\ \vdots \\ \vdots \\ x(N) \end{pmatrix}}_{\bar{x}} = \underbrace{\begin{pmatrix} A \\ \vdots \\ \vdots \\ A^N \end{pmatrix}}_{S_x} x(0) + \underbrace{\begin{pmatrix} B & 0 & \dots & 0 \\ AB & \ddots & \ddots & \vdots \\ \vdots & \ddots & \ddots & \vdots \\ A^{N-1}B & \dots & \dots & B \end{pmatrix}}_{S_u} \underbrace{\begin{pmatrix} u(0) \\ u(1) \\ \vdots \\ u(N-1) \end{pmatrix}}_{\bar{u}}. \quad (2.5)$$

The weighing matrices may change over the course of the optimization horizon and can also be expressed in block diagonal matrix form

$$\bar{Q} = \begin{pmatrix} Q(1) & & 0 \\ & \ddots & \\ 0 & & Q(N) \end{pmatrix}, \quad \bar{R} = \begin{pmatrix} R(0) & & 0 \\ & \ddots & \\ 0 & & R(N-1) \end{pmatrix}. \quad (2.6)$$

The objective function (2.4) formulated in matrix form is

$$\phi(\bar{u}, x(0)) = \bar{x}^T \bar{Q} \bar{x} + \bar{u}^T \bar{R} \bar{u}. \quad (2.7)$$

The state vector x is replaced in (2.7) with (2.5). Hence the objective function is given through

$$\begin{aligned} \phi(\bar{u}; x(0)) &= \bar{u}^T \underbrace{(S_u^T \bar{Q} S_u + \bar{R})}_H \bar{u} + 2x^T(0) \underbrace{(S_x^T \bar{Q} S_u)}_F \bar{u} + x^T(0) \underbrace{(S_x^T \bar{Q} S_x)}_Y x(0) \\ &= \bar{u}^T H \bar{u} + 2x(0)^T F \bar{u} + x^T(0) Y x(0). \end{aligned} \quad (2.8)$$

Since the positive definiteness of \bar{R} is transferable to H (2.8) is a positive definite QP-problem. Hence, the minimum of (2.8) is calculated with

$$\frac{\partial \phi(\bar{u}; x(0))}{\partial \bar{u}} = 0 \quad (2.9)$$

and the optimal trajectory is given through

$$\bar{u}^*(x(0)) = -H^{-1}F^T x(0). \quad (2.10)$$

2.3 Model predictive control with constraints

If the control problem needs to consider constraints the QP-problem can be extended [5]. The constraints include additional input inequalities $A_{u,in}\bar{u}^{(k)} \leq b_{u,in}^{(k)}$ and state inequalities $A_{x,in}x^{(k)} \leq b_{x,in}^{(k)}$. With the help from (2.5) the state inequalities/equations can be formulated in dependence of x_0 and \bar{u} .

$$\underbrace{\begin{bmatrix} A_{u,in} & 0 & \dots & 0 \\ 0 & A_{u,in} & \ddots & \vdots \\ \vdots & \ddots & \ddots & 0 \\ 0 & \dots & 0 & A_{u,in} \\ A_{x,in}B & 0 & \dots & 0 \\ A_{x,in}AB & A_{x,in}B & \dots & 0 \\ \vdots & \ddots & \ddots & 0 \\ A_{x,in}A^{N-1}B & A_{x,in}A^{N-2}B & \dots & A_{x,in}B \end{bmatrix}}_{A_{in}} \bar{u} - \underbrace{\begin{bmatrix} 0 \\ \vdots \\ 0 \\ -A_{x,in}A \\ -A_{x,in}A^2 \\ \vdots \\ -A_{x,in}A^N \end{bmatrix}}_{E_{in}} x_0 \leq \underbrace{\begin{bmatrix} b_{u,in}^{(0)} \\ b_{u,in}^{(1)} \\ \vdots \\ b_{u,in}^{(N-1)} \\ -b_{x,in}^{(1)} \\ -b_{x,in}^{(2)} \\ \vdots \\ -b_{x,in}^{(N)} \end{bmatrix}}_{W_{in}}$$

$$\underbrace{\begin{bmatrix} A_{u,eq} & 0 & \dots & 0 \\ 0 & A_{u,eq} & \ddots & \vdots \\ \vdots & \ddots & \ddots & 0 \\ 0 & \dots & 0 & A_{u,eq} \\ A_{x,eq}B & 0 & \dots & 0 \\ A_{x,eq}AB & A_{x,eq}B & \dots & 0 \\ \vdots & \ddots & \ddots & 0 \\ A_{x,eq}A^{N-1}B & A_{x,eq}A^{N-2}B & \dots & A_{x,eq}B \end{bmatrix}}_{A_{eq}} \bar{u} - \underbrace{\begin{bmatrix} 0 \\ \vdots \\ 0 \\ -A_{x,eq}A \\ -A_{x,eq}A^2 \\ \vdots \\ -A_{x,eq}A^N \end{bmatrix}}_{E_{eq}} x_0 = \underbrace{\begin{bmatrix} b_{u,eq}^{(0)} \\ b_{u,eq}^{(1)} \\ \vdots \\ b_{u,eq}^{(N-1)} \\ -b_{x,eq}^{(1)} \\ -b_{x,eq}^{(2)} \\ \vdots \\ -b_{x,eq}^{(N)} \end{bmatrix}}_{W_{eq}}$$

$$\min_{\bar{u}} \phi(\bar{u}, x_0) = \bar{u}^T H \bar{u} + 2x_0^T F \bar{u} + x_0^T Y x_0 \quad (2.11)$$

The objective function (2.4) in the general form is extended with equalities and inequalities constraints

$$A_{in} \bar{u} \leq \underbrace{W_{in} + E_{in} x_0}_{b_{in}} \quad (2.12)$$

$$A_{eq} \bar{u} = \underbrace{W_{eq} + E_{eq} x_0}_{b_{eq}}. \quad (2.13)$$

As promising and potent as MPC might be, power systems pose a very complex system and therefore optimization problem. MPC in large scale applications is under research, but practical implementations in the industry are limited.

Partitioning a large scale problem into sub-systems, can effectively reduce the computational complexity. In Chapter 3 and Chapter 6 cooperative measures are introduced, which will compute a solution close to the global optimum and reduce the computational complexity.

Chapter 3

Cooperative Multi-area Optimization

3.1 Introduction

In Chapter 1.1.1 an overview is given on how secure stationary operation is guaranteed. This approach increases flexible grid operation and allows TSOs to reduce redispatch costs caused by intermittent renewable energy sources (RES). The cooperative multi-area optimization strategy presented here enables transmission system operators (TSOs) to dispatch/redispatch interconnected networks securely, while reducing dispatch/redispatch costs. Schedules for storage devices, conventional- and renewable generation are obtained considering network constraints and ramping rates [80]. An optimal schedule for several control areas is attained, including storage operation to achieve congestion relief. The distributed approach preserves control area responsibilities. All participating control areas attain a schedule close to the global optimum. TSOs implement agreements to share resulting profits. Problem decomposition reduces the complexity compared to a global optimization and makes it suitable for large scale optimization. The multi-step optimization considers RES and load forecast over an optimization horizon. The functionality was shown successfully using stressed 14 and 118 node systems. A cross border dispatch with use of storage devices is realized to maintain a high share of RES feed-in, while reducing overall dispatch costs.

In an unbundled market environment each market player receives unrestricted access to the market and therefore to the network. The TSO validates the day-ahead schedule for adherence to standards for a secure operation of the transmission system. Several arrangements are in place to avoid day-ahead congestion and make efficient operation possible. However, in case temporary or unexpected congestion arises, the TSO is obliged to alter the power flow with all necessary means. Possible means are topology changes, the use of FACTS elements, redispatch of generation and RES curtailment. This chapter focuses on the efficient short term dispatch and redispatch of generation, RES curtailment and storage operation.

Redispatch volume and costs are becoming increasingly significant factors in grid operation. The main drivers of this trend are: the hesitant extensions of the power grid, the expansion of RES and the growing demand for electrical power. Furthermore, the introduction of energy trading through a common market has led to an additional aggravation of the problem. In Europe generator unit locations are selected solely by economical considerations, whereas costs of transmission grid reinforcements are not considered. The increasing redispatch and control power costs in Europe can be avoided partially by using a shorter dispatch interval. With the applied dispatch interval of up to 1 hour, TSOs need to operate the power system well within its physical limits [19]; for comparison Australia is using a 5 minute dispatch interval. As a second measure to reduce redispatch cost and volume, cooperative redispatch strategies involving several control areas are promising.

Network operational flexibility is essential to accommodate a high share of RES. Means to enable more flexibility are storage devices, demand side management, energy balancing from RES and combined heat power plants (CHP), improved demand and RES feed-in predictions [70]. Furthermore, the ramping capability of generators has to be taken into account. A lack of coordination between control areas during dispatch or redispatch may result in non-optimal use of generation or balancing power [2]. Due to the high costs for storage and hot standby operation of conventional power plants, grid operation needs to be as close as possible to the global optimum.

The following chapter presents an advanced dispatch/redispatch algorithm, which coordinates several control areas optimally including the existing storage devices and avoids unwanted interaction. Each control area executes a local optimization with simplified external generation costs. Through iterative calculation of the local optimization problems, the algorithm converges close to the global optimum.

3.1.1 Coordination of control areas to ensure operational security

In order to guarantee operational security between control areas, the European Network of Transmission System Operators for Electricity (Entso-E) published guidelines in the operation handbook [14].

3.1.1.1 N-1 operation

The TSOs are obliged to guarantee operational security within their control zone, and have the means to redispatch the available generation. The operational security limits need to hold before and after a contingency took place. Contingencies are for example line, generator, power station or transformer outages. Operational security subsumes the N-1 principle, line constraints and generation constraints.

The TSO creates a list of possible faults, according to a risk assessment analysis. External contingencies are possible faults from neighboring control areas. Each element in the contingency list needs to be considered in the N-1 simulation. An external contingency is considered in the N-1 simulation, and added to the list, if there is a considerable influence on its own area. An optimal redispatch restores the system from a state with possible constraint violations to a system without constraint violations at minimum redispatch costs.

3.1.1.2 Observability

An online model is implemented to evaluate the network condition and assess the security situation. The scope of the online model is the observability area including the own and parts of the neighboring network. The observability area includes all external contingencies. Each TSO needs to be able to perform N-1 calculations for any external contingency.

3.1.1.3 Coordination

The Entso-E operation handbook [14] defines the following procedures regarding TSO interaction:

Collaboration of TSOs is essential and includes the exchange of relevant information on risks and the preparation of coordinated remedial actions one day in advance as necessary. Control areas cannot act independently and redispatch strategies often influence neighboring TSOs. Consequently, a globally optimal redispatch involves cooperation of TSOs. Desired effects are inter-TSO assistance in the event of failures and the prevention of disturbances. Communication between neighbors to change the generation pattern abroad and defined mechanisms to launch cross border redispatching need to be implemented. The TSOs are able to share information on redispatching costs with each other.

The above statements, especially those on the cooperation of TSOs, concern redispatch and are applicable to short term dispatch as well.

3.1.2 Multi-area optimization

Within the environment defined by the Entso-E a distributed cooperative multi-area optimization is introduced, with the goal of a cost optimal (re-)dispatch involving several areas with compliance of constraints.

The advantages are

- defined and controlled way of cross border (re-)dispatching

- consideration of control area interaction
- more flexible and efficient grid operation
- reduction of (re-)dispatch cost in comparison to a decentralized approach
- consideration of a continuously updated wind forecast
- optimal storage operation to achieve congestion relief

Each TSO conducts its own optimization with inclusion of approximated neighboring generation costs. The generation pattern, load and RES feed-in forecasts are exchanged. Through an iterative approach, a solution close to the global optimum is reached.

As described above and in compliance with [14], the following features are used. The TSOs exchange the (re-)dispatch costs and prepare a comprehensive network model, including all participating control areas. Furthermore, TSOs exchange load and RES feed-in forecasts, current network states and generation patterns. Each TSO keeps its field of responsibility and independence. Thus, the TSO (re-)dispatches the generation in its area of responsibility and is able to define individual cost functions and constraints.

3.1.2.1 Literature Overview

Efficient network operation can be interpreted as an optimization problem under consideration of constraints. The solution of the optimal power flow (OPF) leads to an optimized grid operation. Several solution strategies have recently made it possible to cope with these economic challenges in optimal grid operation. In order to include storage devices, [13] presented a sequential OPF. The sequential OPF only considers storage operation over a limited time interval, to ease computational complexity. In case the full optimization horizon is considered, MPC and sequential OPF pose the same problem formulation. Several distributed OPF formulations are available [4], [43]. [39] presented a multi-step optimization and extended the formulation to a distributed approach with a Lagrangian decomposition [2]. An extensive review of congestion management is given in [48]. Redispatch strategies are the focus of [58] and [78]. For example [58] proposes an approach to improve cross border redispatch. [60] and [51] deploy a generalized Nash equilibrium to achieve joint cross border redispatch. [6] compares national and joint cross border redispatch. [78] adapts an OPF formulation to redispatch generation and operate FACTS devices.

3.2 Power Node Framework

This unified modeling framework is able to represent complex structures within a model environment introduced by [30], [71] and [16]. It can be used to explicitly consider renewable energy sources and storage devices. Also energy efficiency, environmental impact and cost of a technologically diverse unit portfolio can be evaluated. A model of a power system with consideration of grid and generation constraints allows optimal operation with the use of a system model. The power node domain is linked with the grid side under the use of power generation u_g and power demand u_l . A power node is described by the following variables. The demanded power is denoted by $\xi < 0$ and the provided power is denoted by $\xi > 0$. In case of RES curtailment or unserved load process variables $w > 0$ or $w < 0$ are introduced. A power node is defined in the most general case with

$$x(k+1) = Ax(k) + TC^{-1}(\eta_l u_l - \eta_g^{-1} u_g + \xi - w), \quad (3.1)$$

where x represents the state of the storage, A is the system matrix and C denotes the capacity of the storage device. Equation (3.1) is a discrete state space system, where k is the time variable and T the sample rate. The following model descriptions were used for the problem formulation.

3.2.1 Dispatch Formulation

3.2.1.1 Generation

The power output of conventional generation such as thermal power plants and CHP can be chosen arbitrarily. Thus, u_g is an optimization variable. ξ represents the fuel consumption of the plant.

$$0 = -\eta_g^{-1}(u_g) + \xi \quad (3.2)$$

Constraints include min/max power output and ramping rates.

$$\begin{aligned} u_g^{min} &\leq u_g \leq u_g^{max} \\ r_g^{min} &\leq u_g(k) - u_g(k-1) \leq r_g^{max} \end{aligned} \quad (3.3)$$

Renewable Energy Sources are curtailable, hence w is an optimization variable. The process variable ξ is in this case the estimated solar radiation or wind powering the generator, based on weather forecasts.

$$0 = -\eta_g^{-1} u_g - w + \xi \quad (3.4)$$

Since curtailment can never be greater than the estimation of the supply,

$$0 \leq w \leq |\xi|. \quad (3.5)$$

3.2.1.2 Storage Devices

For each storage device a dynamic equation is introduced

$$x(k+1) = x(k) + TC^{-1}(\eta u_s - \eta_g^{-1} u_g), \quad (3.6)$$

where u_s denotes storage charging and C denotes the capacity of the storage device. A state variable change will occur if an imbalance between supply and demand arises at the power node. Optimization variables are u_g and u_s . The normalized state variable is limited to a minimum and maximum of stored energy. Constraints also include min/max power output and ramping rates.

$$\begin{aligned} 0 &\leq x \leq 1 \\ u_g^{min} &\leq u_g \leq u_g^{max} \\ u_s^{min} &\leq u_s \leq u_s^{max} \end{aligned} \quad (3.7)$$

$$r_g^{min} \leq u_g(k) - u_g(k-1) \leq r_g^{max} \quad (3.8)$$

In order to distinguish between controllable and uncontrollable loads u_s is introduced as a controllable variable in addition to u_l , which is an uncontrollable variable.

3.2.1.3 System formulation

For each power node a corresponding equation of the type (3.1) is deployed. Nodes with storage can be formulated with

$$x(k+1) = Ax(k) + B \begin{pmatrix} u \\ z \end{pmatrix} \quad (3.9)$$

and nodes without storage with

$$0 = B \begin{pmatrix} u \\ z \end{pmatrix}, \quad (3.10)$$

where u is the set of all optimization variables, z is the set of all uncontrollable variables and A is an identity matrix. (3.9) and (3.10) are time discrete state space equations, with

$$\begin{aligned} B &= TC^{-1} \begin{pmatrix} B_g & B_s & B_w & B_\xi & B_l \end{pmatrix} \\ z &= \begin{pmatrix} \xi & u_l \end{pmatrix}^T \\ u &= \begin{pmatrix} u_g & u_s & w \end{pmatrix}^T. \end{aligned} \quad (3.11)$$

3.2.2 Redispatch Formulation

In order to formulate an optimization problem regarding redispatch costs, the dispatch formulation of [30] stated in Section 3.2.1 is extended:

$$u_g = \Delta u_{g+} + \Delta u_{g-} + u_{g0} \quad (3.12)$$

$$u_s = \Delta u_{s+} + \Delta u_{s-} + u_{s0} \quad (3.13)$$

is introduced where u_{g0}/u_{s0} is power generation/demand of the day-ahead schedule. Δu_{g+} is the increment of generation and Δu_{g-} is the decrement of generation. Furthermore, Δu_{s+} denotes the increment of charging power, whereas Δu_{s-} denotes the decrement of charging power. Distinguishing increment and decrement enables the differentiation of increment and decrement generation costs and avoids nonlinear equation sets [6].

3.2.2.1 Generation

As a consequence u_g is replaced by (3.12) to deduce a redispatch formulation. Hence,

$$0 = -\eta_g^{-1}(\Delta u_{g+} + \Delta u_{g-} + u_{g0}) + \xi. \quad (3.14)$$

Constraints include min/max power output and ramping rates.

$$\begin{aligned} 0 &\leq \Delta u_{g+} \leq u_g^{max} - u_{g0} \\ u_g^{min} - u_{g0} &\leq \Delta u_{g-} \leq 0 \\ r_g^{min} &\leq u_g(k) - u_g(k-1) \leq r_g^{max} \end{aligned} \quad (3.15)$$

Note for algebraic sign handling, the constraint on Δu_{g-} ensures $\Delta u_{g-} \leq 0$.

3.2.2.2 Storage Devices

Furthermore, u_g and u_s is replaced by (3.12) and (3.13) for storage devices.

$$x(k+1) = x(k) + TC^{-1}(\eta_l(\Delta u_{s+} + \Delta u_{s-} + u_{s0}) - \eta_g^{-1}(\Delta u_{g+} + \Delta u_{g-} + u_{g0})) \quad (3.16)$$

Analogous to (3.15) the constraints for storage devices are

$$\begin{aligned} 0 &\leq x \leq 1 \\ 0 &\leq \Delta u_{g+} \leq u_g^{max} - u_{g0} \\ u_g^{min} - u_{g0} &\leq \Delta u_{g-} \leq 0 \end{aligned} \quad (3.17)$$

$$\begin{aligned} 0 &\leq \Delta u_{s+} \leq u_s^{max} - u_{s0} \\ u_s^{min} - u_{s0} &\leq \Delta u_{s-} \leq 0 \end{aligned} \quad (3.18)$$

$$r_g^{min} \leq u_g(k) - u_g(k-1) \leq r_g^{max} \quad (3.19)$$

3.2.3 Network mapping

A problem formulation in accordance with the power node framework can be used with any kind of network model. Possible candidates are DC power model, AC power model and successive linearization of the AC power model [17], [77], [1].

The power flow model for the case study is a DC power flow. The power flow is calculated with the admittance matrix B_{DC} .

$$P_{bus} = B_{DC} \theta \quad (3.20)$$

The network model can be mapped to the system (3.9), (3.10) with

$$P_{bus} = \underbrace{\begin{pmatrix} c_1^T & b_1^T \\ c_2^T & b_2^T \\ \vdots & \vdots \\ c_n^T & b_n^T \end{pmatrix}}_{G_{map}} \begin{pmatrix} u_g \\ u_l \end{pmatrix} \quad (3.21)$$

where G_{map} is a bus mapping matrix and c_{ik} and b_{ik} are defined with

$$c_{ik} = \begin{cases} 0 & : \text{no grid injection} \\ 1 & : \text{generator injection} \end{cases} \quad b_{ik} = \begin{cases} 0 & : \text{no grid injection} \\ -1 & : \text{load injection} \end{cases} .$$

The bus mapping matrix and admittance matrix are integrated into one equation set

$$G_{map} \begin{pmatrix} u_g \\ u_l \end{pmatrix} - B_{DC} \theta = 0. \quad (3.22)$$

The transferred power over a line is calculated with

$$p_{line} - B_f \theta = 0 \quad (3.23)$$

where B_f is the admittance of the corresponding line. (3.22) and (3.23) can also be replaced by the power transfer distribution factor. p_{line} is limited to the maximum transfer capacity p_{line}^{max} , hence

$$|p_{line}| - p_{line}^{max} \leq 0. \quad (3.24)$$

3.2.4 Modeling example - Dispatch Problem

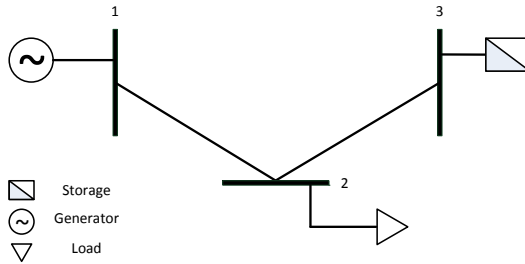


Figure 3.1: Three node modeling example

The example describes a three node network with one storage device. A combined heat power plant (CHP) is connected at node 1 and a load is positioned at node 2. CHP and storage have the following data.

Table 3.1: Generation parameter of a three node example

	P_{max} in MW	Cap. in MW/h	η_g	η_l	Costs in €
CHP	100	0	0.42	/	145
Storage	40	5000	0.9	0.85	5

Two lines, with parameters as in Table 3.2, link the corresponding nodes. Optimization variables are u_{g1} , u_{g2} and u_s . For the sake of simplicity ramping and line constraints are neglected. Furthermore, the optimization horizon is $N = 1$.

Table 3.2: Line parameter of a three node example

	X_L in Ω
line 1-2	8
line 2-3	2

3.2.4.1 Combined Heat and Power Plant

The power of the CHP is described with (3.25) based on the energy conservation law. The fuel consumption ξ is the product of efficiency η and the power feed-in.

$$\begin{aligned}\xi &= \eta_g^{-1} u_{g1} \\ &= 0.42^{-1} u_{g1}\end{aligned}\tag{3.25}$$

Additional constraints for the CHP are

$$0 \leq u_{g1} \leq 100.\tag{3.26}$$

3.2.4.2 Storage

The system equation of the storage device can be formulated according to (3.6) with sample rate $T = 15 \text{ min} = 0.25 \text{ h}$.

$$\begin{aligned}x(k+1) &= x(k) + TC^{-1} \begin{pmatrix} -\eta_g^{-1} & \eta_s \end{pmatrix} \begin{pmatrix} u_g \\ u_l \end{pmatrix} \\ &= x(k) + \frac{0.25}{5000} \begin{pmatrix} -0.9^{-1} & 0.85 \end{pmatrix} \begin{pmatrix} u_{g2} \\ u_s \end{pmatrix}\end{aligned}\tag{3.27}$$

Maximum and minimum constraints are considered with

$$\begin{aligned}0 &\leq x \leq 1 \\ 0 &\leq u_{g2} \leq 40 \\ 0 &\leq u_s \leq 40.\end{aligned}\tag{3.28}$$

The optimization starts with an initial charge of for example 0% (i.e. $x(0) = 0$).

3.2.4.3 Network

The DC power flow model of the three node network is

$$P_{bus} = B_{DC} \theta$$

$$\begin{pmatrix} u_{g1} \\ u_{g2} - u_s \\ -u_l \end{pmatrix} = \begin{pmatrix} \frac{1}{8} & 0 & \frac{-1}{8} \\ 0 & \frac{1}{2} & \frac{-1}{2} \\ \frac{-1}{8} & \frac{-1}{2} & \frac{5}{8} \end{pmatrix} \theta, \quad (3.29)$$

where P_{bus} is the net nodal power injection which is equal to

$$G_{map} u = \begin{pmatrix} 1 & 0 & 0 & 0 \\ 0 & 1 & -1 & 0 \\ 0 & 0 & 0 & -1 \end{pmatrix} \begin{pmatrix} u_{g1} \\ u_{g2} \\ u_s \\ u_l \end{pmatrix}. \quad (3.30)$$

3.2.4.4 Constraint LP-Problem

The constraint LP-problem is formulated as follows:

A control strategy shall be deployed optimizing the system

$$x(k+1) = x(k) + \frac{0.25}{5000} \begin{pmatrix} -0.9^{-1} & 0.85 \end{pmatrix} \begin{pmatrix} u_{g2} \\ u_s \end{pmatrix} \quad (3.31)$$

subject to state constraints

$$0 \leq x \leq 1 \quad (3.32)$$

which can be translated into

$$\begin{pmatrix} 1 \\ -1 \end{pmatrix} x \leq \begin{pmatrix} 1 \\ 0 \end{pmatrix}. \quad (3.33)$$

Assuming the optimization horizon of $N = 1$, the state variable x is

$$x(1) = x(0) + \frac{0.25}{5000} \begin{pmatrix} -0.9^{-1} & 0.85 \end{pmatrix} \begin{pmatrix} u_{g2} \\ u_s \end{pmatrix}. \quad (3.34)$$

x is replaced in (3.33) with (3.34), which leads to

$$\frac{0.25}{5000} \begin{pmatrix} -0.9^{-1} & 0.85 \\ 0.9^{-1} & -0.85 \end{pmatrix} \begin{pmatrix} u_{g2} \\ u_s \end{pmatrix} + \begin{pmatrix} 1 \\ -1 \end{pmatrix} x_0 \leq \begin{pmatrix} 1 \\ 0 \end{pmatrix}. \quad (3.35)$$

Let $u_{el} = (u_{g1} \ u_{g2} \ u_s)^T$. In accordance with Chapter 2.3 are the inequalities formulated with

$$\frac{0.25}{5000} \begin{pmatrix} 0 & -0.9^{-1} & 0.85 \\ 0 & 0.9^{-1} & -0.85 \end{pmatrix} \begin{pmatrix} u_{g1} \\ u_{g2} \\ u_s \end{pmatrix} \leq \begin{pmatrix} -1 \\ 1 \end{pmatrix} x_0 + \begin{pmatrix} 1 \\ 0 \end{pmatrix} \quad (3.36)$$

$$A_{in1} u_{el} \leq b_{in1}.$$

The input constraints are

$$\begin{aligned} 0 &\leq u_{g1} \leq 100 \\ 0 &\leq u_{g2} \leq 40 \\ 0 &\leq u_s \leq 40, \end{aligned} \quad (3.37)$$

analogous to (3.33) the input constraints are equal to

$$\begin{pmatrix} 1 & 0 & 0 \\ 0 & 1 & 0 \\ 0 & 0 & 1 \\ -1 & 0 & 0 \\ 0 & -1 & 0 \\ 0 & 0 & -1 \end{pmatrix} \begin{pmatrix} u_{g1} \\ u_{g2} \\ u_s \end{pmatrix} \leq \begin{pmatrix} 40 \\ 100 \\ 40 \\ 0 \\ 0 \\ 0 \end{pmatrix} \quad (3.38)$$

$$A_{in2} u_{el} \leq b_{in2}.$$

Additional equations are DC power flow equations (3.29) with

$$\underbrace{\begin{pmatrix} -G_{map} & B_{DC} \end{pmatrix}}_{A_{eq}} \begin{pmatrix} u_{el} \\ u_l \\ \theta \end{pmatrix} = 0. \quad (3.39)$$

In order to calculate the optimization variables over the course of the optimization horizon, the demand of the u_l is defined by a H_0 profile. An equation set for each time step is defined by the length of the optimization horizon N . The optimization

variables u_{g1} , u_{g2} , u_s are calculated minimizing the objective function over the optimization horizon. Consideration of generation costs leads to

$$\begin{aligned} \phi &= \sum_{k=1}^N L u(k) \\ &= \sum_{k=1}^N \begin{pmatrix} 145 & 0 & 0 \\ 0 & 5 & 0 \\ 0 & 0 & 0 \end{pmatrix} \underbrace{\begin{pmatrix} u_{g1}(k) \\ u_{g2}(k) \\ u_s(k) \end{pmatrix}}_{u_{el}} \\ &\stackrel{N=1}{=} L u_{el} \end{aligned} \quad (3.40)$$

3.2.4.5 Linear Programming

The optimization problem as stated in Section 3.2.4.4 can be solved using the simplex algorithm, which is using an augmented matrix form. The matrix form will be derived in the following. The inequality constraints are converted into equality constraints with the introduction of slack variables z . The equation set with slack variables is

$$\begin{aligned} \phi - L u_{el} &= 0 \\ A_{in} u_{el} + z &= b_{in} \\ A_{eq1} u_{el} + A_{eq2} \underbrace{\begin{pmatrix} u_l \\ \theta \end{pmatrix}}_{u_{ad}} &= b_{eq}, \end{aligned} \quad (3.41)$$

and the corresponding augmented matrix form with the objective to minimize ϕ is

$$\begin{pmatrix} E & -L & 0 & 0 \\ 0 & A_{in} & 0 & E \\ 0 & A_{eq1} & A_{eq2} & 0 \end{pmatrix} \begin{pmatrix} \phi \\ u_{el} \\ u_{ad} \\ z \end{pmatrix} = \begin{pmatrix} 0 \\ b_{in} \\ b_{eq} \end{pmatrix} \quad \text{with } z > 0, \quad (3.42)$$

where E is an identity matrix. The optimum can be attained by using the simplex algorithm.

The example has only one dynamic equation, but has 8 inequality constraints and 4 equality constraints. In general, the number of dynamic equations is equal to the number of storage devices, which is very low compared to the number of constraints. Hence, the optimization is primarily static in nature. Cooperation as introduced by [73], which relies on a coupled system matrix (coupling the state variables x) will fail, since the matrix is only sparsely populated. In the following

section novel cooperative optimization strategies have been developed to overcome these limitations.

3.3 Feasible Cooperation MPC

Goal of the multi-step optimization is to attain the optimal control sequence u^* over an optimization horizon N , complying with the constraints (3.3), (3.5), (3.7), (3.8) and (3.24). Predicted RES feed-in and load forecast over the optimization horizon are considered. Optimization variables are electrical power u_g of conventional generation, curtailment w of RES and demand and supply u_d, u_s of storage devices.

Based on a process model and past control variable inputs $u(k-1)$, the controller calculates how changes of the control variables effect the process. The best control sequence is selected using an objective function. Only the first step of the calculated control sequence is applied. Subsequently, based on the principle of the receding horizon, the next step of the optimal control sequence is calculated to account for prediction and model errors.

3.3.1 Cooperation of control areas

Ensuring a feasible cooperation of control areas, the following requirements have to be met:

- Through iterative calculation of the local optimization problems, the algorithm shall converge close to the global optimum.
- Communication of the current state and input variables to all subsystems is mandatory.
- A cooperation is only possible, if a subsystem adapts its state away from its local optimum towards the global optimum, while demand and supply are balanced.
- The objective function of each subsystem needs to make a cooperation possible [73], therefore simplified external generation costs are included.
- Calculated state and input trajectories must satisfy the model and input constraints of the global system to ensure feasibility.
- The local optimization needs to have a significantly lower complexity in comparison to the global problem in order to achieve calculation time benefits.

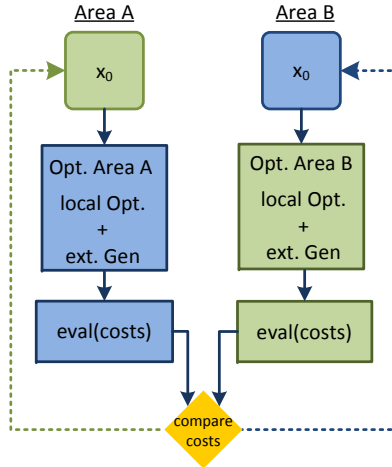


Figure 3.2: Cooperative optimization

A cooperative MPC algorithm is now presented, which complies with the requirements stated above.

The procedure is implemented for each subsystem. For the sake of simplicity Fig. 3.2 depicts only two areas. The algorithm starts with an initial condition calculated with the approach presented in Section 3.3.4. The initial condition includes values for all subsystems. At the optimization stage the local optimization considers the sum of external generation and its costs additionally. The costs of the produced results are evaluated. Results of all control areas are compared and the cheapest solution is distributed to all areas. Each area uses the favored solution for the next iteration.

3.3.1.1 Subsystem building

Each subsystem is defined as an area, where the corresponding operator has the responsibility of a secure network operation and the means to redispatch the generation units and storage devices. Subsystem m at iterate p is defined through

$$x_m^p(k+1) = A_m x_m^p(k) + B_m \begin{pmatrix} u_m^p \\ z_m \end{pmatrix}. \quad (3.43)$$

Nodes without storage lead to

$$0 = B_m \begin{pmatrix} u_m^p \\ z_m \end{pmatrix}. \quad (3.44)$$

The vector z_m is not an optimization variable and is therefore constant during the iterative process.

Each subsystem defined through (3.43) and (3.44) has no direct coupling to third party subsystems, the only exchange takes place through the network equations (3.22). The solution of external subsystems u_j^{p-1} with $\forall j \neq m$ is made available for the p -th iteration to subsystem m .

3.3.2 Cooperative Dispatch

The optimization variables are dispatched electrical power u_g of conventional generation, curtailment w of RES and dispatched demand and supply u_g, u_s of storage devices.

3.3.2.1 Cooperative optimization of generation

At any time throughout the iterative process, the supply is required to be equal to the demand to fulfill the power flow equations. One control area needs to be able to influence the power generation in external control areas to achieve power exchange from one area to another. In order to establish this, one control area has the ability to reduce the sum of the overall generation of each external control area. As generation can only be reduced, line limits and generation constraints will always hold and do not have to be evaluated explicitly. Reduction of generation is also coherent with the load flow calculation. The described procedure is implemented for $\forall j \neq m$ with

$$u_{g,j}^p = c_j u_{g,j}^{p-1} \quad (3.45)$$

where c_j is an optimization variable of the dimension (1×1) . External generation can be reduced from 100% to 0%, which leads to

$$0 \leq c_j \leq 1. \quad (3.46)$$

3.3.2.2 Cooperative optimization of storage

Storage management is adapted analogously to the cooperative behavior of generation. The residual charging power available in the storage can be calculated with

$$u_{sR} = u_s^{max} - u_s. \quad (3.47)$$

The remaining storage load of external systems can be accessed with k_j and varied from 0% to 100%. The adapted storage load for $\forall j \neq m$ is

$$u_{s,j}^p = u_{s,j}^{p-1} + k_j u_{sR,j}^{p-1}, \quad (3.48)$$

where k_j is an optimization variable of dimension (1×1) :

$$0 \leq k_j \leq 1 \quad (3.49)$$

Due to the introduction of k_j all storage devices of one area can be equally weighted and thus activated from an external subsystem. In order to prohibit a charging if the storage device has reached 100% state of charge (SOC) capacity, u_s is not allocatable for this time step. Since power generation from storage devices is in the set of u_g , an allocation is implemented analogously to Section 3.3.2.1.

The complexity is reduced significantly since only two additional optimization variables are needed per external subsystem.

3.3.2.3 Network equation

The exchange of iteration results takes place through (3.20). The vector u_g and u_l is assembled from all participating TSOs.

$$\begin{aligned} u_g &= \left(u_{g,1}^p \quad u_{g,2}^p \quad \dots \quad u_{g,m}^p \right)^T \\ u_l &= \left(u_{l,1} \quad u_{l,2} \quad \dots \quad u_{l,m} \right)^T. \end{aligned} \quad (3.50)$$

The complete equation set (3.20) is kept intact to maintain the coupling of the optimization problem.

3.3.2.4 Cost function

The cost function of the m -th subsystem is defined as

$$\begin{aligned} \phi_m(u_m) = \sum_{k=1}^N & \left[L_m u_m(k-1) + r_m(k)^T Q_m r_m(k) \right. \\ & \left. + \sum_{\substack{j=1 \\ j \neq m}}^M L_{gen,j}(c_j u_{g,j}^{p-1}) \right], \end{aligned} \quad (3.51)$$

where N is the optimization horizon. Cost matrix of the m -th system L_m includes generation and curtailment costs, whereas Q_m includes ramping costs. Furthermore, costs from external subsystems are also considered, where $L_{gen,j}$ are the full dispatch costs. Note that the power of external subsystems $u_{gen,j}^{p-1}$ is constant for each time step.

3.3.3 Cooperative Redispatch

This section describes the realization of cooperative redispatch. The optimization variables are redispatched electrical power Δu_g of conventional generation, curtailment w of RES and redispatched demand and supply $\Delta u_g, \Delta u_s$ of storages devices.

3.3.3.1 Cooperative optimization of generation

In order to compute a cooperative redispatch strategy of multiple control areas two optimization variables c_j, v_j with the dimensions (1×1) are introduced. Both variables are defined within the range

$$\begin{aligned} 0 &\leq c_j \leq 1 \\ 0 &\leq v_j \leq 1 \end{aligned} \quad (3.52)$$

and lead as in Section 3.3.2.1 to a reduction of all conventional generation and storage devices of neighboring subsystems.

$$\begin{aligned} \Delta u_{g+,j}^p &= c_j \Delta u_{g+,j}^{p-1} \\ \Delta u_{g-,j}^p &= -u_{g0} + u_g^{min} + v_j(u_{g0} + \Delta u_{g-,j}^{p-1} - u_g^{min}) \end{aligned} \quad (3.53)$$

c_j is capable of reducing any positive deviation of u_{g0} originated from previous iterations. Furthermore, v_j reduces all conventional generation and storage devices in neighboring subsystems within the range $0 \leq \Delta u_{g-} \leq u_{g0}$.

The implementation of cooperative optimization of storage devices is described in Section 3.3.2.2. Equations (3.47), (3.48) and (3.49) are applied.

3.3.3.2 Cost function

Analogous to Section 3.3.2.4 the cost function for the cooperative redispatch is defined with

$$\begin{aligned} \phi_m(u_m) = \sum_{k=1}^N & \left[L_{+,m} \Delta u_{g+,m} - L_{-,m} \Delta u_{g-,m} \right. \\ & + L_{w,m} w_m + r_m(k)^T Q_m r_m(k) \\ & \left. + \phi_{ext,m} \right], \end{aligned} \quad (3.54)$$

where $L_{+,m}$ are redispatch costs of incremental generation and $L_{-,m}$ are redispatch costs of decremental generation of the m -th subsystem. $L_{w,m}$ denotes curtailment costs, Q ramping costs and $\phi_{ext,m}$ costs from external subsystems. The external costs can be subdivided into incremental redispatch costs of all neighboring subsystems and decremental redispatch costs of all neighboring subsystems.

$$\begin{aligned} \phi_{ext,m}(u_m) = \sum_{j \neq m}^M & (L_{+,j} c_j \Delta u_{g+,j}^{p-1} - L_{-,j} (-u_{g0} \\ & + v_j (u_{g0} + \Delta u_{g-,j}^{p-1} - u_g^{max}))) \end{aligned} \quad (3.55)$$

Fig. 3.3 shows the generation of a power unit in a neighboring subsystem exem-

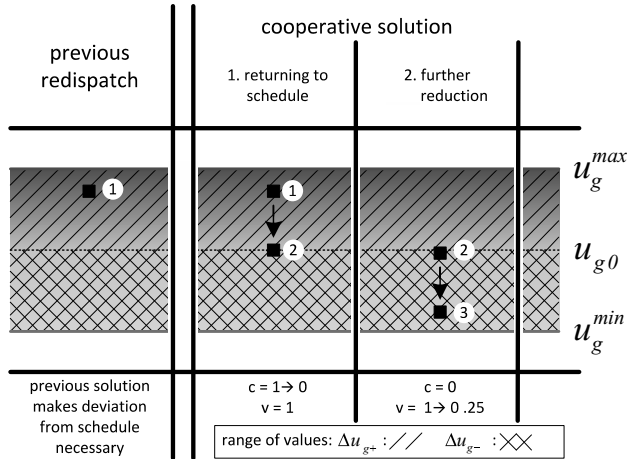


Figure 3.3: Cooperative redispatch example

plarily - a previous optimization iteration led to the case that Δu_{g_i} was chosen to be non-zero. c_j will preferably be used in comparison to v_j as it is economically beneficial to return to the day ahead schedule instead of deviating from the schedule

with v_j . Consequently, c_j can reduce this neighboring area to u_{g0} marked in Fig. 3.3 as point 2. If a further power decrease of this unit is profitable, v_j is applied reducing the generated power in this control area within the range u_{g0} to u_g^{min} . This is shown exemplarily in Fig. 3.3 with point 3.

3.3.4 Initial Values

The following algorithm is designed to attain initial values for the cooperative multi-step optimization.

In phase one a purely decentralized optimization of subsystem m is executed, i.e. the load and generation of external subsystems are set to zero. System (3.43), (3.44) is optimized considering the network equations (3.20) with $u_{g,j}^p = 0$ and $u_{l,j} = 0 \forall j \neq m$. A decentralized solution of subsystem m with network constraints is calculated and communicated to all subsystems. In the second phase a decentralized optimization considering the prior attained solution is executed to produce a consistent load flow. System (3.43), (3.44) is optimized considering the network equations (3.20) with $u_{g,j}^{p-1}$ and $u_{l,j}^{p-1} \forall j \neq m$ from the decentralized solution. The local optimum may not be achieved.

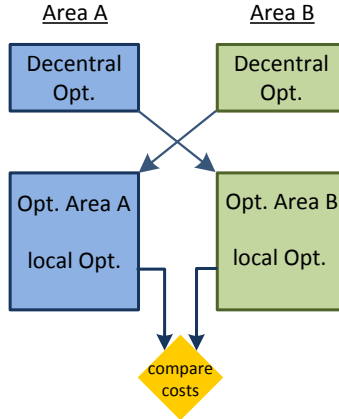


Figure 3.4: Flow chart initial values

3.3.5 Complexity

The central dispatch problem formulation has one optimization variable per generator g including RES and two optimization variables per storage s . Furthermore, two constraints per generator, four constraints per storage and one constraint per line

l are used. Consequently, the number of optimization variables n and the number of constraints m is

$$\begin{aligned} n &= g + 2s \\ m &= 2g + 4s + l, \end{aligned} \tag{3.56}$$

Let $W = m + n$. The complexity can be estimated according to [40] with the big O notation

$$\mathcal{O}\left((WN)^{k_p}\right). \tag{3.57}$$

where N is the optimization horizon and k_p depends on the solver algorithm used. The complexity of one subsystem from a total of M subsystems can be estimated with

$$\begin{aligned} n_i &= g_i + 2s_i \\ m_i &= 2g_i + 4s_i + l, \end{aligned} \tag{3.58}$$

where s_i and g_i denote the number of storage devices and generators in subsystem i . Let $W_i = m_i + n_i$. The complexity per iterate of a subsystem can be estimated with

$$\mathcal{O}\left(\left((2(M-1) + W_i)N\right)^{k_p}\right). \tag{3.59}$$

Since $(2(M-1) + W_i) \ll W$, a significant reduction of complexity is achieved. Each subsystem can be solved independently using parallel computing methods.

3.4 Case Study

In this section the results of the developed cooperative optimization are presented. As the central optimization of the considered networks is still solvable, it is possible to compare the quality of the calculated cooperative optimization. The IEEE 14 and IEEE 118 networks are equipped with additional RES and storage devices. Simulations are done using Yalmip [55].

3.4.1 General setup

The simulations are conducted with the following assumptions. The process model has accurate prediction for load and RES feed-in, therefore it possesses perfect foresight. The N-1 principle is accomplished, if the used line capacity is $< 80\%$ of the rated line capacity. External subsystems cannot dispatch renewable generation of neighboring systems. Line constraints are defined according to [34]. The scenarios are defined with a load profile for each load for a period of 72 h. Further, wind speed and solar radiation are defined for the same time interval.

3.4.2 IEEE 14 network

The IEEE 14 benchmark network is used to illustrate the capabilities of the developed algorithm. The case study especially focuses on generation and storage cross border dispatch. The costs, efficiency η and maximum power output are defined in Appendix C.2. The generation consists of four biomass power plants, two pumped-hydro plants, a wind park, a PV and a feeder. The pumped storage plants have a capacity of 5000 MWh each.

The IEEE 14 network is divided into 4 subsystems as depicted in Fig. 3.5. Both pumped storage plants are in separate areas. Hence, the subsystems need to coordinate the storage devices and biomass power plants in order to attain an optimal schedule.

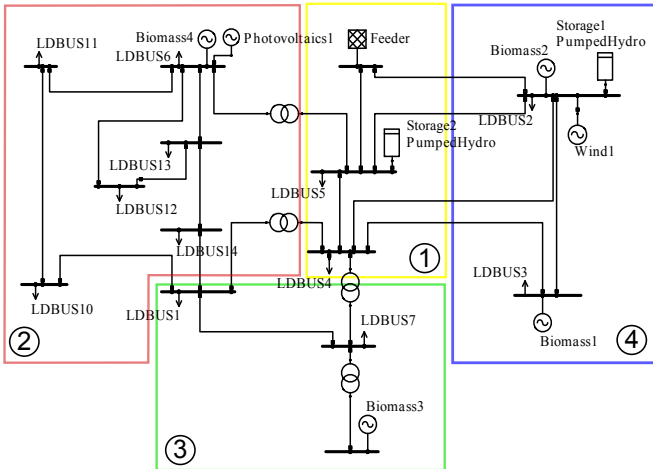
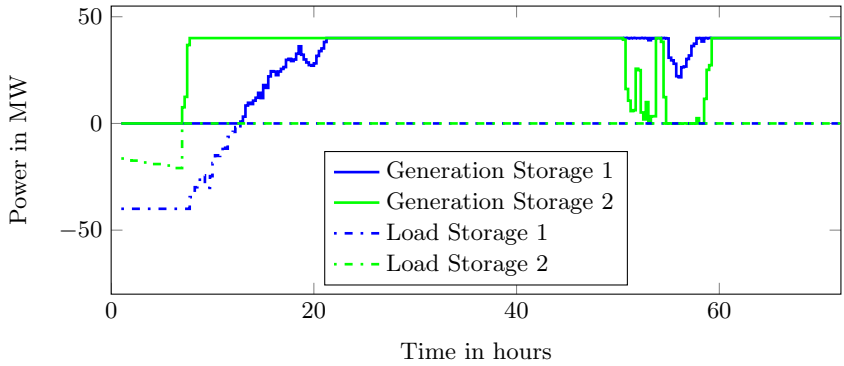


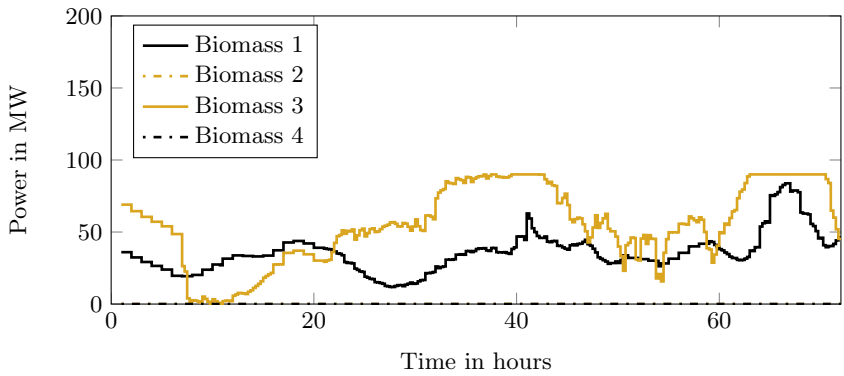
Figure 3.5: Extended IEEE 14 network with RES and storage devices divided into four areas

3.4.2.1 Cooperative solution

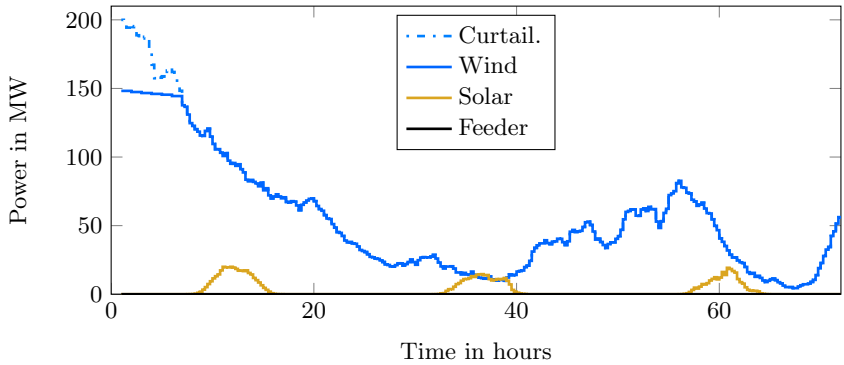
At the beginning of the simulation very high wind feed-in in area 4 endangers grid security. Area 4 could curtail wind feed-in significantly and solve the incident by itself. However, from a global perspective it is preferable to use the storage capacity of area 1. Consequently, both storage devices are charged. Storage 1 is located at the same busbar as the wind farm and is able to charge with full load (40 MW) as depicted in Fig. 3.6a. Due to the line restrictions not all wind energy can be transferred to storage 2. Storage device 2 is able to buffer with a peak load of



(a) Storage operation



(b) Biomass 1 to 4 operation



(c) Wind power, solar power and feeder operation

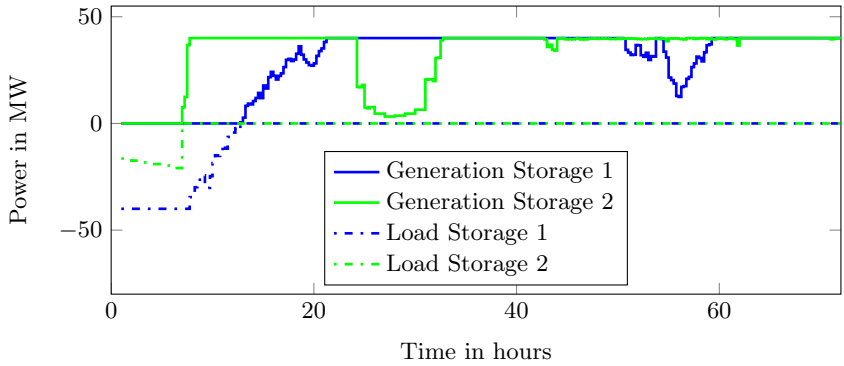
Figure 3.6: Cooperative operation of the IEEE 14 network

20 MW during high wind feed-in. Furthermore, the biomass power of areas 3 and 4 is dispatched as depicted in Fig. 3.6b. The residual wind energy is curtailed as depicted in Fig. 3.6c. In the further course of the simulation at hour 10 both pumped storage hydro power plants of area 1 and area 4 are discharging, while the wind feed-in decreases and hence the power output of biomass power plant 3 can be reduced. During day time solar power is fed into the network, curtailment is not necessary. The biomass power plant 3 is operated counter-cyclical to the wind feed-in. Furthermore, the feeder is only used sporadically during the simulation interval. Biomass power plant 2 and 4 are not in operation.

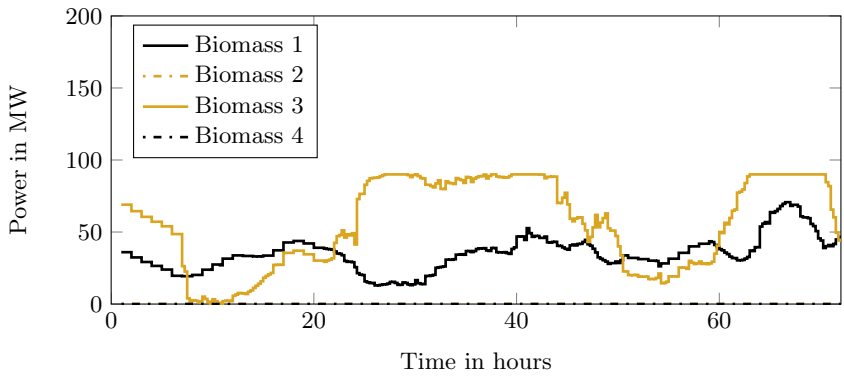
3.4.2.2 Central solution

The centralized controller has full system knowledge and is able to schedule any control variable u . Consequently, the global optimum is defined with the trajectories of the central solution as depicted in Fig. 3.7c-3.7a. The central controller has the identical wind and solar feed-in as depicted in Fig. 3.7c. Also the load curve of both storages are identical as depicted in Fig. 3.7a. The generation of the storage devices has some discrepancies. The centralized optimization operates storage 2 at maximum power output, apart from hour 50 - 60. In comparison storage 2 of the cooperative solution is operated at maximum power output, apart from hour 22 - 32 (Fig. 3.6a). The power decrease from storage 2 is balanced by biomass 3 (Fig. 3.7b). Storage 1 has minor discrepancies at hour 58. The feeder is not needed for the central scenario.

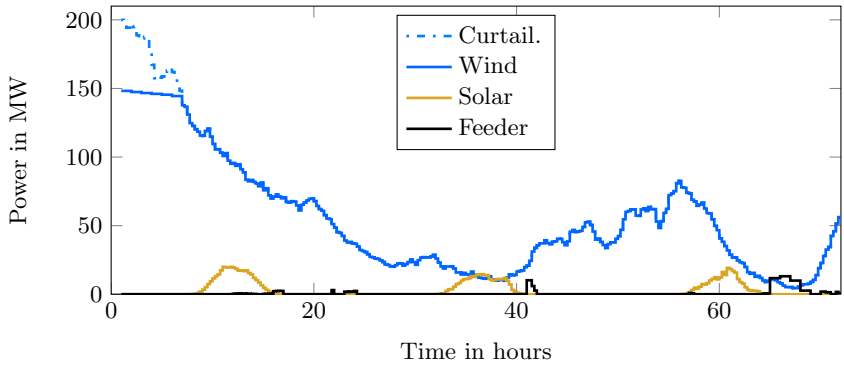
A discrepancy may only lead to minimal additional costs depending on the generation used. The centralized optimization spends € 2.627 million to satisfy the demand. In comparison the cooperative approach spends € 2.699 million. Therefore, the cooperative optimization is reaching 97% of the global optimum after 7 iterations.



(a) Storage operation



(b) Biomass 1 to 4 operation



(c) Wind power, solar power and feeder operation

Figure 3.7: Central operation of the IEEE 14 network

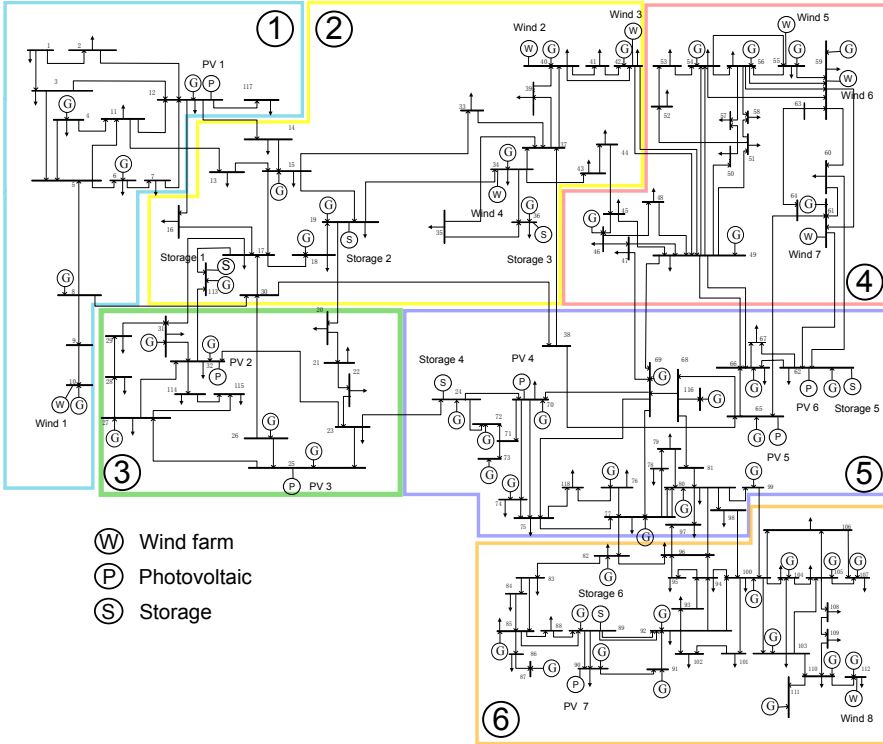


Figure 3.8: Extended IEEE 118 network with RES and storage devices divided into six areas

3.4.3 IEEE 118 network

It is possible to compare the time line of the IEEE 14 network. However, this is not the case for the IEEE 118 network. Due to the high degree of freedom caused by receding horizon optimization a simple visual comparison of the schedules does not necessary reveal, if two solutions are close. Different operating strategies may lead to an economic solution very close to the global optimum. Therefore, the monetary comparison as introduced in Section 3.4.2.2 is chosen. The network has a total installed generation of 9.7 GW satisfying a total demand of 4.2 GW. The costs, efficiency and maximum power output are defined in Appendix C.3. The total generation is produced from 52 generators, 8 wind farms, 7 solar power plants and 6 pumped-storage hydro power plants. The network is divided into 6 control areas as depicted in Fig. 3.8.

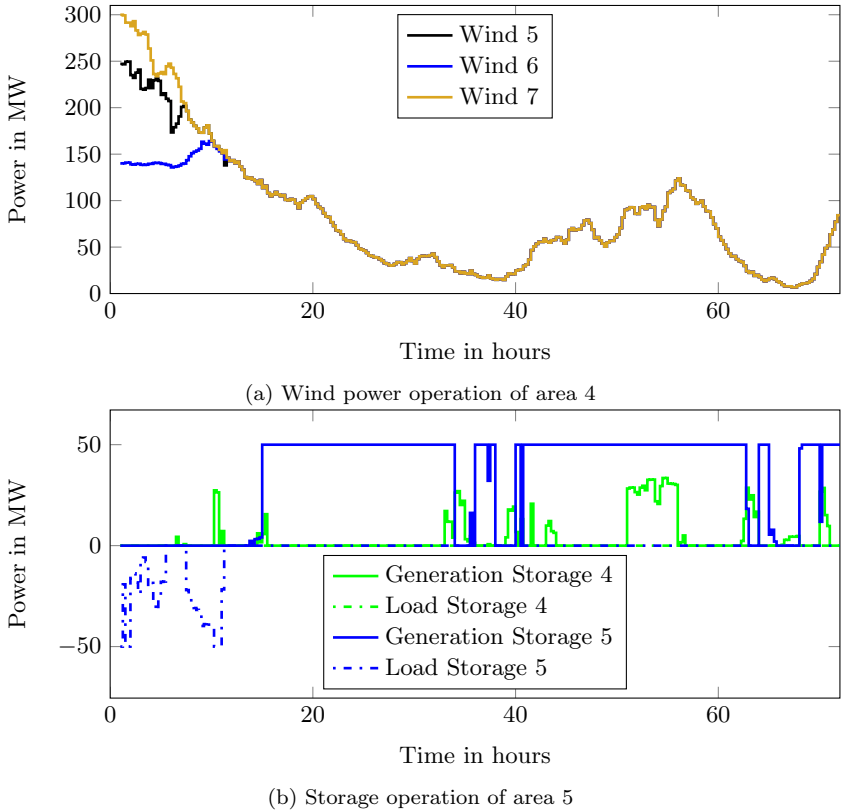


Figure 3.9: Cooperative operation of the IEEE 118 network

Three wind farms are located in area 4 with a maximum power output of 300 MW each. As depicted in Fig. 3.9a storage device 5 located in area 5 buffers the wind energy. In order to comply with line constraints, curtailment of wind farms 5 and 6 is needed as illustrated in Fig. 3.9a. The centralized optimization spends € 29.7 million to satisfy the demand. In comparison the cooperative approach spends after 7 iterations €33.5 million. Therefore, the cooperative optimization is reaching 89% of the global optimum.

3.5 Conclusion

Decentralized optimization faces the challenge, that each local optimum may differ significantly from the global optimum. The method presented in this work ensures

secure operation of several control areas with high RES feed-in, while reducing overall costs. A safe and efficient way of cross border dispatching can be deployed. Wind forecast and optimal storage operation are explicitly considered. Control area responsibilities are maintained. Through cooperation rather than competition the solution gets closer to the global solution per iteration. The cooperative strategy will reduce redispatch costs and ensure flexible grid operation. The overall complexity is reduced by dividing the optimization into subproblems. Furthermore, the method is scalable and makes parallel computing possible. Functionality of the algorithm was successfully shown using an extension of the IEEE 14 and an extension of the IEEE 118 grid. Both scenarios represent stressed systems with very high RES feed-in. A secure cross border redispatch with use of storage devices is realized to maintain a high share of RES feed-in. All line constraints are met with the help of the new schedule.

3.5.1 Outlook

Explicit N-1 calculation can be added to the presented method with the approach of [33]. A full Newton-Raphson AC power flow would further support the model quality. Also the influence of prediction errors needs to be evaluated. Future versions can also be applied in grid planning tasks.

Chapter 4

Dynamic Security

4.1 Motivation

Dynamic security also known as dynamic stability of the power system is one of the key requirements of a secure operation. Programs which assess the dynamic stability are heavily used in the industry, however most of the developed programs for instance [75], [50] neglect the influence of network dynamics. The programs work with algebraic network equations assuming all frequencies very are close to $f_N = 50\text{Hz}/60\text{Hz}$. Furthermore, the system models including algebraic network equations not only describe frequencies very close to f_N , but also superimposed frequencies from $0.01 - 5\text{Hz}$. The system modes are preserved also for low frequency oscillations, since the sinusoidal waveform of the $50\text{Hz}/60\text{Hz}$ signal is altered very little. However, the following phenomena are not described with a static network model [35]: Torsional oscillations, controller interactions, harmonic interactions and resonance, ferroresonance.

This thesis focuses on the avoidance of controller interactions, while the methodology used is also applicable to the phenomena mentioned above. Control interactions are crucial for controller synthesis, which implies a successful coordinated control strategy. With the increasing number of power system devices with closed loop controls, the number of control modes also increases. In general modern power system devices like FACTs, HVDC, but also AVR and PSS have natural oscillation modes at $1 - 35\text{Hz}$. Furthermore, RES with closed-loop controls for the reactive power supply create additional control modes. Depending on the electrical distance between devices and control parameters, control interactions may result in small-signal instability. Additionally, closed-loop control systems and natural oscillatory modes can interact. This leads to the situation that advantages associated with smart grid applications, i.e. the increasing number of power system devices able to influence the power flow including RES [54] [44] [7], also significantly increases the number of control modes. Hence, the traditionally used models relying on static network equations may lead to false conclusions. Furthermore, the coordination of

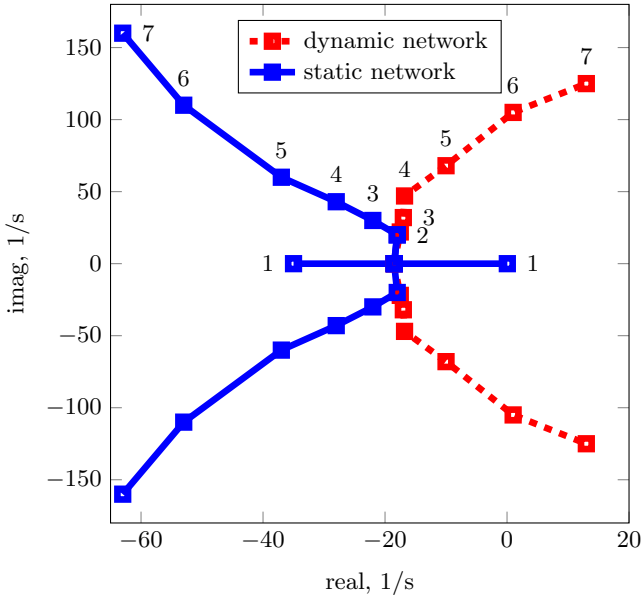


Figure 4.1: Root loci of radial network with three SVCs developed by [63]

Point 1: $k_p = 0$	Point 5: $k_p = 2.1$
Point 2: $k_p = 0.2$	Point 6: $k_p = 4.2$
Point 3: $k_p = 0.4$	Point 7: $k_p = 6.3$
Point 4: $k_p = 0.8$	

multiple controllers, as proposed in Chapter 6, needs to explicitly consider control modes. [41] shows that the interaction of multiple HVDC feed-ins are described unsatisfactorily by static network equations and suggests dynamic network models as a remedy.

Moreover, [63] presented an illustrative example for control interactions and compares the stability assessments from static and dynamic network models. A radial network is used with a total of 650 km and three SVCs in operation. The block diagram and the system data can be found in Appendix C.1.

All SVCs are operated in closed-loop control. The root loci of the dominant mode of SVC 3 is depicted in Figure 4.1. A root loci plot calculates the eigenvalues of the overall system in dependence of the SVC controller gain k_p . The dominant eigenvalues calculated with static network equations are compared to the dominant eigenvalues of the system calculated with a dynamic network model. Both models show the same results for small gains ($k_p \leq 0.2$). For gains $k_p > 0.2$ the static net-

work predicts good overall dampening of the system, whereas the dynamic network shows a significant deteriorating dampening behavior. The root loci plot created with the dynamic network indicates an unstable overall system with gains higher than $k_p = 4.2$, while the model with static network equations indicates high dampening of the mode with a gain of that value. Hence, the modes calculated with static network equations provide unsatisfactory results.

Engineers working with the widespread software packages relying on static network equations make fundamental errors when assessing the dynamic behavior of the overall model. The insight attained by a comprehensive small signal analysis is essential, especially for complex systems.

In this chapter a model is developed suitable for small signal analysis. The network model presented, based on [31], explicitly considers network dynamics and hence is suitable for the prevention of resonant control modes or harmonic interactions. Moreover, models for synchronous generators and static var compensators are developed. The small signal model is used for an eigenvalue comparison, where models relying on static network equations and the model relying on dynamic network equations are compared.

4.1.1 Network Model Overview and Applications

This section first gives a short overview of existing network models including dynamics. The second subsection contains examples of applications using dynamic network equations, sometimes also called dynamic phasors.

E.S. Kuh [47] demonstrated as one of the first in 1965 the state-variable approach to network analysis. He developed a state description for linear, passive networks. [27] developed the first commercial software package including network dynamics and demonstrated its effectiveness using the New England test system. Variations of the two model representations are used by [53]. [24] extends the approach also to distributed parameter line models. Furthermore, [42] developed a hybrid network model, mixing dynamic and static network equations in order to reduce the number of state variables. [56] developed a model for the unsymmetrical operation.

Applications

The work of [32] and [8] uses dynamic network models for simulation purposes. Dynamic network representation is able to improve simulation performance, while achieving a higher accuracy, compared to available commercial software. [28] and [11] apply dynamic networks to damp torsional oscillations. Furthermore, [29] investigates interactions of turbo-generator sets and power electronics.

[10] and [79] developed controllers for HVDC applying network dynamics. [72] used dynamic networks to create reduced order equivalents, whereas [25] developed a tool for harmonic analysis.

4.2 Dynamic network model

The network model proposed by [32], [56] and [31] describes the dynamic in/- output behavior of a network. This thesis presents an extension which is able to calculate all feed-in and node voltages and hence can be used in further applications. The method is able to represent transformers, transmission lines and loads using a resistance network. Within the network two nodes can only be connected by one series RL-branch in addition to a parallel capacitance.

The dynamic model is based on the admittance matrix $I = Y_m U$. Where Y_m is the modified node-point admittance matrix of Y with the last column and row omitted. Y_m has the dimensions $(n \times n)$. To develop a dynamic model, each element of the admittance matrix is interpreted in Laplace space, which leads to the substitution $j\omega = s$. In general this is only true if the initial condition is equal to zero, which can be assumed here. Hence the modified admittance matrix Y_m is a function of s

$$\begin{pmatrix} i_F \\ i_N \end{pmatrix} = Y_m(s) \underbrace{\begin{pmatrix} u_F \\ u_N \end{pmatrix}}_u, \quad (4.1)$$

where u_F and u_N denote the feeder and node voltages, respectively. The admittance matrix is based on Kirchhoff's current law as $i_N = 0$. Therefore, with a given impedance matrix with loads included, the voltage for every node can be calculated with the knowledge of i_F . The inverse of Y_m can be calculated when $\det(Y_m) \neq 0$ as the adjugate divided by the determinant of Y_m .

$$\begin{aligned} u &= Y_m^{-1}(s) i_F = Z_m(s) i_F \\ &= \frac{\text{adj}(Y_m)}{\det(Y_m)} i_F \end{aligned} \quad (4.2)$$

In order to obtain a polynomial denominator and numerator of minimal order $Z_m(s)$ needs to be extended by N_Δ . N_Δ is the product of the denominators of the upper triangular matrix, i.e. the denominator of Y_{ij} , ($j > i$).

$$u = \frac{\text{adj}(Y_m) N_\Delta}{\det(Y_m) N_\Delta} i_F \quad (4.3)$$

The poles of $Z_m(s)$ can be calculated with the determinant of Y_m .

$$u = \frac{adj(Y_m)N_\Delta}{V(s - \sigma_1) \dots (s - \sigma_{n_0})} i_F \quad (4.4)$$

For every row of Y_m which consists only of terms of the form $Y = \frac{1}{R+sL}$ and zeros, the order of the numerator is greater than the order of the denominator. Hence a partial fraction decomposition is needed and gives

$$u = \left(R + sL + \sum_{l=1}^{n_0} \frac{1}{s - \sigma_l} Z_l \right) i_F. \quad (4.5)$$

Where n_0 is the number of poles. Z_l is calculated with the residue theorem

$$Z_l = \frac{adj(Y_m)N_\Delta}{V \prod (s - \sigma)} \Big|_{s=\sigma_l}. \quad (4.6)$$

Moreover, Z_l can be decomposed into

$$Z_l = V_l \Lambda_l W_l, \quad (4.7)$$

where Λ_l are the eigenvalues of Z_l , and V_l and W_l are left- and right-hand eigenvectors. The matrices Z_l have several properties as described by [31],[56]. Since Y_m is symmetric and the properties of the adjugate are transferable to Z_l , the following properties can be formulated for Z_l .

Properties of Z_l

$$\begin{aligned} &\text{if } \text{rank}(Y_m(\sigma_l)) = n - 1 \\ &\quad \Rightarrow \text{rank}(adj(Y_m(\sigma_l))) = 1 \\ &\text{if } \text{rank}(Y_m(\sigma_l)) < n - 1 \\ &\quad \Rightarrow \text{rank}(adj(Y_m(\sigma_l))) = 0 \end{aligned} \quad (4.8)$$

Y_m is symmetric
 $\Rightarrow adj(Y_m)$ is symmetric

If Z_l is of rank 0 the decomposition is not unique and Λ_l may be set to 0. Furthermore, if Z_l is of rank 1, the eigenvalue Λ_l has only one non-zero element. Thus, Λ_l can be reduced to one element μ_l with the corresponding eigenvectors v_l , w_l with the dimensions $(n \times 1)$ and $(1 \times n)$.

$$Z_l = \mu_l v_l w_l \quad (4.9)$$

$$C = \left(\begin{array}{cccc} \mu_1 v_1 & \dots & \operatorname{Re}\{\mu_{l+1} v_{l+1}\} & \operatorname{Im}\{\mu_{l+1} v_{l+1}\} & \dots \end{array} \right) \quad (4.15)$$

and the dimensions, where F is the number of feeds. As $i_N = 0$, the matrices A, B, C, R, L have the dimension

$$\begin{aligned} \dim(A) &= (n_0 \times n_0) & \dim(R) &= (n \times F) \\ \dim(B) &= (n_0 \times F) & \dim(L) &= (n \times F) \\ \dim(C) &= (n \times n_0) \end{aligned} \quad (4.16)$$

4.2.2 dq-Transformation of the model

The model described is only valid for the symmetrical three phase current case, but can be extended to the asymmetrical case [31] as well.

The state space matrices for a three-phase system are equal to those of a single-phase system since all phases are structurally the same. E is the identity matrix with the dimension (3×3) . a_{ij} is element ij of (4.13).

$$A_{abc} = \left(\begin{array}{ccc} a_{11}E & \cdots & a_{1n_0}E \\ \vdots & \ddots & \vdots \\ a_{n_0 1}E & \cdots & a_{n_0 n_0}E \end{array} \right) \quad (4.17)$$

The transformation from 3-phase to $\alpha\beta 0$ does not alter the system matrices ($A_{\alpha\beta 0} = A_{abc}$), but only the state variables. The 0-component can be omitted for the symmetrical case.

Since the dq-Transformation is a time-variant transformation the system matrices and the state variables change due to the transformation. With

$$T = \left(\begin{array}{cc} \cos \Theta & \sin \Theta \\ -\sin \Theta & \cos \Theta \end{array} \right) \quad (4.18)$$

and $\Theta = 2\pi ft$ the state space equation is

$$\begin{aligned} \frac{d}{dt}(T\zeta_{dq}) &= A_{\alpha\beta}T\zeta_{dq} + B_{\alpha\beta}T i_{dq} \\ \omega DT\zeta_{dq} + T\dot{\zeta}_{dq} &= A_{\alpha\beta}T\zeta_{dq} + B_{\alpha\beta}T i_{dq} \\ \dot{\zeta}_{dq} &= (-\omega D + A_{\alpha\beta})\zeta_{dq} + B_{\alpha\beta} i_{dq} \\ \dot{\zeta}_{dq} &= A_N \zeta_{dq} + B_N i_{dq} \end{aligned} \quad (4.19)$$

Analogous to (4.2.2) the state equation is

$$\begin{aligned} u_{dq} &= C_{\alpha\beta}\zeta_{dq} + (R_{\alpha\beta} + L_{\alpha\beta}\omega D)i_{dq} + L_{\alpha\beta}\dot{i}_{dq} \\ u_{dq} &= C_N\zeta_{dq} + R_N i_{dq} + L_N \dot{i}_{dq} \end{aligned} \quad (4.20)$$

since

$$\frac{d}{dt}(T) = \omega D(T) \quad (4.21)$$

with

$$\begin{aligned} \omega &= 2\pi f \\ D &= \begin{pmatrix} 0 & -1 \\ 1 & 0 \end{pmatrix}. \end{aligned} \quad (4.22)$$

The system from d-phase and q-phase are the structurally the same

$$T \begin{pmatrix} c & 0 \\ 0 & c \end{pmatrix} T^{-1} = \begin{pmatrix} c & 0 \\ 0 & c \end{pmatrix} \quad (4.23)$$

and

$$T^{-1} \begin{pmatrix} c & 0 \\ 0 & c \end{pmatrix} DT = \begin{pmatrix} c & 0 \\ 0 & c \end{pmatrix} D. \quad (4.24)$$

The state space model for the grid used in the following is

$$\dot{\zeta}_{dq} = A_N\zeta_{dq} + B_N i_{dq} \quad (4.25)$$

$$u_{dq} = C_N\zeta_{dq} + R_N i_{dq} + L_N \dot{i}_{dq}. \quad (4.26)$$

In case only the in-/output behavior is of interest (4.1) can be partitioned into

$$\begin{pmatrix} i_F \\ 0 \end{pmatrix} = \begin{pmatrix} Y_{FF} & Y_{NF} \\ Y_{FN} & Y_{NN} \end{pmatrix} \begin{pmatrix} u_F \\ u_N \end{pmatrix}. \quad (4.27)$$

The method described in (4.3) - (4.15) with consideration of Y_{FF} instead of Y_m can be applied.

(4.26) can be reformulated into

$$u_F = C_F \zeta_{dq} + R_F i_F + L_F \dot{i}_F. \quad (4.28)$$

The matrices of (4.28) are the same as (4.26), but with the row dimension F .

$$\begin{bmatrix} u_F \\ 0 \end{bmatrix} = \begin{bmatrix} L_F & 0 \\ 0 & -E \end{bmatrix} \begin{bmatrix} i_F \\ \zeta \end{bmatrix}^\bullet + \begin{bmatrix} R_F & C_F \\ B_F & A_N \end{bmatrix} \begin{bmatrix} i_F \\ \zeta \end{bmatrix} \quad (4.29)$$

In order to deploy (4.29) the same matrix definitions as (4.13) - (4.15) apply. The eigenvectors of (4.9) v_l, w_l have only the dimensions $(F \times 1)$ and $(1 \times F)$.

In the following chapter an overall model of the network model given in (4.29), the dynamic model of synchronous machine and static var compensator (SVC) is developed. In order to distinguish the feed-in currents and voltages of synchronous machines and SVCs (4.29) is partitioned into

$$\begin{bmatrix} u_{Fg} \\ u_{Fs} \\ 0 \end{bmatrix} = \begin{bmatrix} L_{Fg} & 0 & 0 \\ 0 & L_{Fs} & 0 \\ 0 & 0 & -E \end{bmatrix} \begin{bmatrix} i_{Fg} \\ i_{Fs} \\ \zeta \end{bmatrix}^\bullet + \begin{bmatrix} R_{Fg} & 0 & C_{Fg} \\ 0 & R_{Fs} & C_{Fs} \\ B_{Fg} & B_{Fs} & A_N \end{bmatrix} \begin{bmatrix} i_{Fg} \\ i_{Fs} \\ \zeta \end{bmatrix}. \quad (4.30)$$

Where the index g indicates generator feed-in and s SVC feed-in, respectively. (4.30) assumes R_F and L_F in diagonal form with is in general the case.

4.3 Model of the Synchronous Generator

The plurality of electrical power is generated by synchronous machines. The dynamic and transient behavior of power systems is strongly influenced by synchronous generators. Hence, the correct dynamic description of synchronous generators is essential for the assessment of small signal stability. A nonlinear model of a 3-phase salient-pole synchronous generators is presented, which represent hydro, steam generators and synchronous motors.

4.3.1 Nonlinear Model

The generator model (4.31) - (4.36) derived from [46] is used for the small signal stability analysis. The rotor is equipped with one field winding and in total three damper windings. One damper winding (kd) is in-line with the field winding (kf), whereas the remaining two damper windings (kq1) and (kq2) are orthogonal to

the field winding. As depicted in Fig. 4.2 both damper windings (kq1), (kq2) are orthogonal to the d-axis and the field winding (kf) is orthogonal to the q-axis. The stator of the 3 phase system has three windings displaced by 120° . As shown in Fig. 4.2 each stator winding has the resistance r_s and the reactance X_s , creating three terminals. With the aid of park's transformation the stator variables can be transformed to dq-components. For simplicity the 0-component has been omitted and hence the model assumes symmetric operation. The model neglects the mutual inductance between field winding and d-axis damper winding, sometimes referred to as canay reactance. Furthermore, all saturation effects have been neglected. kq1, kq2 have the resistance r_{kq1} , r_{kq2} and the reactance X_{kq1} , X_{kq2} . Furthermore, fd, kd have the resistance r_{kfd} , r_{kd} and the reactance X_{kfd} , X_{kd} . The excitation of the synchronous generator is controlled via u_{fd} , whereas all damper windings are short-circuited windings. The q- and d-axis are rotating with the electrical angular velocity ω_r . The angle difference between the a-axis and q-axis is the rotor angle θ .

$$\dot{\psi}_{qs}^r = \omega_b \left(u_{qs}^r - \frac{\omega_r}{\omega_b} \psi_{ds}^r + \frac{r_s}{X_{ls}} (\psi_{mq}^r - \psi_{qs}^r) \right) \quad (4.31)$$

$$\dot{\psi}_{ds}^r = \omega_b \left(u_{ds}^r + \frac{\omega_r}{\omega_b} \psi_{qs}^r + \frac{r_s}{X_{ls}} (\psi_{md}^r - \psi_{ds}^r) \right) \quad (4.32)$$

$$\dot{\psi}_{kq1}^r = \omega_b \left(u_{kq1}^r + \frac{r'_{kq1}}{X'_{lkq1}} (\psi_{mq}^r - \psi_{kq1}^r) \right) \quad (4.33)$$

$$\dot{\psi}_{kq2}^r = \omega_b \left(u_{kq2}^r + \frac{r'_{kq2}}{X'_{lkq2}} (\psi_{mq}^r - \psi_{kq2}^r) \right) \quad (4.34)$$

$$\dot{\psi}_{fd}^r = \omega_b \left(\frac{r'_{fd}}{X_{md}} u_{fd} + \frac{r'_{fd}}{X'_{lfd}} (\psi_{md}^r - \psi_{fd}^r) \right) \quad (4.35)$$

$$\dot{\psi}_{kd}^r = \omega_b \left(u_{kd}^r + \frac{r'_{kd}}{X'_{lkd}} (\psi_{md}^r - \psi_{kd}^r) \right) \quad (4.36)$$

The state variables of the nonlinear model are the magnetic flux per second of the stator windings ψ_d^r , ψ_q^r as well as the magnetic flux per second of the rotor windings ψ_{kq1} , ψ_{kq2} , ψ_{fd} , ψ_{kd} . The input variables are u_d^r , u_q^r (terminal voltage), and u_{fd} excitation voltage. $\omega_b = 2\pi f_N$ is the angular grid frequency.

The differential equation set (4.31 - 4.32) of the stator and (4.33 - 4.36) of the rotor are coupled over the main flux

$$\psi_{mq}^r = X_{aq} \left(\frac{\psi_{qs}^r}{X_{ls}} + \frac{\psi_{kq1}^r}{X'_{lkq1}} + \frac{\psi_{kq2}^r}{X'_{lkq2}} \right) \quad (4.37)$$

$$\psi_{md}^r = X_{ad} \left(\frac{\psi_{ds}^r}{X_{ls}} + \frac{\psi_{fd}^r}{X'_{lfd}} + \frac{\psi_{kd}^r}{X'_{lkd}} \right). \quad (4.38)$$

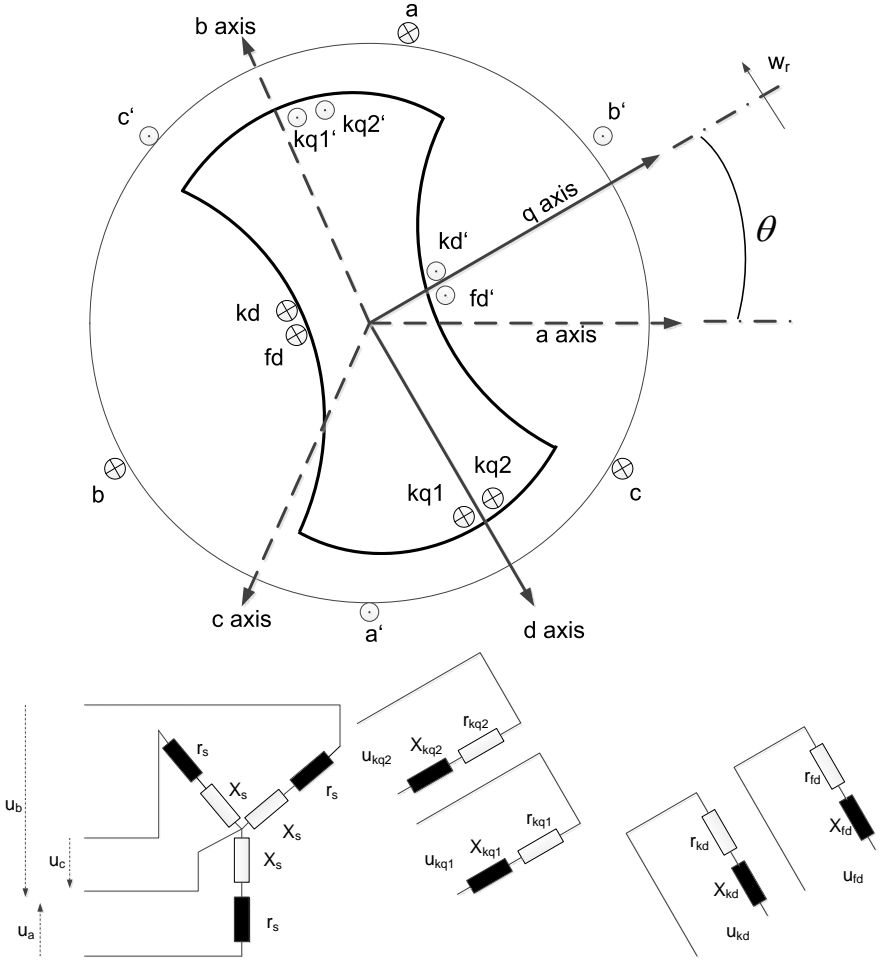


Figure 4.2: Salient-pole synchronous generators [46]

Additionally, let

$$X_{aq} = \left(\frac{1}{X_{mq}} + \frac{1}{X_{ls}} + \frac{1}{X'_{lkq1}} + \frac{1}{X'_{lkq2}} \right)^{-1} \quad (4.39)$$

$$X_{ad} = \left(\frac{1}{X_{md}} + \frac{1}{X_{ls}} + \frac{1}{X'_{lfd}} + \frac{1}{X'_{lkd}} \right)^{-1} \quad (4.40)$$

The terminal currents can be expressed in dependence of the state variables with

$$i_{qs}^r = -\frac{1}{X_{ls}}(\psi_{qs}^r - \psi_{mq}^r) \quad (4.41)$$

$$i_{ds}^r = -\frac{1}{X_{ls}}(\psi_{ds}^r - \psi_{md}^r). \quad (4.42)$$

All introduced states denoted with superscript r are dq-transformed variables referring to rotor frequency ω_r .

4.3.2 Torque equations

Changes of the rotor frequency are caused by an unbalance of electrical and mechanical torque. The electrical torque is

$$M_e = (i_{qs}^r \psi_{ds}^r - i_{ds}^r \psi_{qs}^r) \quad (4.43)$$

and the mechanical torque M_m is generated by the turbine. Let

$$\dot{\omega}_r = -\frac{\omega_b}{2H} \left((i_{qs}^r \psi_{ds}^r - i_{ds}^r \psi_{qs}^r) - M_m \right), \quad (4.44)$$

where H is the inertia constant created by the mass of the powering turbine and the generator. The turbine torque M_m is assumed to be constant during the analysis.

4.3.3 Reference Frame Theory

Regarding a multi-generator network, multiple reference frames applying the park-transformation are introduced. Each generator is transformed with w_r , the rotor frequency of the corresponding generator. Hence, each generator has terminal currents i_{dq}^r and voltages u_{dq}^r only valid in the corresponding reference frame. However, the variables rotating with ω_r can be transformed to the stationary reference frame rotating with angular grid frequency w_b . Consequently, the stationary reference frame is transformed with $\Theta = \omega_b t$ and a generator reference frame is transformed with $\Theta_r = \omega_r t$, where $\theta = \omega_b t - \omega_r t$ is the rotor angle of a corresponding synchronous generator. States in the stationary reference frame are denote with superscript n . The angular position of the stationary reference frame is defined with $\theta_b = 0$.

$$\begin{pmatrix} i_d^n \\ i_q^n \end{pmatrix} = K^{-1} \begin{pmatrix} i_d^r \\ i_q^r \end{pmatrix} = \begin{pmatrix} \cos \theta & -\sin \theta \\ \sin \theta & \cos \theta \end{pmatrix} \begin{pmatrix} i_d^r \\ i_q^r \end{pmatrix} \quad (4.45)$$

$$\begin{pmatrix} u_d^r \\ u_q^r \end{pmatrix} = K \begin{pmatrix} u_d^n \\ u_q^n \end{pmatrix} = \begin{pmatrix} \cos \theta & \sin \theta \\ -\sin \theta & \cos \theta \end{pmatrix} \begin{pmatrix} u_d^n \\ u_q^n \end{pmatrix} \quad (4.46)$$

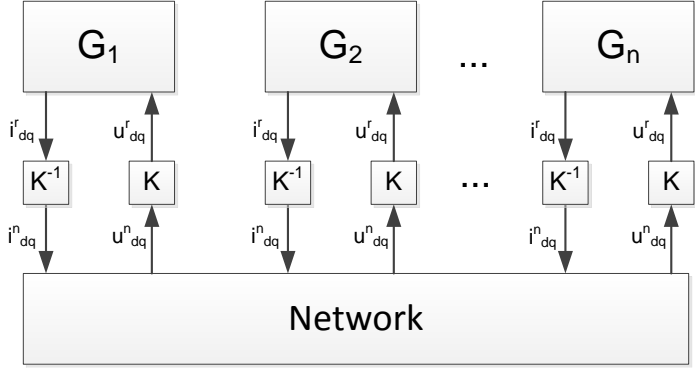


Figure 4.3: dq reference frames for a multi generator network

In order to create a consistent equation set, the generator inputs u_{dq}^r are replaced with (4.46) and the output equation (4.41 - 4.42) is transformed with (4.45). Consequently, the nonlinear generator model is dependent on θ .

4.3.4 Linearized Model

In order to apply the derived nonlinear model to small signal analysis, (4.31 - 4.36), (4.44), (4.45) needs to be linearized. Regarding the linearization of a state space model refer to Appendix A.1. The nonlinear state space model depends on ω_r , θ and the flux per seconds. The state variables are

$$x_{Gen} = \left(\psi_q^r \quad \psi_d^r \quad \psi_{kq1} \quad \psi_{kq2} \quad \psi_{fd} \quad \psi_{kd} \quad \omega_r \quad \theta \right)^T. \quad (4.47)$$

Initial values for ψ_{dq} and θ are attained with load flow calculation. Moreover, $\psi_{kq1} = 0$, $\psi_{kq2} = 0$, $\psi_{kd} = 0$, $\omega_r = \omega_b$ leads to a linearized model around the operating point x_{G0} . Applying (4.45) and (4.46), the stator current i_{dq}^n and voltage u_{dq}^r become

$$\Delta i_{dq}^n = \begin{pmatrix} \cos \theta \Delta i_d^r - \sin \theta \Delta i_q^r - \underbrace{(\sin \theta i_d^r + \cos \theta i_q^r)}_{i_q^n} \theta \\ \sin \theta \Delta i_d^r + \cos \theta \Delta i_q^r + \underbrace{(\cos \theta i_d^r - \sin \theta i_q^r)}_{i_d^n} \theta \end{pmatrix} \quad (4.48)$$

$$\Delta u_{dq}^r = \begin{pmatrix} \cos \theta \Delta u_d^n - \sin \theta \Delta u_q^n + \underbrace{(-\sin \theta u_d^n + \cos \theta u_q^n)}_{u_q^r} \theta \\ -\sin \theta \Delta u_d^n + \cos \theta \Delta u_q^n - \underbrace{(\cos \theta u_d^n + \sin \theta u_q^n)}_{u_d^r} \theta \end{pmatrix}. \quad (4.49)$$

The linear generator model is defined with the state equation

$$\begin{aligned} \Delta \dot{x}_{Gen} &= A_{Gen} \Delta x_{Gen} + B_{Gen1} \Delta u_{dq}^n + B_{Gen2} \Delta u_{fd} \\ \Delta \dot{x}_{Gen} &= \begin{pmatrix} A_{Gen1} & A_{Gen2} \end{pmatrix} \Delta x_{Gen} + B_{Gen1} \Delta u_{dq}^n + B_{Gen2} \Delta u_{fd} \end{aligned} \quad (4.50)$$

and the output equation

$$\begin{aligned} \Delta i_{dq}^n &= C_{Gen} \Delta x_{Gen} \\ \Delta i_{dq}^n &= \begin{pmatrix} C_{Gen1} & C_{Gen2} \end{pmatrix} \Delta x_{Gen}, \end{aligned} \quad (4.51)$$

with the matrices

$$B_{Gen1} = \begin{pmatrix} -\omega_b \sin \theta & \omega_b \cos \theta \\ \omega_b \cos \theta & \omega_b \sin \theta \\ 0 & 0 \\ 0 & 0 \\ 0 & 0 \\ 0 & 0 \end{pmatrix} \quad (4.52)$$

$$B_{Gen2} = \left(0 \quad 0 \quad 0 \quad \frac{r'_{fd}}{X_{md}} \quad \omega_b \quad 0 \quad 0 \quad 0 \right)^T \quad (4.53)$$

$$C_{Gen1} = \begin{pmatrix} \left[\frac{\sin \theta}{X_{ls}} \left(1 - \frac{X_{aq}}{X_{ls}} \right) \right] & \left[\frac{-\cos \theta}{X_{ls}} \left(1 - \frac{X_{ad}}{X_{ls}} \right) \right] & \frac{-\sin \theta X_{aq}}{X_{ls} X'_{lkq1}} \\ \left[\frac{-\cos \theta}{X_{ls}} \left(1 - \frac{X_{aq}}{X_{ls}} \right) \right] & \left[\frac{-\sin \theta}{X_{ls}} \left(1 - \frac{X_{ad}}{X_{ls}} \right) \right] & \frac{\cos \theta X_{aq}}{X_{ls} X'_{lkq1}} \end{pmatrix} \quad (4.54)$$

$$C_{Gen2} = \begin{pmatrix} \frac{-\sin \theta X_{aq}}{X_{ls} X'_{lkq2}} & \frac{\cos \theta X_{ad}}{X_{ls} X'_{lfd}} & \frac{\cos \theta X_{ad}}{X_{ls} X'_{lkd}} & 0 & -i_{q0}^n \\ \frac{\cos \theta X_{aq}}{X_{ls} X'_{lkq2}} & \frac{\sin \theta X_{ad}}{X_{ls} X'_{lfd}} & \frac{\sin \theta X_{ad}}{X_{ls} X'_{lkd}} & 0 & i_{d0}^n \end{pmatrix} \quad (4.55)$$

$$A_{Gen1} = \begin{pmatrix} \frac{\omega_b r_s}{X_{ls}} \left(\frac{X_{\alpha q}}{X_{ls}} - 1 \right) & -\omega_r 0 & \frac{\omega_b r_s X_{\alpha q}}{X_{ls} X_{lkq1}} & \frac{\omega_b r_s X_{\alpha q}}{X_{ls} X_{lkq2}} \\ \omega_r 0 & \frac{\omega_b r_s}{X_{ls}} \left(\frac{X_{\alpha d}}{X_{ls}} - 1 \right) & 0 & 0 \\ \frac{\omega_b r'_{kq1} X_{\alpha q}}{X_{lkq1} X_{ls}} & 0 & \frac{\omega_b r'_{kq1}}{X_{lkq1}} \left(\frac{X_{\alpha q}}{X_{lkq1}} - 1 \right) & \frac{\omega_b r_{kq1} X_{\alpha q}}{X_{\alpha q} X_{lkq2}} \\ \frac{\omega_b r'_{kq2} X_{\alpha q}}{X_{lkq2} X_{ls}} & 0 & \frac{\omega_b r'_{kq2} X_{kq2}}{X_{ls} X'_{lkq1}} & \frac{\omega_b r'_{kq2}}{X_{lkq2}} \left(\frac{X_{\alpha q}}{X_{lkq2}} - 1 \right) \\ 0 & \frac{\omega_b r'_{fd} X_{\alpha d}}{X_{lfd} X_{ls}} & 0 & 0 \\ 0 & \frac{\omega_b r'_{kd} X_{\alpha d}}{X'_{lkd} X_{ls}} & 0 & 0 \\ \frac{\omega_b}{2H} \left[\frac{\psi'_{d0}}{X_{ls}} (1 - \frac{X_{\alpha q}}{X_{ls}}) + i_{d0} \right] & -\frac{\omega_b}{2H} \left[i'_{q0} + \frac{\psi'_{q0}}{X_{ls}} (1 - \frac{X_{\alpha d}}{X_{ls}}) \right] & -\frac{\omega_b}{2H} \frac{\psi'_{q0} X_{\alpha q}}{X_{ls} X_{lkq1}} & -\frac{\omega_b}{2H} \frac{\psi'_{d0} X_{\alpha q}}{X_{ls} X_{lkq2}} \\ 0 & 0 & 0 & 0 \end{pmatrix} \quad (4.56)$$

$$A_{Gen2} = \begin{pmatrix} 0 & 0 & -\psi'_{d0} & -\omega_b \cdot u'_{d0} \\ \frac{\omega_b r_s X_{\alpha d}}{X_{ls} X'_{lfd}} & \frac{\omega_b r_s X_{\alpha d}}{X_{ls} X_{lkd}} & \psi'_{q0} & \omega_b \cdot u'_{q0} \\ 0 & 0 & 0 & 0 \\ \frac{\omega_b r'_{fd}}{X_{lfd}} \left(\frac{X_{\alpha d}}{X_{lfd}} - 1 \right) & \frac{\omega_b r'_{fd} X_{\alpha d}}{X_{lfd} X_{lkd}} & 0 & 0 \\ \frac{\omega_b r'_{kq} X_{\alpha d}}{X_{lkq} X_{lfd}} & \frac{\omega_b r'_{kq} X_{\alpha d}}{X_{lkd} X_{lkd}} & 0 & 0 \\ \frac{\omega_b}{2H} \frac{\psi'_{q0} X_{\alpha d}}{X_{ls} X'_{lfd}} & \frac{\omega_b}{2H} \frac{\psi'_{q0} X_{\alpha d}}{X_{ls} X_{lkd}} & 0 & -\frac{\omega_b}{2H} (\psi'_{d0} i'_{d0} + \psi'_{q0} i'_{q0}) \\ 0 & 0 & 1 & 0 \end{pmatrix} \quad (4.57)$$

4.4 External Loads and Static Var Compensator

4.4.1 External Loads

The simplest case of a load model is a series RL-impedance, where R and L are calculated with

$$R_L = \frac{(|U_L| \cos \varphi_s)^2}{P_L}$$

$$L_L = \frac{(|U_L| \sin \varphi_s)^2}{\omega Q_L}$$

where $\varphi_s = \tan^{-1} \left(\frac{Q_L}{P_L} \right)$ and $|U_L| = (u_d^2 + u_q^2)^{\frac{1}{2}}$.

After dq-transformation the load model has the structure

$$u_{dq} = - \begin{bmatrix} L_L & 0 \\ 0 & L_L \end{bmatrix} \dot{i}_{dq} - \begin{bmatrix} R_L & -\omega L_L \\ \omega L_L & R_L \end{bmatrix} i_{dq}. \quad (4.58)$$

The load model neglects frequency dependencies, but is voltage dependent. For non-static load behavior more complex load models need to be considered.

4.4.2 Static Var Compensator

Based upon the load model the equations for a static var compensator (SVC) can be formulated. Dynamic models of a static var compensator (SVC) have been developed from [26], [37]. Based on [26] a TCR-type SVC can be formulated and integrated into an overall model including network dynamics. The dynamic equations in dq-components of a TCR-type SVC are deployed with the aid of branches shown in Fig. 4.4.

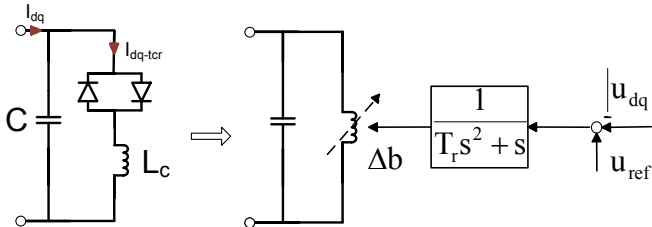


Figure 4.4: Dynamic model of a TCR-type static var compensator

Branch of inductance

With $b = \frac{1}{L_c}$

$$bu_{dq} = \dot{i}_{dq-tcr} + \omega D i_{dq-tcr} \quad (4.59)$$

u_{dq} and b are dependent upon the firing angle, where D is defined according to (4.22). Assuming small changes of the firing angle (4.59) can be linearized for stability analysis to

$$b_0 \Delta u_{dq} + u_{dq0} \Delta b = \Delta \dot{i}_{dq-tcr} + \omega D \Delta i_{dq-tcr}. \quad (4.60)$$

u_{dq} is substituted with (4.28)

$$b_0 (R_{Fs} \Delta i_{dq} + L_{Fs} \Delta \dot{i}_{dq} + C_{Fs} \Delta \zeta_{dq}) + u_{dq0} \Delta b = \Delta \dot{i}_{dq-tcr} + \omega D \Delta i_{dq-tcr}, \quad (4.61)$$

where the subscribed F_s denotes SVC feed-in nodes.

Branch of capacitor

Let

$$\Delta i_{dq} - \Delta i_{dq-tcr} = C (\Delta \dot{u}_{dq} + \omega D \Delta u_{dq}). \quad (4.62)$$

Δu_{dq} is substituted with the network model (4.28) which leads to

$$\begin{aligned} \Delta i_{dq} - \Delta i_{dq-tcr} = C & ((R_{Fs} \Delta i_{dq} + L_{Fs} \Delta \dot{i}_{dq} + C_{Fs} \Delta \zeta_{dq}) \dot{} \\ & + \omega D (R_{Fs} \Delta i_{dq} + L_{Fs} \Delta \dot{i}_{dq} + C_{Fs} \Delta \zeta_{dq})). \end{aligned} \quad (4.63)$$

As additional virtual state variable

$$\Delta \dot{i}_{dq} = \Delta x_{vi} \quad (4.64)$$

is introduced. This leads to the final equation of the capacitor branch

$$\begin{aligned} \Delta i_{dq} - \Delta i_{dq-tcr} = C & ((R_{Fs} \Delta i_{dq} + L_{Fs} \Delta x_{vi} + C_{Fs} \Delta \zeta_{dq}) \dot{} \\ & + \omega D (R_{Fs} \Delta i_{dq} + L_{Fs} \Delta \dot{i}_{dq} + C_{Fs} \Delta \zeta_{dq})). \end{aligned} \quad (4.65)$$

Control system

The control system adapts the firing angle according to the voltage deviation $|u_{dq}|$. Considering an integral behavior of the controller and a *PT1* behavior with the time constant T_r of the TCR, the control system and TCR can be approximated with

$$\begin{aligned} b &= \frac{1}{T_r s^2 + s} (u_{ref} - |u_{dq}|) \\ &= G_T(s) (u_{ref} - |u_{dq}|). \end{aligned} \quad (4.66)$$

$G_T(s)$ is transformed into the time domain with the state variables $\begin{bmatrix} b & x_c \end{bmatrix}^T$.

Linearizing $|u_{dq}|$ leads to

$$\begin{aligned} K_{rms} \Delta u_{dq} &= \begin{bmatrix} \frac{\partial |u_{dq}|}{\partial u_d} & \frac{\partial |u_{dq}|}{\partial u_q} \end{bmatrix} \Delta u_{dq} \\ &= \begin{bmatrix} \frac{u_{d0}}{\sqrt{u_{d0}^2 + u_{q0}^2}} & \frac{u_{q0}}{\sqrt{u_{d0}^2 + u_{q0}^2}} \end{bmatrix} \Delta u_{dq} \end{aligned} \quad (4.67)$$

Δu_{dq} is substituted with (4.28) in Laplace space.

$$\Delta b = G_T(s) (\Delta u_{ref} - K_{rms} (R_{Fs} \Delta i_{dq} + s L_{Fs} \Delta i_{dq} + C_{Fs} \Delta \zeta_{dq})) \quad (4.68)$$

Transforming (4.68) into the time domain leads to

$$K_{rms} L_{Fs} \Delta \dot{i}_{dq} + T_r \Delta \dot{x}_c + K_{rms} R_{Fs} \Delta i_{dq} + E \Delta x_c + K_{rms} C_{Fs} \Delta \zeta_{dq} = \Delta u_{ref} \quad (4.69)$$

$$\Delta \dot{b} = \Delta x_c. \quad (4.70)$$

(4.61), (4.64), (4.65) and (4.68) can be compiled into

$$M_{svc} \begin{bmatrix} \Delta x_{svc} \\ \Delta \zeta_{dq} \end{bmatrix} \dot{\bullet} + A_{svc} \begin{bmatrix} \Delta x_{svc} \\ \Delta \zeta_{dq} \end{bmatrix} = \Delta u_{svc} \quad (4.71)$$

with

$$\Delta x_{svc} = \begin{bmatrix} \Delta i_{dq} & \Delta i_{dq-tcr} & \Delta x_{vi} & \Delta b & \Delta x_c \end{bmatrix}^T, \quad (4.72)$$

$$\Delta u_{svc} = \begin{bmatrix} 0 & 0 & 0 & \Delta u_{ref} & 0 \end{bmatrix}^T, \quad (4.73)$$

and

$$M_{svc} = \begin{bmatrix} M_{s1} & M_{s2} \end{bmatrix}, \quad A_{svc} = \begin{bmatrix} A_{s1} & A_{s2} \end{bmatrix}, \quad (4.74)$$

where M_{s1} denotes the influence from x_{svc} and M_{s2} denotes the influence from ζ_{dq} . The model neglects any control dynamics resulting from the phase locked loop.

$$M_{s1} = \begin{bmatrix} CR_{Fs} + CWDL_{Fs} & 0 & CL_{Fs} & 0 & 0 \\ -b_0L_{Fs} & E & 0 & 0 & 0 \\ -E & 0 & 0 & 0 & 0 \\ K_{rms}L_{Fs} & 0 & 0 & 0 & T_r \\ 0 & 0 & 0 & E & 0 \end{bmatrix} \quad (4.75)$$

$$M_{s2} = \begin{bmatrix} CC_{Fs} & 0 & 0 & 0 & 0 \end{bmatrix}^T \quad (4.76)$$

$$A_{s1} = \begin{bmatrix} CWDR_{Fs} - E & E & 0 & 0 & 0 \\ -b_0R_{Fs} & wD & 0 & u_{dq0} & 0 \\ 0 & 0 & E & 0 & 0 \\ K_{rms}R_{Fs} & 0 & 0 & 0 & E \\ 0 & 0 & 0 & 0 & -E \end{bmatrix} \quad (4.77)$$

$$A_{s2} = \begin{bmatrix} CWDC_{Fs} & -b_0C_{Fs} & 0 & K_{rms}C_{Fs} & 0 \end{bmatrix}^T \quad (4.78)$$

4.5 Overall model including dynamic network and generators

An overall model consisting of dynamic network and generators can be formulated with the deployed network model (4.30), where u_{Fg} are generator feed-in voltages, i_{Fg} generator feed-in currents and ζ_{dq} virtual state variables.

$$\Delta u_{Fg} = L_{Fg} \Delta \dot{i}_{Fg} + R_{Fg} \Delta i_{Fg} + C_{Fg} \Delta \zeta_{dq} \quad (4.79)$$

$$0 = -E \Delta \dot{\zeta}_{dq} + B_{Fg} \Delta i_{Fg} + A_N \Delta \zeta_{dq} \quad (4.80)$$

and generator model

$$\Delta \dot{x}_{Gen} = A_{Gen} \Delta x_{Gen} + B_{Gen1} \Delta u_{dq}^n + B_{Gen2} \Delta u_{fd} \quad (4.81)$$

with the output equation

$$\Delta \dot{i}_{dq}^n = C_{Gen} \Delta x_{Gen}. \quad (4.82)$$

A multi-generator model is hence

$$\begin{aligned} \Delta \dot{x}_G &= A_G \Delta x_G + B_{G1} \Delta u_{dq}^n + B_{G2} \Delta u_{fd} \\ \Delta \dot{i}_{dq}^n &= C_G \Delta x_G \end{aligned} \quad (4.83)$$

with

$$\begin{aligned} A_G &= \begin{bmatrix} A_{Gen1} & & 0 \\ & \ddots & \\ 0 & & A_{Gen n} \end{bmatrix} & B_{G1} &= \begin{bmatrix} B_{Gen11} & & 0 \\ & \ddots & \\ 0 & & B_{Gen1 n} \end{bmatrix} \\ B_{G2} &= \begin{bmatrix} B_{Gen21} & & 0 \\ & \ddots & \\ 0 & & B_{Gen2 n} \end{bmatrix} & C_G &= \begin{bmatrix} C_{Gen1} & & 0 \\ & \ddots & \\ 0 & & C_{Gen n} \end{bmatrix} \\ \Delta x_G &= [\Delta x_{Gen1} \quad \dots \quad \Delta x_{Gen n}]^T. \end{aligned} \quad (4.84)$$

Δu_{dq}^n is replaced with (4.79) in (4.83) since generator feed-in voltages are equal to the terminal voltages $\Delta u_{dq}^n = \Delta u_{Fg}$.

$$\begin{aligned} \Delta \dot{x}_G - A_G \Delta x_G - B_{G1} (L_{Fg} C_G \Delta \dot{x}_G + R_{Fg} C_G \Delta x_G + C_{Fg} \Delta \zeta_{dq}) &= B_{G2} \Delta u_{fd} \\ \underbrace{(E - B_{G1} L_{Fg} C_G)}_{M_{11}} \Delta \dot{x}_G - \underbrace{(A_G + B_{G1} R_{Fg} C_G)}_{A_{11}} \Delta x_G - B_{G1} C_{Fg} \Delta \zeta_{dq} &= B_{G2} \Delta u_{fd} \end{aligned} \quad (4.85)$$

Leading to the overall model

$$\begin{bmatrix} B_{G2} \\ 0 \end{bmatrix} \Delta u_{fd} = \begin{bmatrix} M_{11} & 0 \\ 0 & -E \end{bmatrix} \begin{bmatrix} \Delta x_G \\ \Delta \zeta_{dq} \end{bmatrix} + \begin{bmatrix} A_{11} & -B_{G1} C_{Fg} \\ B_{Fg} C_G & A_N \end{bmatrix} \begin{bmatrix} \Delta x_G \\ \Delta \zeta_{dq} \end{bmatrix}. \quad (4.86)$$

4.6 Interaction of Grid, Generators and SVCs

To describe the overall system behavior the systems of network (4.28), (4.25), generator (4.50) and SVC (4.71) can be formulated into an overall system (4.87).

Analogous to (4.86) the overall system including dynamic network, generators and SVCs is formulated as

$$\Delta u_{sys} = M_{sys} \dot{\Delta x}_{sys} + A_{sys} \Delta x_{sys} \quad (4.87)$$

$$M_{sys} = \begin{bmatrix} M_{11} & 0 & 0 \\ 0 & M_{s1} & M_{s2} \\ 0 & 0 & -E \end{bmatrix} \quad (4.88)$$

$$A_{sys} = \begin{bmatrix} -A_{11} & 0 & -B_{G1}C_{Fg} \\ 0 & A_{s1} & A_{s2} \\ B_{Fg}C_G & B_{Fs} & A_N \end{bmatrix}$$

$$\Delta u_{sys} = \begin{pmatrix} 0 \\ B_{G2} \Delta u_{fd} \\ 0 \\ \Delta u_{svc} \\ 0 \end{pmatrix} \Delta x_{sys} = \begin{pmatrix} \Delta x_G \\ \Delta x_{svc} \\ \Delta \zeta_{dq} \end{pmatrix} \quad (4.89)$$

4.6.1 Applications small signal stability

Small signal stability analysis is an effective way to evaluate the influence of regulators and electric equipment. Consequently, commissioning regulators as deployed generator controllers, control systems for HVDC and FACTS will in general be done using small signal stability analysis. Transient simulations use detailed models of all involved network components. Simulation results give information on the time evolution of the nonlinear dynamic system. If the influence from several parameter sets is from interest, simulation time can get excessive. Small signal stability gives information about the dynamic behavior and is only valid around an operation point. The dynamic influence of parameter sets is analyzed effectively with small signal stability. Moreover, the behavior of several power system devices and countermeasures against phenomena like torsional oscillations, controller interactions, harmonic interactions are formulated applying a small signal model. This leads to the design of the presented controllers in Chapter 6 and estimators in Chapter 5. Moreover, the developed model is used for the validation of a planned generator schedule as introduced in Chapter 1.

4.7 Eigenvalue comparison

To evaluate the deployed models, eigenvalues found in literature are compared to the eigenvalues presented in this thesis. Since the error created by linearization and a possible error of the deployed model is difficult to distinguish time-domain comparisons are be inconclusive if nonlinear simulation results are compared against time-domain simulations of the linearized model.

The generator model (4.50) is compared to the eigenvalues presented in [46] for the machine with the parameters as shown in Table 4.1.

Table 4.1: Steam Turbine Generator

Rating: 835 MVA	
Line-to-line voltage: 26 kV	
Power factor: 0.85	
Poles: 2	
Speed: 3600 r/min	
Combined inertia of generator and turbine:	
$j = 0.0658 \cdot 10^6 \text{ J s}^2$	
$r_s = 0.003 \text{ pu}$	
$X_{ls} = 0.19 \text{ pu}$	
$X_q = 1.8 \text{ pu}$	$X_d = 1.8 \text{ pu}$
$r_{kq1} = 0.00178 \text{ pu}$	$r_{fd} = 0.000929 \text{ pu}$
$X_{kq1} = 0.8125 \text{ pu}$	$X_{lfd} = 0.1414 \text{ pu}$
$r_{kq2} = 0.00841 \text{ pu}$	$r_{kd} = 0.01334 \text{ pu}$
$X_{kq2} = 0.939 \text{ pu}$	$X_{lkd} = 0.08125 \text{ pu}$

Table 4.2: Eigenvalues of Steam Turbine Generator

Ref. [46]	Eigenvalues of (4.50)
-4.45 ± j377	-4.45 ± j376.89
-1.70 ± j10.5	-1.588 ± j10.64
-32.2	-32.04
-11.1	-11.42
-0.349	-0.351
-0.855	-0.83

As shown in Table 4.2 the eigenvalues of [46] are very close to the eigenvalues presented of (4.50). This confirms the correctness of the generator model used for the dynamic security assessment.

4.7.1 Evaluation of the dynamic network model

4.7.1.1 A two Area benchmark network

A widely-used benchmark model is the 2 area - 4 generator network developed by [49]. Both areas are connected by a weak tie line. The network data can be found in Appendix C.4.

Table 4.3 presents the dominant eigenvalues, with excitation regulators on manual control. Only slow evolving dynamics, which have a significant influence on the overall behavior are depicted. The eigenvalues presented in this thesis are based on the dynamic model (4.86), and are compared to the eigenvalues calculated using the MASS [49] software package. Furthermore, [69] published the eigenvalues calculated with PSS/E [9] and Simpow [36].

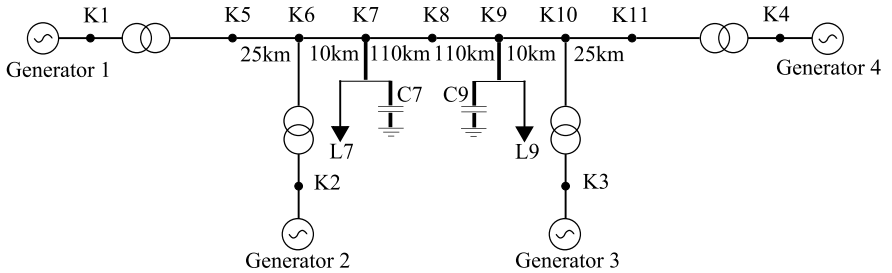


Figure 4.5: 2 area - 4 generator benchmark model developed by [49]

All software packages MASS [49], PSS/E [9], Simpow [36] used for the comparison rely on static network models. Furthermore, only six-order generator models are applied. The software packages assume static stator equations, with is

$$0 = \omega_b \left(u_{qs}^r - \frac{\omega_r}{\omega_b} \psi_{ds}^r + \frac{r_s}{X_{ls}} (\psi_{mq}^r - \psi_{qs}^r) \right) \quad (4.90)$$

$$0 = \omega_b \left(u_{ds}^r + \frac{\omega_r}{\omega_b} \psi_{qs}^r + \frac{r_s}{X_{ls}} (\psi_{md}^r - \psi_{ds}^r) \right). \quad (4.91)$$

PSS/E, Simpow and the presented model (4.86) have mechanical power as input variable, whereas [49] uses electrical power. Inter-area modes occur at a low frequency range from 0.01 – 1 Hz, hence the static grid models provided are able to describe those modes correctly. This has also been reported in [35] and [42]. The eigenvalues calculated with the model developed in this thesis show a very good match to those presented in [49]. The inter-area modes are in close proximity, as well as the eigenvalues associated with the amortisseur flux linkages.

Table 4.3: Eigenvalue comparison of a 2 area network

PSS/E	Simpow	MASS [49] p. 815	EVs of (4.86)	Dominant States
0.32	0	-0.001 ± j0.002	-0.025 ± j5.79	
-0.106	0	-0.096	-0.136	
-0.151 ± j3.41	-0.152 ± j3.42	-0.111 ± j3.43	-0.122 ± j4.09	
-0.606 ± j6.74	-0.661 ± j6.64	-0.492 ± j6.82	-0.458 ± j8.62	
-0.619 ± j6.94	-0.678 ± j6.84	-0.506 ± j7.02	-0.472 ± j8.08	
-0.217	-0.1 ± j0.069	-0.117	-0.235	
-0.225	-0.191	-0.265	-0.265	
-0.25 ± j0.21	-0.210	-0.276	-0.291	
-2.93	-3.6	-3.428	-2.299	
-3.85	-5.1	-4.139	-3.202	
-5.19	-8.04	-5.287	-4.788	
-5.21	-8.11	-5.303	-4.856	
-28.43	-34.12	-31.03	-10.24 ± 376.79	} ψ_{dq}
-29.92	-35.01	-32.45	-10.81 ± j376.79	
-33.32	-36.02	-34.07	-13.55 ± j16974	} ζ
-34.71	-37.48	-35.01	-13.47 ± j17728	
-35.67	-37.48	-36.02	-13.25 ± j17753	
			-17.29 ± j28984	
			-17.25 ± j29006	
			-17.28 ± j29738	} ζ
			-17.23 ± j29760	
			-21.33	
			-21.47	} ψ_{kd}
			-22.54	
			-22.56	} ζ
			-25.04 ± j7781	
			-25.04 ± j7027	} ψ_{dq}
			-28.50	
			-29.50 ± j376.82	
			-30.10	
			-35.94	
			-36.09	

As deduced in [49] the formulation used by MASS [49] and Simpov [36] use absolute changes in machine rotor speed and angle as state variables, which create two zero eigenvalues. One of the zero eigenvalues is caused by the lack of uniqueness of the absolute rotor angle used. The rotor angle is described only in dependence of internal generator variables, assuming a constant network frequency. However, since the network is not connected to an infinite bus, the correct rotor angle is calculated with

$$\Delta\dot{\theta}_i = \omega_i - \bar{\omega} \quad (4.92)$$

$$= \omega_i - \frac{1}{H_{sum}} \sum_{j=1}^n H_j \omega_j, \quad (4.93)$$

where $\bar{\omega}$ is the average system frequency, H_j is the inertia constant of generator j and $H_{sum} = \sum H_j$.

The second zero eigenvalue can be eliminated, if a speed governor is included or the speed deviations are measured with respect to a reference machine. [69] suggests that also the first and second entry of the eigenvalues calculated by PSS/E are caused by the phenomena mentioned above. This is also validated by time-domain simulations. Both cases are addressed in the presented model (4.86). Consequently, the results of the reviewed commercial programs need to be interpreted with care, if no excitation regulator or speed governor is included.

The additional eigenvalues (indicated in red), which do not occur in MASS [49], Simpov [36] or PSS/E [9] can be traced back to the additional states used in (4.86).

The relative participation of state variables and eigenvalues can be deduced with the help of sensitivity analysis.

$$sen(i, j) = V_{sys}(i, j) \cdot W_{sys}(j, i) \quad (4.94)$$

where V_{sys}, W_{sys} are the left- and righthand eigenvectors of the overall system (4.86). (4.94) gives the sensitivity of eigenvalue λ_i . sen is a $n \times n$ matrix, where columns are associated with eigenvalues and rows are associated with state variables. Large values of (4.94) indicate a strong coupling, whereas small values indicate a weak coupling of state variables with the corresponding eigenvalues. Eigenvalues with frequencies of j376 are associated with ψ_{dq} , whereas frequencies higher than j5000 are associated with network dynamics.

4.7.1.2 5 Area benchmark network

The second assessed benchmark network has 14 generator groups, 59 busbars and 5 SVCs. The benchmark network is a contribution to the IEEE Benchmark Systems for Stability Controls Task Force [76]. The network data can be found in Appendix C.5.

It was developed to demonstrate the ability of small-signal analysis and the design of multi-machine controllers. The network has low frequency inter-area modes as well as high frequency local modes. The test-bed includes 6 load cases, in order to evaluate the proposed control method for several load scenarios. Each generator group is a generation equivalent representing a power station of 2 to 12 units. Furthermore, high order excitation models are included.

The assessed benchmark grid has long lines and also includes shunt capacitors and reactor banks. Hence, the eigenvalues from (4.25) and (4.26) are close to the imaginary axis.

The quoted load cases 1 and 6, represent a high load and a moderate load scenario. The eigenvalues and transient behavior are compared and discussed. As depicted in Table 4.4 load case 6 has only 65 % of the energy demand compared to load case 1. Consequently, the number of generator units online, is significantly lower, which also affects the total inertia of the network.

Table 4.5 shows the eigenvalues of both load cases including the dominant state participation. Load case 1 and load case 6 represent unstable systems, without dampening controllers. Furthermore, load case 6 has greater negative dampening. Similar, to the 2 area network presented in Chapter 4.7.1.1, low frequency oscillations are influenced by the states ω and the flux per second ψ in the majority of modes. However, since the 5 area benchmark network is equipped with reactor banks, which create additional modes very close to the imaginary axis. Those modes have dominant state participation from network states ζ and no significant participation from generators. The modes are significant for the system behavior and do not occur with static grid models. Apart from modes created by reactor banks, dominant state participation of network states occur from eigenvalues smaller than -3.3 .

Table 4.4: Overview of two load cases provided by [20]

Load Case 1	Load Case 6	
22.3 GW	14.63 GW	Total demand P
5.5 GVar	0.4 GVar	Total demand Q
62	40	Generator units
932 MWs	589 MWs	H_{sum}

Table 4.5: Eigenvalue comparison of a 5 area network calculated with (4.87)

Case 1	Dominant States	Case 6	Dominant States
$0.183 \pm j8.41$	} ω	$0.455 \pm j10.41$	} ω
$0.04 \pm j5.69$		$0.156 \pm j7.13$	
$-0.134 \pm j6.22$	} ζ	$-0.0005 \pm j8.05$	} ζ
$-0.143 \pm j314.16$		$-0.13 \pm j314.16$	
$-0.161 \pm j7.13$	ω	$-0.143 \pm j7.83$	ω
-0.236	ψ	-0.218	ψ
$-0.234 \pm j314.16$	ζ	$-0.221 \pm j314.16$	ζ
-0.247	} ψ	-0.233	} ψ
-0.262		-0.246	
-0.282		-0.279	
-0.321		-0.28	
-0.323		-0.304	
$-0.338 \pm j0.01$		-0.316	
$-0.349 \pm j0.03$		-0.318	
-0.388	} ω	-0.332	} ω
-0.407		-0.338	
$-0.435 \pm j12.59$	} ψ	-0.351	} ω
-0.46		-0.364	
-0.486	} ψ	-0.382	} ψ
-0.549		$-0.493 \pm j13.51$	
-0.681		-0.504	
-0.772	} ω	-0.504	} ψ
$-0.802 \pm j15.15$		-0.586	
-0.831	} ψ	$-0.88 \pm j314.16$	} ζ
-0.83		-0.895	
-0.913	} ζ	$-0.914 \pm j15.71$	} ω
$-0.951 \pm j314.56$		-0.96	
$-3.316 \pm j14569$		$-3.316 \pm j14569$	ζ

Dampening controllers need to show good performance for several operating conditions. The eigenvalues of load case 1 and 6 can be used to specify the robustness requirements of a control system. Fig. 4.7 shows the singular values of both load cases. Computed are the input of generator BPS 2 located in area 2 versus all model outputs. The resonant frequency changed considerable comparing case 1 and case 6 especially in the frequency range of 5 - 10 rad per second.

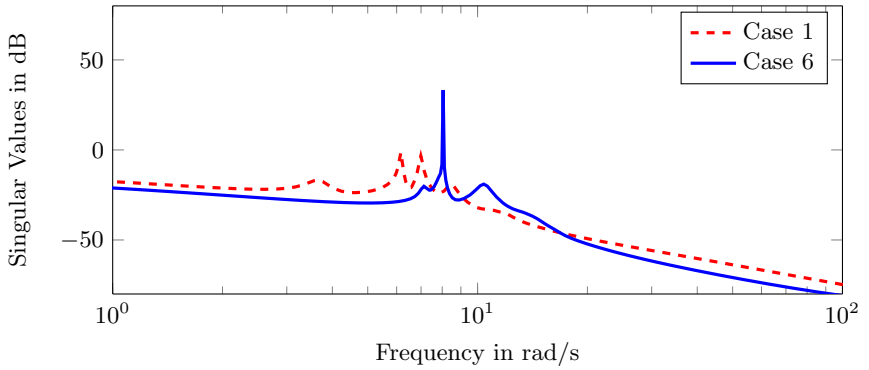


Figure 4.7: Singular values of case 1 and case 6 calculated with (4.87)

Chapter 5

State Estimation

For monitoring purposes state estimators have become an invaluable asset. Phase measurement units (PMUs) have the ability to improve the quality of estimators, since the transfer rate is higher than in traditional measurement systems. Moreover, the estimation problem becomes a linear problem as voltage magnitude and angle are measured. With the exact knowledge of the grid state, voltage stability and low frequency oscillations can be detected and appropriate countermeasures may be initiated. Most of the advanced control schemes assume the knowledge of the state variable x , in case the state variable is not measured it is estimated using an observer structure as proposed in the following section.

5.1 Observer

With the introduction of PMUs it is possible to track dynamic incidents of power systems. PMUs measure voltage and current phasors. Depending on the proposed model structure the measurements are interpreted as inputs or outputs of the model. The observer is able to estimate all states x of the process model developed in Section 4.2, if the observability criterion is fulfilled. The state equations are

$$\dot{x} = A x + B u \quad (5.1)$$

$$y = C x \quad (5.2)$$

with the given measurements y and input variables u . The observer includes a model of the process which makes it possible to predict the estimated state variables \hat{x} with the given input variables. $\hat{y} = C \hat{x}$ allows the estimation of the output variables. \hat{y} is then compared to the process measurements y . The observer gain L will compensate the error $y - \hat{y}$ and \hat{x} will converge to x . One method for an observer synthesis is to solve the Riccati equation

$$A X + X A^T - X^T C^T S^{-1} C X + Q = 0, \quad (5.3)$$

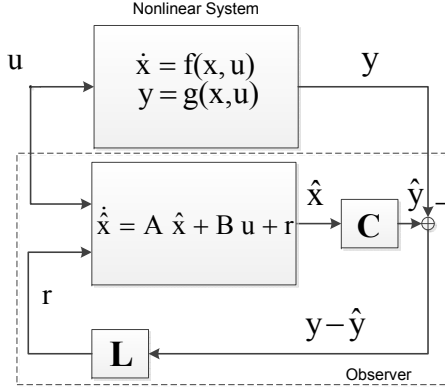


Figure 5.1: Observer structure

for X . X needs to be positive definite, which in this context is defined as $X > 0$. Where Q and S are positive definite weighting matrices minimizing the objective function

$$J = \int_{-\infty}^{\infty} u(t)^T S u(t) + x(t)^T Q x(t) dt. \quad (5.4)$$

Solving the Riccati equation after X leads to the observer gain

$$L = (S^{-1} C X^T)^T. \quad (5.5)$$

The deployed network model as derived in equation (4.29) is

$$\begin{bmatrix} u_F \\ 0 \end{bmatrix} = \underbrace{\begin{bmatrix} L_F & 0 \\ 0 & -E \end{bmatrix}}_{M_F} \begin{bmatrix} i_F \\ \zeta \end{bmatrix} + \underbrace{\begin{bmatrix} R_F & C_F \\ B_F & A_N \end{bmatrix}}_{A_F} \begin{bmatrix} i_F \\ \zeta \end{bmatrix} \quad (5.6)$$

The network model is rearranged into state space form

$$\begin{bmatrix} i_F \\ \zeta \end{bmatrix} \bullet = -M_F^{-1} A_F \begin{bmatrix} i_F \\ \zeta \end{bmatrix} + M_F^{-1} \begin{bmatrix} u_F \\ 0 \end{bmatrix}. \quad (5.7)$$

In the following u_F is defined as input and i_F as measured output, which makes

$$i_F = \begin{bmatrix} E & 0 \end{bmatrix} \begin{bmatrix} i_F \\ \zeta \end{bmatrix}. \quad (5.8)$$

Estimated are the state variables $\left[i_F \quad \zeta \right]^T$. The nodal voltages u_{dq} are calculated with the help from (4.25).

5.2 Results

To prove the capabilities of the observer for monitoring purposes, the two area benchmark network according to Section 4.7.1.1 was chosen. The specific network data can be found in the Appendix. Every feeding node, i.e. nodes 1 to 4, has a phasor measuring unit. In practice the data would be transmitted to a data concentrator, whose data would be available to the observer. Simulation results for the given network and a 3-phase short circuit with a duration of 150 ms at node 8 are depicted in Fig. 5.2. The estimates of the observer are compared with the simulation results created with a commercial power system software package. Fig. 5.2 depicts the magnitude and phase voltage of the estimated nodal voltages. During the short circuit the simulation and the estimates have a discrepancy. This is due to the fact that the estimator has no knowledge about the short circuit. It only has sensory input from PMUs located at great distance to the node where the short circuit occurs. Immediately after the fault is resolved, angle and magnitude of the simulated and estimated voltages are almost identical. Although the ability to estimate the voltage evolution after a fault is imperative to assess voltage stability and inter-area oscillations, the presented results of the estimated voltage magnitude during transient events have not been accomplished before. A procedure to estimate the state variables of synchronous generators has been presented in [83].

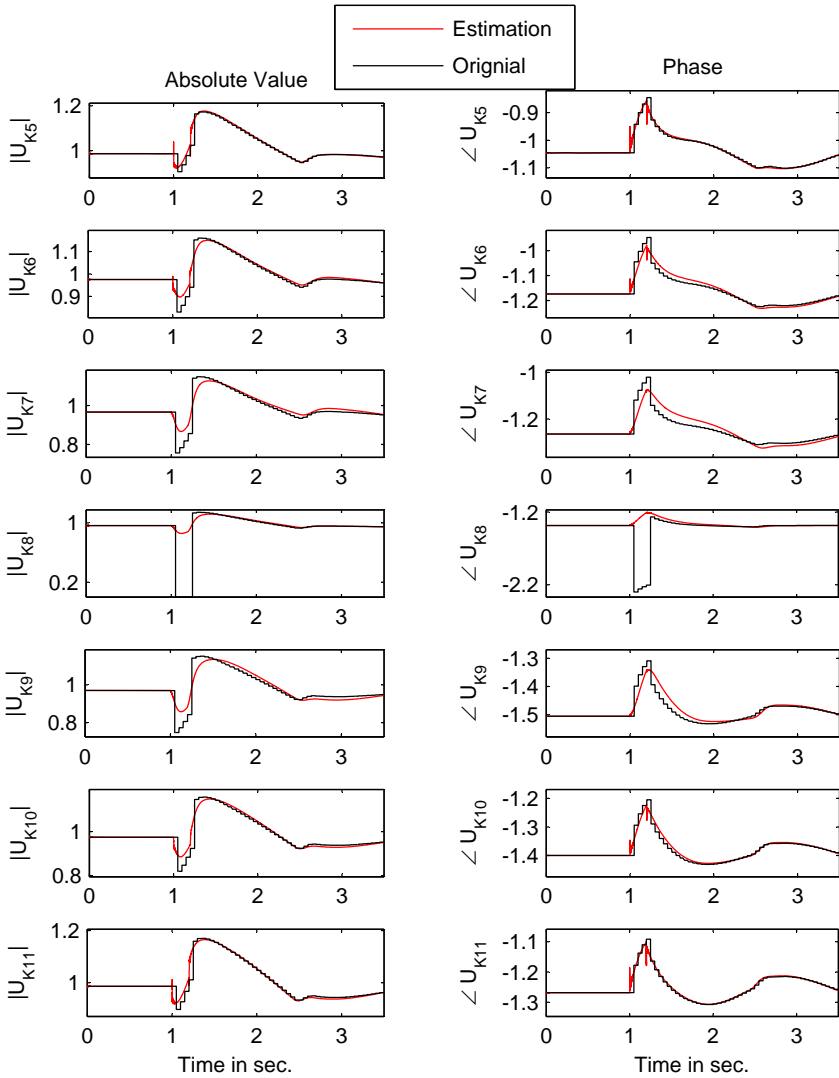


Figure 5.2: Absolute value and phase of nodal voltages of a 2 area network, after 1 sec. a short circuit occurs at node 8

Chapter 6

FC-MPC to improve dynamic stability

6.1 Motivation

This chapter presents an integral control strategy that integrates data from phase measurement units to damp inter-area oscillations. The proposed distributed model predictive control (dMPC) method has one control unit for each controllable device (Generators, FACTS, HVDC) and coordinates their behavior after a fault. Each unit is designed by applying a systematic controller synthesis. The distributed MPC has a significantly improved performance compared to a standard power system stabilizer.

Power system stabilizer (PSS) methods can be divided into damping torque, frequency response and eigenvalue techniques. In [22] the damping torque concept has been developed, whereby the proportionality between electrical damping torque and speed perturbations is applied to damp the system. PSSs based on the damping torque concept tend to perform worse in field tests as compared to results attained by analysis. This can be traced back to the interaction of PSSs and has been observed for local and inter-area modes [21]. Multiple-input and multiple-output (MiMo) models describe interaction system coupling. The resulting MiMo controllers account explicitly for couplings of the system and achieve an optimal control, considering all generators and power converters. Especially complex, coupled systems with several in- and outputs perform significantly better with MiMo control. Model predictive control is an advanced control method and in its classical form is a central MiMo controller. Central controllers are not applicable due to the spatially distributed nature of power systems. However, [65] developed distributed MPC variants, which can be applied in a power system setting [74].

In 2000 Bonneville Power Administration was the first TSO to put a wide area measurement system (WAMS) into service, consisting of phase measurement units (PMUs) and a data concentrator. PMUs measure the absolute value and angle of voltage and currents with very high accuracy and sample time. The measured data is transmitted to the data concentrator, where data packages are synchronized and

made available. WAMS are in application in many states of the USA and Canada. Furthermore, Europe, China and India have WAMS in operation.

The existing electrical power systems in Europe and North America have multiple monitoring systems at transmission level. However, the control systems of power plants rely only on local measurements. The control law is therefore not based on the overall grid state, but only on the measured terminal voltages and frequency deviations. Assuming a wide area measurement system, a controller which relies not only on local measurements, but also on several PMU measurements, becomes feasible.

Control design methods for fast acting controllable devices (Exciters, HVDC, FACTS) need dynamic network equations to describe the behavior satisfactorily if these devices are electrically close to each other. A model including dynamic network equations is developed in Chapter 4.

The distributed MPC presented here is based on this model and inherently considers the interaction between generators, power converters and grid dynamics correctly. Furthermore, dMPC control is based on MPC control, which is a MIMO controller with the described advantages.

Dynamic stability is especially critical in low inertia systems. Examples are island systems and wind farms where the generation is supplied from power converters [79]. Scenarios where only low inertia is available are for instance the island operation of large AC networks after tripping of a crucial component and the black start of a power network. Consequently, advanced control schemes were applied first in island systems. For instance ABB [67] and Hitachi [45] are working on advanced protection and control schemes, that integrate remote signals from WAMS.

The dMPC control strategy described here achieves results very close to the global optimum for the following reasons. Each distributed control unit considers all state variables for the optimization. Every controller has a global objective and considers the couplings of the overall system. The controller relies primarily on local measurements and uses global measurements when available.

6.1.1 Literature Review

[64] and [62] propose a robust approach using linear matrix inequalities based on pole placement and H_∞ , respectively. The controllers are robust against influence from neighboring plants resulting in a decentralized controller. [52] is using mixed H_2/H_∞ synthesis controlling HVDC and FACTS devices. [38] integrates wide area dynamical information into the control system based on a selective modal performance index, damping inter-area modes. [59] develops a PSS based on fuzzy control using remote signals. [61] as well as [12] develop a central control scheme improving

the PSS performance considering signal transmission delays. [18] presents a central MPC coordinating several HVDC devices. [3] gives an overview on published supervisory PSS. [73] formulates dMPC strategies and applies control methods to the automatic generation control problem. [73] shows that the performance benefits obtained from MPC can be realized through dMPC for large scale systems.

This chapter is organized as follows: The implemented control scheme with distributed control units and one data concentrator state estimator is explained. First followed by a description of the MPC strategy developed. The potential of the dMPC controller in comparison to pure PSS dampening is demonstrated with simulation results for 2 and 5 area networks.

6.1.2 Controller Structure

A distributed control method for the nonlinear process of generation units and SVC connected over a network, is introduced as shown in Fig. 6.1. The control method relies primarily on local measurements. This thesis uses standard PSS as presented in [49], [20] as local control method, any decentralized method is applicable.

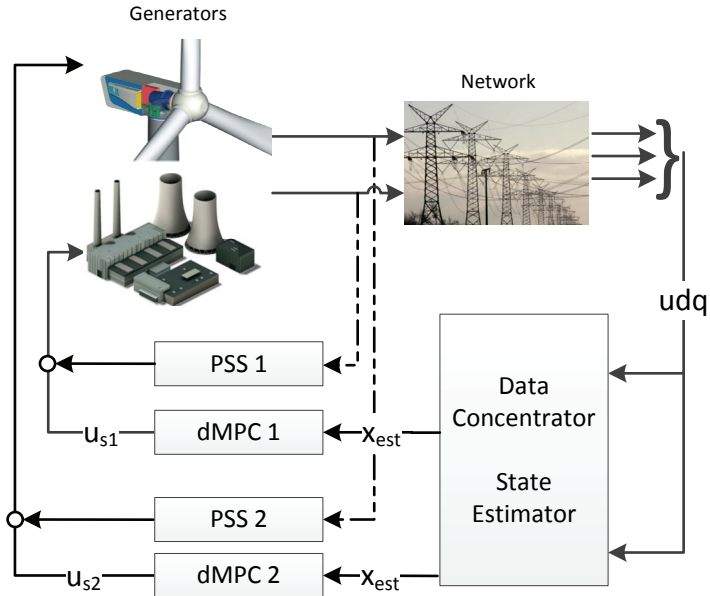


Figure 6.1: Block diagram of a power system represented by 2 generators and network controlled by a multi-machine controller structure

The applied PSS methods use the rotor speed deviation as input and provide a stabilizing signal as output. An implementation without PSS is presented in [82]. The corresponding network has a WAMS available, which measures \underline{U} , \underline{I} , ω at several locations throughout the grid. As indicated in [23], it is advantageous to position the PMUs at the feed-in nodes involved in frequency and/or voltage control. Consequently, every major feed-in node has one PMU available.

The measurements are transferred to the data concentrator, where data synchronization is established. The measurements are used to estimate the network state variables ζ , as introduced in Chapter 5. The state variables of all controllable devices (generators, SVC) can be calculated/estimated directly at the device and need to be transferred to the data concentrator. The number of state variables can be reduced further by using model reduction methods [66]. The synchronized and assembled state variables are transferred to all participating controllable devices as a global signal. The distributed MPC developed provides an additional stabilizing signal, which corrects the PSS output with the help of the global signal. One dMPC controller is implemented for each controllable device and is located, as for the PSS, directly at the device. The dMPC works with sample times up to 1 second.

The control loops of a conventional power plant are depicted in Fig. 6.2 in more detail. The power plant control consists of two main loops, one for the excitation and one for the torque control. Both control loops remain intact in comparison to the conventional implementation. The resulting stabilizing signal u_s attained from PSS and dMPC output is used as a set point update of the excitation control. The absolute value of the voltage and the rotor speed of the generator are measured. The excitation voltage u_{fd} and the torque M_m are inputs to the generator.

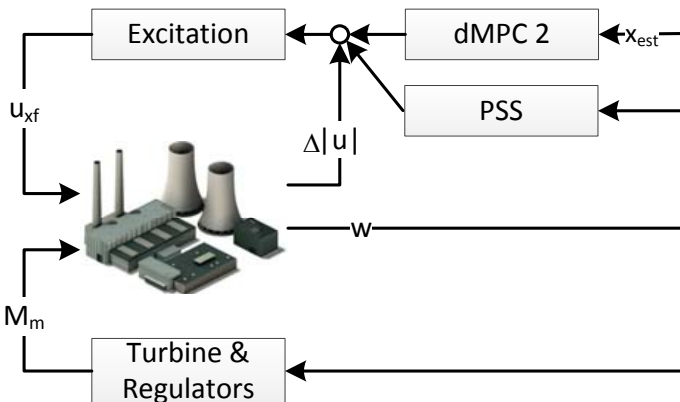


Figure 6.2: Block diagram of a conventional control system including PSS and dMPC

6.2 Modeling Framework

A modeling framework using subsystems is introduced to develop a distributed control method. An overall model is divided into M subsystems. Model partitions are made depending on the given control problem. For the stated circumstances a subsystem is defined for each controllable device. Thus, for each generator, HVDC, SVC subsystems are defined. Furthermore, one subsystem is deployed for the network, which has no controllable inputs. Consequently, the network can only be influenced indirectly by coupled subsystems.

The discrete linear time-invariant model is used for the design of a model predictive controller. Additional information regarding the discretization can be found in Appendix A.2. The developed model (4.87) is transformed into a discrete model with the sample time T_s ,

$$x_{sys}(k+1) = A_{sys} x_{sys}(k) + B_{sys} u_{sys}(k) \quad (6.1)$$

$$y_{sys}(k) = C_{sys} x_{sys}(k) \quad (6.2)$$

where A_{sys} is the discrete system matrix, B_{sys} is the discrete input matrix and C_{sys} the output matrix with

$$A_{sys} = \begin{pmatrix} A_{11} & \cdots & A_{1M} \\ \vdots & \ddots & \vdots \\ A_{M1} & \cdots & A_{MM} \end{pmatrix}, B_{sys} = \begin{pmatrix} B_{11} & \cdots & B_{1M} \\ \vdots & \ddots & \vdots \\ B_{M1} & \cdots & B_{MM} \end{pmatrix} \quad (6.3)$$

$$C_{sys} = \begin{pmatrix} C_{11} & \cdots & C_{1M} \\ \vdots & \ddots & \vdots \\ C_{M1} & \cdots & C_{MM} \end{pmatrix} \quad (6.4)$$

$$\begin{aligned} x(k) &= \begin{pmatrix} x_1(k) & \cdots & x_M(k) \end{pmatrix}^T \\ u(k) &= \begin{pmatrix} u_1(k) & \cdots & u_M(k) \end{pmatrix}^T \\ y(k) &= \begin{pmatrix} y_1(k) & \cdots & y_M(k) \end{pmatrix}^T. \end{aligned} \quad (6.5)$$

k indicates the time variable. The partitioned model for subsystem j describes the influence of the state x_j fully

$$x_j(k+1) = A_{jj}x_j(k) + B_{jj}u_j(k) + \sum_{p=1, p \neq j}^M [A_{jp}x_p(k) + B_{jp}u_p(k)] \quad (6.6)$$

where A_{jj} , B_{jj} is the effect of local subsystem variables and A_{jp} , B_{jp} the effect of interconnected subsystems.

The output equation is defined with

$$y_j(k) = \sum_{p=1}^M C_{jp} x_p(k). \quad (6.7)$$

In comparison traditional PSS are decentralized control methods, relying only on local subsystem variables. Any influence of interconnected subsystems is not considered in the design process. A decentralized model is defined with

$$x_j(k+1) = A_{jj} x_j(k) + B_{jj} u_j(k). \quad (6.8)$$

6.3 Feasible Cooperation MPC

[73] developed a feasible cooperative model predictive controller. The controllers are distributed and can be located close to the actuators. In order to apply a distributed, predictive control approach the central MPC as described in Chapter 2 needs to be adapted.

6.3.1 Model manipulation

Analogously to the central MPC introduced in Chapter 2, the distributed MPC is derived from (6.8), which is equal to the first prediction time step

$$x_j(k+1) = A_{jj} x_j(k) + B_{jj} u_j(k) + \sum_{p \neq j}^M [A_{jp} x_p(k) + B_{jp} u_p(k)]. \quad (6.9)$$

The second time step with $k \Rightarrow k+1$ is

$$x_j(k+2) = A_{jj} x_j(k+1) + B_{jj} u_j(k+1) + \sum_{p \neq j}^M [A_{jp} x_p(k+1) + B_{jp} u_p(k+1)]. \quad (6.10)$$

Substituting $x_j(k+1)$ with (6.9) leads to

$$\begin{aligned}
 x_j(k+2) &= A_{jj}^2 x_j(k) + \begin{pmatrix} A_{jj} B_{jj} & B_{jj} \end{pmatrix} \begin{pmatrix} u_j(k) \\ u_j(k+1) \end{pmatrix} \\
 &+ \sum_{p \neq j}^M \left[A_{jj} A_{jp} x_p(k) + A_{jp} x_p(k) + \begin{pmatrix} A_{jj} B_{jp} & B_{jp} \end{pmatrix} \begin{pmatrix} u_p(k) \\ u_p(k+1) \end{pmatrix} \right],
 \end{aligned} \tag{6.11}$$

where (6.9) defines the first time step for sub-model j and (6.11) the second time step for sub-model j . The formulation for N time steps and one subsystem is given with

$$\bar{x}_j = \bar{E}_{jj} \bar{u}_j + \bar{f}_{jj} x_j(k) + \sum_{p \neq j}^M \bar{E}_{jp} \bar{u}_p + \bar{f}_{jp} x_j(k) + \bar{g}_{jp} \bar{x}_p, \tag{6.12}$$

where

$$\bar{E}_{jp} = \begin{pmatrix} B_{jp} & 0 & \cdots & \cdots & 0 \\ A_{jj} B_{jp} & B_{jp} & 0 & \cdots & 0 \\ \vdots & \ddots & \ddots & \ddots & \vdots \\ A_{jj}^{N-1} B_{jp} & \cdots & \cdots & \cdots & B_{jp} \end{pmatrix},$$

$$\bar{f}_{jp} = \begin{pmatrix} A_{jp} & A_{jj} A_{jp} & \cdots & A_{jj}^{N-1} A_{jp} \end{pmatrix}^T,$$

$$g_{jp} = \begin{pmatrix} 0 & 0 & \cdots & \cdots & 0 \\ A_{jp} & 0 & 0 & \cdots & 0 \\ \vdots & \ddots & \ddots & \ddots & \vdots \\ A_{jj}^{N-2} A_{jp} & A_{jj}^{N-3} A_{jp} & \cdots & \cdots & 0 \end{pmatrix}.$$

\bar{x}_j and \bar{u} are defined with

$$\bar{x}_j = \begin{pmatrix} x_j(1) & \cdots & x_j(N) \end{pmatrix}^T, \tag{6.13}$$

$$\bar{u}_j = \begin{pmatrix} u_j(1) & \cdots & u_j(N) \end{pmatrix}^T. \tag{6.14}$$

\bar{E} and \bar{f} have the same structure as S_u, S_x of the central formulation. However, the presented distributed formulation is consistent with the subsystems defined in Section 6.2. Converting (6.12) leads to

$$\bar{x}_j - \sum_{p \neq j}^M \bar{g}_{jp} \bar{x}_p = \bar{E}_{jj} \bar{u}_j + \bar{f}_{jj} x_j(k) + \sum_{p \neq j}^M \bar{E}_{jp} \bar{u}_p + \bar{f}_{jp} x_j(k). \quad (6.15)$$

The model for N time steps and the overall model is

$$\mathcal{A} \begin{pmatrix} \bar{x}_1 \\ \vdots \\ \bar{x}_M \end{pmatrix} = \mathcal{E} \begin{pmatrix} \bar{u}_1 \\ \vdots \\ \bar{u}_M \end{pmatrix} + \mathcal{G} x(k) \quad (6.16)$$

$$\begin{pmatrix} \bar{x}_1 \\ \vdots \\ \bar{x}_M \end{pmatrix} = \underbrace{\mathcal{A}^{-1} \mathcal{E}}_E \begin{pmatrix} \bar{u}_1 \\ \vdots \\ \bar{u}_M \end{pmatrix} + \underbrace{\mathcal{A}^{-1} \mathcal{G}}_f x(k) \quad (6.17)$$

where

$$\mathcal{A} = \begin{pmatrix} I & -\bar{g}_{12} & \cdots & -\bar{g}_{1M} \\ -\bar{g}_{21} & I & & -\bar{g}_{2M} \\ \vdots & \ddots & \ddots & \ddots \\ -\bar{g}_{M1} & -\bar{g}_{M2} & \cdots & I \end{pmatrix},$$

$$\mathcal{E} = \begin{pmatrix} \bar{E}_{11} & \cdots & \bar{E}_{1M} \\ \vdots & \ddots & \vdots \\ \bar{E}_{M1} & \cdots & \bar{E}_{MM} \end{pmatrix},$$

$$\mathcal{G} = \begin{pmatrix} \bar{f}_{11} & \cdots & \bar{f}_{1M} \\ \vdots & \ddots & \vdots \\ \bar{f}_{M1} & \cdots & \bar{f}_{MM} \end{pmatrix}.$$

The central formulation (2.5) represents a model with prediction horizon and $\bar{x} = f(x(k), \bar{u})$. (6.17) assembles the same model including prediction horizon, but also preserves subsystem boundaries.

Hence:

$$\boxed{\bar{x}_j = f_{jj} x_j(k) + E_{jj} \bar{u}_j + \sum_{p \neq j}^M f_{jp} x_p(k) + E_{jp} \bar{u}_p} \quad (6.18)$$

where \bar{x}_j gives the model predictive equation set for subsystem j and N time steps only in dependence of $x(k)$ and \bar{u} , which shall be used for the optimization. The matrices E and f are defined by (6.17).

Since the existing problem is an output regulator problem with the control variable ω , the output equation over the prediction horizon is needed. The output y_j is coupled with all subsystems, but is independent of the prediction step.

$$\bar{y}_j = \sum_{i=1}^M \tilde{C}_{ji} \bar{x}_i \quad (6.19)$$

with

$$\tilde{C}_{ji} = \begin{pmatrix} C_{ji} & \cdots & 0 \\ \vdots & \ddots & \vdots \\ 0 & \cdots & C_{ji} \end{pmatrix}. \quad (6.20)$$

6.3.2 Objective Function

For each subsystem j and iterate it the control variable is defined with \bar{u}_j^{it} . Each MPC controller calculates the optimal actuating variable considering the objective function

$$V_j(k) = \sum_{s=1}^M \omega_{js} \left[[\bar{y}_s(k) - \tau_s(k)]^T Q_s(k) [\bar{y}_s(k) - \tau_s(k)] + \bar{u}_s(k)^T R_s(k) \bar{u}_s(k) \right] \quad (6.21)$$

τ_s is the set point for each subsystem and Q , R are positive-definite weighting matrices. Cooperation of the dMPC controllers is needed to achieve system wide objectives. Therefore, the overall system influence and the objectives of all subsystems are incorporated into the cost function V_j of subsystem j . w_{js} is a weighting term for each subsystem with $\sum_s w_{js} = 1$ and $w_{js} > 0$. w_{js} defines the consideration of neighboring subsystems in the controller design. $w_{jj} = 1$ only optimizes the controller with respect to the own subsystem, whereas $w_{js} = \frac{1}{M}$, $\forall s$ optimizes the controller with respect to all subsystems in equal weight.

A quadratic cost function was taken for this example. The matrix \tilde{C}_{ji} is defined with (6.20). Substituting (6.18) into (6.19) and the resulting equation into (6.21) formulates a PQ-problem. In the following the time variable (k) is dropped for simplicity.

$$V_j = \min_{\bar{u}_j} \frac{1}{2} \bar{u}_j^T \Phi_j \bar{u}_j + \left(K_{MPC,j} x + \sum_{p \neq j} W_{MPC,jp} \bar{u}_p^{it-1} \right)^T \bar{u}_j + \text{const} \quad (6.22)$$

The PQ-problem of controller j is given in (6.22). (6.22) has a quadratic term penalizing local control variables \bar{u}_j , additionally the product of $x \cdot \bar{u}_j$ and $\bar{u}_p^{it-1} \cdot \bar{u}_j$ is penalized. Here x is the overall state vector and \bar{u}_p^{it-1} are control variables of neighboring subsystems which are not optimization variables. V_j is only optimized for \bar{u}_j .

To calculate the optimal solution for a trajectory $\bar{u}_{opt,j}$, equation (6.22) is differentiated with respect to \bar{u}_j and set to zero.

$$\frac{dV_j}{d\bar{u}_j} = \left(K_{MPC,j}x + \sum_{p \neq j} W_{MPC,jp} \bar{u}_p^{it-1} \right)^T + \Phi_j \bar{u}_j = 0$$

which leads to the optimal control law:

$$\boxed{\bar{u}_{opt,j} = -\Phi_j^{-1} \left(K_{MPC,j}x + \sum_{p \neq j} W_{MPC,jp} \bar{u}_p^{it-1} \right)^T} \quad (6.23)$$

After considerable work Φ_j , $K_{MPC,j}$ and $W_{MPC,jp}$ are obtained

$$\begin{aligned} \Phi_j &= \left[\omega_{jj} R_j + \sum_{s=1}^M \left[\sum_{i=1}^M (\tilde{C}_{si} E_{ij})^T \omega_{js} Q_s \sum_{i=1}^M (\tilde{C}_{si} E_{ij}) \right] \right] \\ K_{MPC,j}x &= \sum_{s=1}^M \sum_{i=1}^M (\tilde{C}_{si} E_{ij})^T \omega_{js} Q_s \left(\sum_{i=1}^M \tilde{C}_{si} \sum_{p=1}^M [f_{ip} x_p] - \tau_s \right) \\ \sum_{p \neq j} W_{MPC,jp} \bar{u}_p &= \sum_{s=1}^M \sum_{i=1}^M (\tilde{C}_{si} E_{ij})^T \omega_{js} Q_s \left(\sum_{i=1}^M \tilde{C}_{si} \sum_{p \neq j} [E_{ip} \bar{u}_p^{it-1}] - \tau_s \right) \end{aligned}$$

6.3.3 Implementation

The implemented dMPC procedure does not explicitly account for constraints such as the rate of change or saturation effects. Therefore, the dMPC controller is deducible with an analytical solution as shown in (6.23). Hence, a static control matrix can be calculated, which has several inherent advantages.

- The optimization can be calculated offline
- Stability and robustness analysis is possible

In order to penalize input and state changes it is useful to transform the system with $\Delta u = u - u_0$ and $\Delta y = y - y_0$. Thus, Δu are the new optimization variables and Δx the newly obtained state variables after the transition to Δ -values. The set point of the operation point can be reached with $\Delta \tau = 0$. The presented dMPC method is an iterative approach and assumes communication of dMPC controllers. The control law (6.23) is dependent on the input variables of neighboring subsystems. The distributed controller is applying values from the previous iteration $\Delta \bar{u}_p^{it-1}$, consequently assumptions are necessary regarding their initial value $\Delta \bar{u}_p^0$ at iterate $it = 1$. The initial value $\Delta \bar{u}_p^{it-1}$ is assumed to be zero. Simulation results show that the same controller performance is attained if $\Delta \bar{u}_p^{it-1}(k) = \Delta \bar{u}_p^{it-1}(k-1)$. In order to allow several iterations, the data transfer between controllers needs to be considerably faster than the sample time T_s . With a high number of controllers the requirements to transfer rate and data volume would be significant. The implementation presented stops after the first iteration to avoid these obstacles.

6.3.4 Simulation Results - 2 Area Network

A 4 generator benchmark model according to [49] is chosen to demonstrate the performance of the developed dMPC approach. Fig. 6.3 depicts a detailed example of the control structure and data transmissions for the benchmark model. Each feed-in node is equipped with a PMU. The PMU data is transmitted through a data concentrator to the state estimator.

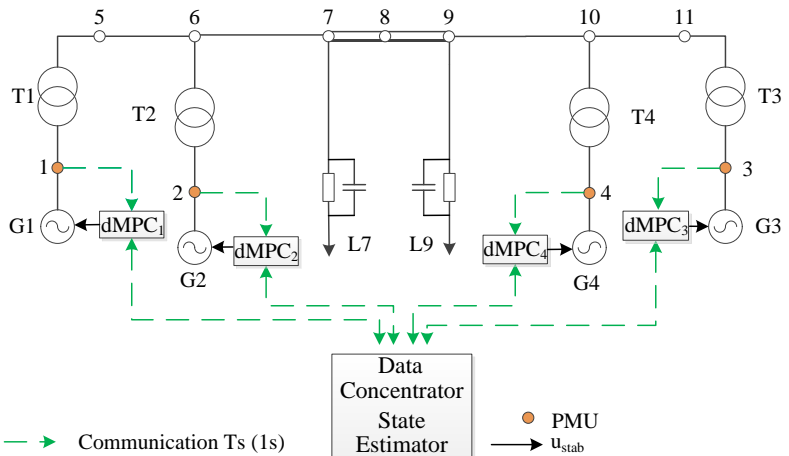


Figure 6.3: Two area network with dMPC control, communication, data concentrator and state estimator

A Kalman-Bucy Filter is used for the estimation as introduced in Chapter 5. By applying (4.29), the filter estimates all network state variables ζ . As indicated in Fig. 6.6b all state variables, except for those x_j available locally, are transferred to the corresponding dMPC controller. The procedure of data transmission and state estimation is time consuming. Thus, the sample time is $T_s = 1$ s. Each generator is equipped additionally with a MB-PSS IEEE type PSS4B, as defined in Appendix B. The PSS is not depicted in Fig. 6.3 for simplicity. The stabilizing signal u_{stab} from each dMPC unit is added to the PSS output. The PSSs compensate for the slow transfer rate of the WAMS.

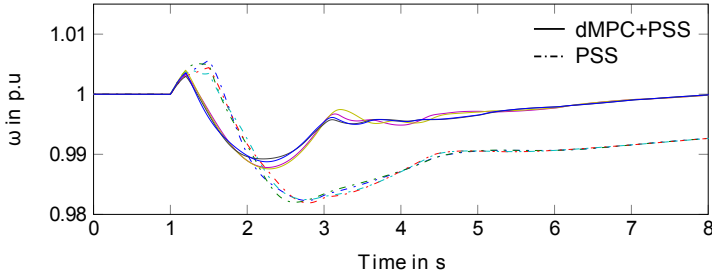


Figure 6.4: ω of dMPC controlled system in comparison to PSS after a 500 ms short circuit

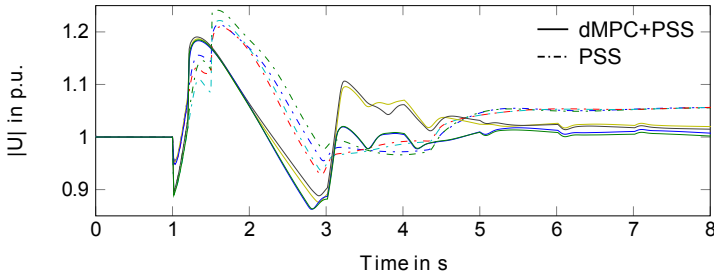


Figure 6.5: $|U|$ of dMPC controlled system in comparison to PSS after a 500 ms short circuit

Fig. 6.4 shows the rotor speed and Fig. 6.5 shows the magnitude of the terminal voltages of all generators. The simulation results created with the dMPC procedure (continuous line) are compared to a MB-PSS IEEE type PSS4B according to IEEE Std 421.5 (dotted line). After one second of simulation time a 3-phase short circuit occurs at node 8 for 500 ms. dMPC and PSS are able to stabilize the system.

However, as depicted in Fig. 6.4 and 6.5, the time evolution of the rotor speed and voltage magnitude of the dMPC controlled system are significantly better than the PSS controlled system. The maximum rotor speed deviation of the dMPC controlled system is 0.01 p.u. compared to 0.02 p.u. for the PSS controlled system. After just 5 s the terminal voltage of the dMPC controlled system is close to the set point. The PSS needs 5.5 s to damp the oscillation, and needs 28.5 s to return the terminal voltage back to its set point.

6.3.5 Simulation Results - 5 Area Network

After successful evaluation of the control method in a 2 area network setting, the control method is evaluated and discussed in a larger network. The system becomes more complex with the rising number of generators and nodes. This effectively entails a rising number of modes and a rising number of control variables. The 5 area network, already shown in Fig. 4.6, includes generators and SVCs as actuators, which are able to control the power flow.

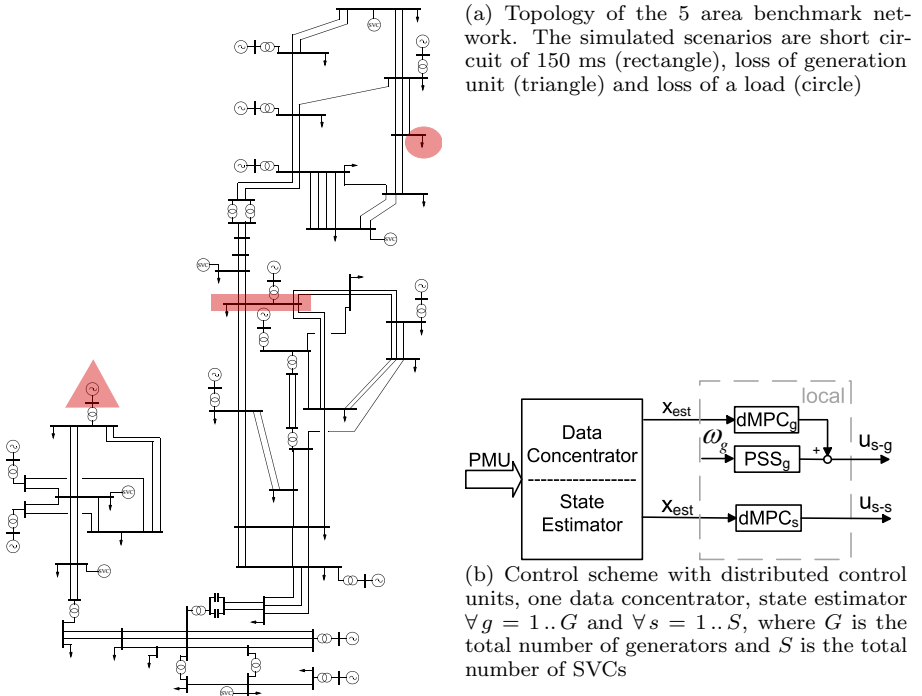


Figure 6.6: Overview of the 5 area network and the implemented control approach

Three contingencies are considered in the 5 area network. As illustrated in Fig. 6.6a considered are: a short circuit at bus 206 (area 2) of 150 ms, the loss of a generation unit at bus 501 (area 5) and the loss of a load at bus 409 (area 4). The control structure of the dMPC for the 5 area network is shown in Fig. 6.6b, which is a simplified scheme of Fig. 6.3. A PMU is located at each generator and SVC feed-in. The data is transferred to the data concentrator and state estimator. The sample time of each dMPC is $T_s = 1$ s; i.e. each controller receives a refreshed estimation of the state variables x_{est} . The optimization horizon is $N = 5$. All generators have a PSS. The distributed MPC developed provides an additional stabilizing signal, which corrects the PSS output with the help of the global signal. In addition the set points of the 5 SVCs deployed at the network are updated with the dMPC controller output. Consequently, 14 dMPC controllers are located at power plants and 5 dMPC controllers are responsible for SVCs.

6.3.5.1 Dynamic stability versus rotor angle stability

Eigenvalues describe the dampening behavior after a contingency and give information on the oscillatory response. Small signal analysis is only valid around an operation point. Rotor angle stability is not considered in small signal analysis. In order to maintain rotor angle stability, θ of all generators needs to be smaller than 90° during stationary operation. Moreover, a rotor angle of all generators $< 180^\circ$ has to be preserved during transients in order to maintain synchronism. The low frequency oscillations also excite rotor angle oscillations during transient operation. A fast deactivation of the excited frequencies is in itself not of paramount importance in power systems [62]. However with the thereby excited rotor angle oscillations and a potential generator failure, a fast dampening with small rotor angle deviations becomes very relevant.

In Chapter 4 load cases 1 and 6 are introduced and an eigenvalue comparison is presented, leading to the following conclusion: The modes of case 6 are more weakly damped and have a strong resonant frequency around 9 rad per second. On the other hand, load case 1 represents a peak load condition, whereas load case 6 is a moderate load condition. Therefore, the rotor angle reserve at case 1 is smaller than in case 6. Load case 1 has a maximum rotor angle of $\theta_{max} = 70^\circ$ and a mean rotor angle of $\theta_{avg} = 48^\circ$, whereas load case 6 has a maximum rotor angle of $\theta_{max} = 59^\circ$ and a mean rotor angle of $\theta_{avg} = 45^\circ$. Even though, load case 6 is dynamically less stable, load case 1 is the more critical case, due to the small rotor angle reserve. For load case 6 the PSS controlled network, has a similar performance as the dMPC controlled network for all contingencies. In the following simulation results are presented discussing load case 1.

6.3.5.2 Short Circuit

The simulation results compare the developed dMPC scheme to PSS developed by [20]. Fig. 6.7a and Fig. 6.7b depict the rotor angle of all generators in reference to generator LPS3. Fig. 6.7c and Fig. 6.7d show the rotor speed of all connected generators. The considered contingency first is a 3-phase short circuit at bus 206 of 150 ms. Due to the short circuit all areas lose steady state and the system performs a transient response. The dMPC controlled system is stable, whereas the PSS controlled system loses rotor angle stability after 5 seconds. The rotor angle reserve for case 1 in area 5 is only 20° . Even though the short circuit occurs far away from area 5 the rotor angle oscillations of generators NFS5, TPS5 and PPS5 lose synchronism. Hence, all generators located in area 5 are disconnected from interconnected operation. The maximum frequency deviation of the dMPC controller system is $\Delta\omega = 0.023$ p.u.

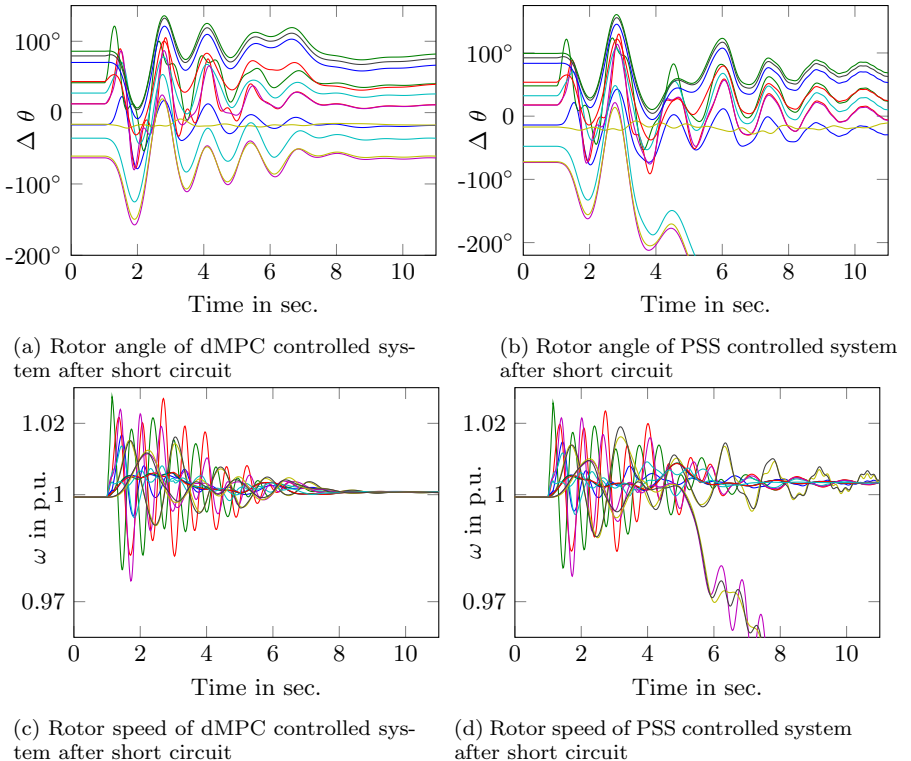


Figure 6.7: Simulation results of the 5 area network

The dMPC controlled system is able to preserve stability and after 7 seconds the frequency of the system is equal to f_N . The rotor angle oscillations of the dMPC controlled system are significantly better damped.

6.3.5.3 Generator unit failure

A power plant in area 5 (NFS5) loses a generation unit, causing a power deficit of 266 MW. Fig. 6.8a and Fig. 6.8b depict the rotor angle of all generators in reference to generator LPS3. Fig. 6.8c and Fig. 6.8d show the rotor speed of all connected generators. The contingency has a small impact on the system and only a minor influence on neighboring areas. However, the PSS controlled system is not able to stabilize the remaining generators and after 5 seconds the generators located in area 5 lose synchronism.

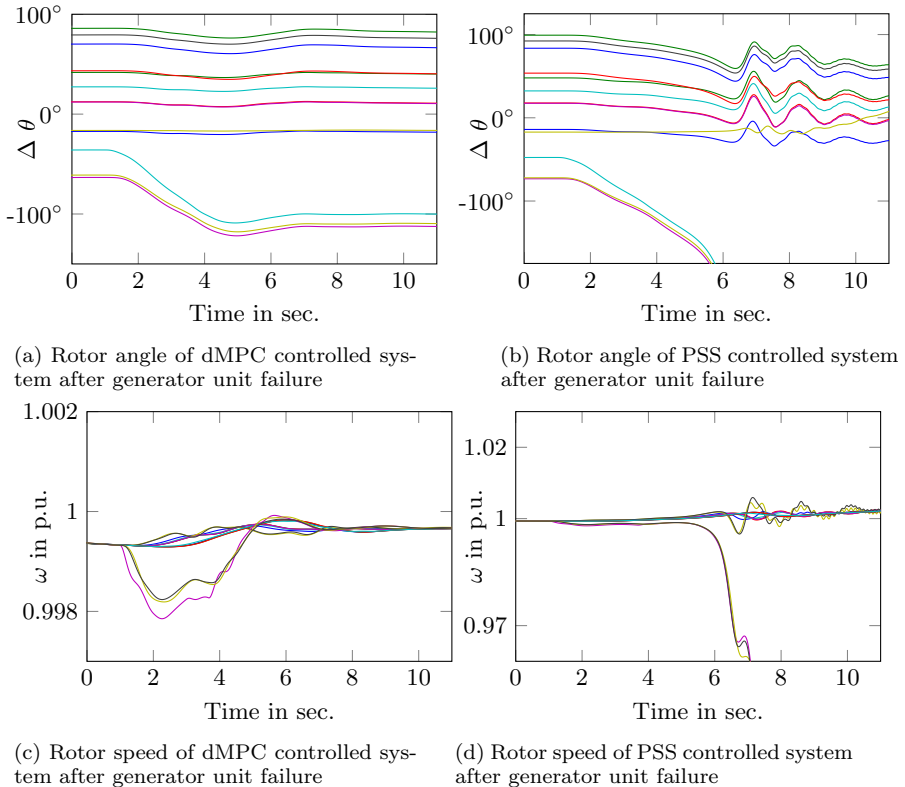


Figure 6.8: Simulation results of the 5 area network

The dMPC controlled system is stable and is able to damp the oscillation. The maximum frequency deviation of the dMPC controlled system is $\Delta\omega = 0.002$. The frequency is equal to the set point after 6 seconds.

As depicted in Fig. 6.8c the rotor speed of all generators has a marginal deviation from f_N at the beginning of the simulation. The deviation is caused by numerical errors of the initial value calculation.

6.3.5.4 Load failure

The last contingency considered is a loss of a load at bus 409 of 260 MW. This contingency appears to be uncritical for both the dMPC and the PSS controlled system, even though the power deviation has the same magnitude as the considered generator unit failure. The load failure is in area 4, which has more rotor angle reserve compared to area 5.

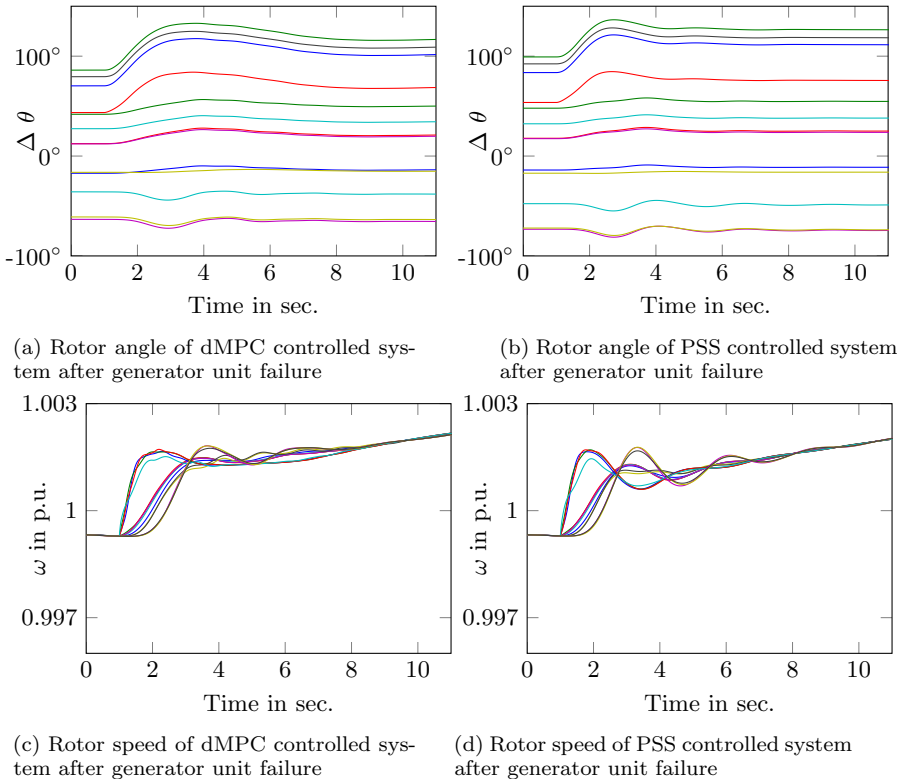


Figure 6.9: Simulation results of the 5 area network

Additionally, area 4 is distant to area 5, hence the power unbalance has very little influence on area 5. The frequency deviation is in both cases $\Delta\omega = 0.0017$. The decay of the oscillation takes 7 seconds.

6.3.6 Discussion

Controller relying on remote signals have superior performance as compared to decentralized PSS; the reviewed publications include many examples showing this. The presented distributed controller significantly improves transient stability, including angle stability. The controller explicitly considers control interaction through the underlying process model which includes network dynamics and through the implementation of a MiMo controller.

All reviewed approaches, except for [18], assume a time-continuous controller and examine the robustness of the controller against communication delays up to 400ms. The presented approach implements a time-discrete controller, explicitly considering transfer/sample rates. The dMPC controller shows good performance for a sample time of 1s for the 2 area network and the 5 area network, respectively. The assumed sample rates are less demanding, i.e. more realistic, compared to the reviewed approaches. Furthermore, central controller schemes such as [18] are vulnerable to communication disturbances or SCADA failures. [81] has presented a central MPC control scheme.

The approach presented here assumes a real-time communication interface, which is able to provide the state variable x_{est} every 1s. This chapter solves the control problem through a distributed approach, but does not address the communication problem. In general, control schemes are preferable which need as few measured variables as possible. Several methods to reduce the estimation and communication effort are available.

- Model reduction methods reduce the number of state variables and therefore the communication needed. Since only a very limited range of the spectrum is of interest, the number of state variables can be significantly reduced [62].
- A hybrid network model reduces the number of state variables and still considers control interaction [42].
- The controllability analysis gives information on which controllers can damp which modes most effectively. Furthermore, the observability analysis gives information on which feedback signals are most conclusive [38]. Hence, not all controllers need a global signal and the cooperating controllers need measurements from only a few locations.

- State estimators which rely on predictor-corrector methods are able to compensate for sporadic communication delays. In case no up-to-date estimation is available due to measurement failure, the predicted variables can be used.
- Robust dMPC implementations will improve control performance against model errors and unmeasured subsystem influence

Note that a reduced system model may result in deteriorating control performance.

6.3.7 Conclusion

The chapter presents a novel approach to systematically integrate PMU-data and coordinate a large number of hardware actuators (Generators, FACTS, HVDC). The optimal trajectories for each control variable are calculated in order to damp inter-area oscillations. Each controller complies with the global objective. Hence, the dMPC approach has a dynamic performance close to a central MPC [74]. The performance is significantly better compared to a PSS, and thus the dMPC approach improves reliability and operational flexibility.

Chapter 7

Conclusion and Outlook

The focus of this thesis lies in the improvement of power system security with high renewable energy sources (RES) in-feed. The first section within this thesis regards the optimal operation of a diverse generation unit portfolio considering operating ranges like transmission line and generation constraints during stationary operation. Generation dispatch and redispatch strategies are developed. In order to integrate a high share of RES, operational flexibility is imperative. Volatile RES challenge one of the fundamental requirements of power system operation, namely the balance of demand and supply.

In order to formulate an optimization problem, a modeling framework is introduced, describing the diverse generation units and the power flow. This thesis presents formulations for normal operation and operation after a contingency took place. The optimization takes place over a prediction horizon, hence inter-temporal dependencies like storage devices and generation ramping constraints are considered. In addition, the optimization accounts for load and RES forecasts.

Since power systems are divided into several control areas with corresponding assignment of responsibilities, it is crucial to consider zoning within the problem formulation. A cooperative optimization is presented in which several control areas attain a verified schedule. For each control area a player is introduced, with the goal to create an iterative procedure which makes cooperation of control areas possible. Each zone conducts its own optimization with inclusion of approximated neighboring generation costs. The generation pattern load and RES feed-in forecasts are exchanged. Through an iterative approach, a solution close to the global optimum is reached. Due to the high costs for storage and hot standby operation of conventional power plants, grid operation needs to be as close as possible to the global optimum.

The functionality is shown successfully using stressed 14 and 118 node systems. A cross border dispatch with use of storage devices is realized to maintain a high share of RES feed-in, while reducing overall dispatch costs.

The second area addressed in this thesis is the transient operation of power systems. Due to the rising numbers of RES and hesitant network reinforcement, transfer capacity reserves as well as total inertia decrease. Thus, the affected power systems have poor transient behavior.

On the other hand controllable devices like generators, FACTS and HVDC located through out the network are able to control the power flow and can improve the transient behavior. In order to avoid cascading blackouts, dampening controllers are implemented which are a significant part of this thesis. This thesis develops dampening controllers improving the performance of local power system stabilizers. In order to coordinate the behavior of the controllable devices a cooperative objective function is used, which optimizes each distributed controller towards a system wide objective.

Furthermore, the distributed controllers are based on an overall network state provided by a dynamic state estimator. This development is also within the scope of the presented thesis. The state estimator is also capable of estimating voltage phase and absolute value of a network assuming a wide area monitoring system. Control design methods for fast acting controllable devices (Exciters, HVDC, FACTS) need dynamic network equations to describe the behavior satisfactorily if these devices are electrically close to each other. This thesis implements a dynamic network model from minimal order, which explicitly considers the control interaction phenomenon. The developed small signal model is applied to control synthesis. Consequently, the deployed dampening controllers avoid interaction. A high number of controllable devices with dampening controllers is difficult to design, therefore a systematic design approach is implemented.

The control scheme is successfully implemented for 11 and 59 node benchmark networks. Contingencies like short circuit, generator unit failure and load tripping are considered. The performance of the control scheme is evaluated against state of the art power system stabilizers. The controller is used as a superordinate control system and only calculates new set points for the local controllers. Consequently, the approach works with a sample time of 1s.

7.1 Outlook

A real world implementation of the presented methods can be disassembled into several steps. The software needs to be implemented on fast and secure running embedded systems. The software implementation can be evaluated using a hardware-in-the-loop test bed, where the in/outputs of the hardware device are used and the real-time capability can be demonstrated. The second step is the evaluation of an experimental plant. For example, a small island network with several generation

units would prove the benefits of the resulting system. Further, resulting cost could be estimated effectively.

There are several possible improvements for both developed methods addressing stationary and transient operation.

In the current implementation the static optimization is using a DC power flow model, whereas a possible AC power flow model will improve modeling quality. An AC model formulation could also consider voltage constraints directly in the optimization without relying on additional iterative procedures. In order to guarantee secure operation, the $N - 1$ principle needs to hold. Therefore, an explicit optimization towards $N - 1$ security will result in maximal economic welfare. The stochastic behavior of renewable generation has not been addressed in this thesis. Future versions may include stochastic effects with the help of Stochastic MPC. Further, the influence of prediction errors has not been considered. The modeling framework is able to represent multi-carrier systems. Consequently, in addition to electric power systems, natural gas systems and head systems could be intergraded in the optimization.

Possible extensions in the field of transient operation are the following: The implemented controller requires full state feedback and therefore requires the maximum of estimation and communication effort. Thus, future research could address model reduction and carefully selected state variables which are effectively needed for the approach. Further, the number of controllers with communication capability can also be reduced. The most efficient control schemes will only implement controllers at locations with strong influence. Robust MPC implementations are able to produce good performance despite model errors.

Appendix A

Control Theory

A.1 Linearization of a nonlinear system around an operating point

In order to apply control design or analysis methods to nonlinear systems, a linearization around an operating point is carried out [15].

$$\begin{aligned} \dot{x} &= f(x, u) \\ y &= g(x, u) \end{aligned} \quad (\text{A.1})$$

In order to attain a linear model, a Taylor series of the nonlinear function $f(x, u)$ is computed

$$\Delta \dot{x} = f(x_0, u_0) + \left. \frac{\partial f}{\partial x} \right|_{x_0, u_0} \Delta x + \left. \frac{\partial f}{\partial u} \right|_{x_0, u_0} \Delta u + r(x, u). \quad (\text{A.2})$$

The Taylor series is discontinued after the first order and since $f(x_0, u_0) = 0$

$$\begin{aligned} \Delta \dot{x} &= \left. \frac{\partial f}{\partial x} \right|_{x_0, u_0} \Delta x + \left. \frac{\partial f}{\partial u} \right|_{x_0, u_0} \Delta u \\ \Delta \dot{x} &= A \Delta x + B \Delta u. \end{aligned} \quad (\text{A.3})$$

Where

$$\left. \frac{\partial f}{\partial x} \right|_{x_0, u_0} = \begin{pmatrix} \frac{\partial f_1}{\partial x_1} & \cdots & \frac{\partial f_1}{\partial x_n} \\ \vdots & & \vdots \\ \frac{\partial f_n}{\partial x_1} & \cdots & \frac{\partial f_n}{\partial x_n} \end{pmatrix}_{x_0, u_0} \quad \left. \frac{\partial f}{\partial u} \right|_{x_0, u_0} = \begin{pmatrix} \frac{\partial f_1}{\partial u_1} & \cdots & \frac{\partial f_1}{\partial u_n} \\ \vdots & & \vdots \\ \frac{\partial f_n}{\partial u_1} & \cdots & \frac{\partial f_n}{\partial u_n} \end{pmatrix}_{x_0, u_0} \quad (\text{A.4})$$

Analogously, the output equation is linearized attaining

$$y = C \Delta x + D \Delta u \quad (\text{A.5})$$

where

$$C = \left. \frac{\partial g}{\partial x} \right|_{x_0, u_0} \quad D = \left. \frac{\partial g}{\partial u} \right|_{x_0, u_0} . \quad (\text{A.6})$$

A.2 Discretization of linear state space models

A control system is normally implemented on digital computers, which process input values in discrete time intervals.

A time discrete state space model

$$\begin{aligned} x(k+1) &= A_d x(k) + B_d u(k) \\ y(k) &= C_d x(k) + D_d u(k) \end{aligned} \quad (\text{A.7})$$

is defined with application of the continues state space model and the sample time T

$$\begin{aligned} A_d &= e^{AT} \\ B_d &= \int_{\tau=0}^T e^{A\tau} d\tau B \\ C_d &= C \\ D_d &= D. \end{aligned} \quad (\text{A.8})$$

Appendix B

Multiband PSS

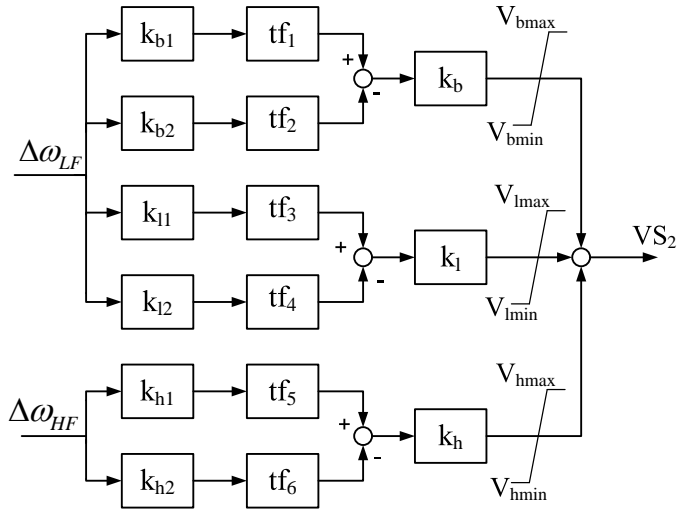


Figure B.1: Simplified representation of PSS4B according to IEEE 421.5

The MB PSS as depicted in Fig. B.1 is a multi-bandpass filter. The PSS as two input variables where $\Delta\omega_{LF}$ is the low frequency speed sensor input and $\Delta\omega_{HF}$ is the high frequency speed sensor input. The bandpass filter can be divided into three frequency ranges: low frequency range for very slow oscillations ($< 0.2\text{Hz}$), intermediate frequency range for inter-area oscillations ($0.2\text{Hz} - 0.8\text{Hz}$) and high frequency range regarding intermachine/local modes. Each set of bandpass filter is based on a gain k and three lead-lad filters, which can be parameterized to adjust for local conditions. The MB PSS has an additional gain and saturation for each frequency range.

Appendix C

Network Data

C.1 SVC Example

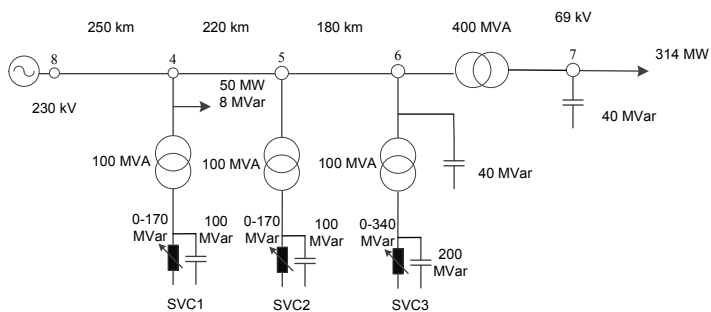


Figure C.1: Radial network from [63] with a total of 650 km and three SVCs in operation

C.2 IEEE 14 Network

Name	η	P_{max} MW	Curtail. costs /€MWh	Disp. costs /€MWh
Wind 1	1	200	200	3.6
Photovoltaics	1	20	200	7
Biomass 1	0.42	100	-	125.6
Biomass 2	0.42	100	-	145.6
Biomass 3	0.42	100	-	55.6
Biomass 4	0.42	100	-	175.6
Feeder	1	1000	-	400
PumpedHy. 1	0.9/0.85	40	-	10
PumpedHy. 2	0.9/0.85	40	-	15

Table C.1: IEEE-14 scenario data

Table C.2: Line IEEE 14 network

ID	node 1	node 2	R' [Ω/km]	X'_L [Ω/km]	l [km]	X'_C [Ω/km]
421	407	408	2.24	9.43	1	2.93
424	409	410	2.57	10.62	1	3.29
427	409	407	0.92	2.82	1	3.53
430	411	410	0.64	2	1	0.86
433	408	411	3.19	8.14	1	2.31
436	407	410	2.71	8.28	1	2.27
439	407	411	2.77	8.39	1	2.50
442	412	413	0.13	0.25	1	0
445	412	414	0.23	0.49	1	0
448	412	415	0.18	0.38	1	0
451	414	413	0.42	0.38	1	0
454	416	415	0.16	0.37	1	0
457	417	418	0.24	0.51	1	0
460	417	416	0.06	0.16	1	0
463	419	417	0	0.21	1	0
466	413	418	0.33	0.66	1	0

Table C.3: Transformer IEEE 14 network

ID	node 1	node 2	U_1 [kV]	U_2 [kV]	S [MVA]	u_x [%]
557	411	419	67.48	13.8	100	20.912
558	410	412	64.30	13.8	100	25.202
559	411	417	66.86	13.8	100	55.618
560	419	420	13.8	18	100	17.615

Table C.4: Load IEEE 14 network

Name	ID	Bus No.	P_{max} [MW]
LDBUS2	686	407	21.7
LDBUS6	687	412	11.2
LDBUS5	688	410	7.6
LDBUS4	689	411	47.8
LDBUS3	690	408	94.2
LDBUS11	691	415	3.5
LDBUS10	692	416	9
LDBUS1	693	417	29.5
LDBUS7	694	419	0
LDBUS14	695	418	14.9
LDBUS13	696	413	13.5
LDBUS12	697	414	6.1

Table C.5: IEEE 14 generation data

Load-ID	Node1	Pgen	Qgen	Pmax	Qmax	Pmin	Qmin	Uset	Name
601	2	40	42.40	100	50	0	-40	104.50	CHP2
602	3	0	23.40	100	40	0	0	101	CHP1
603	6	0	12.20	100	24	0	-6	107	CHP4
604	8	0	17.40	100	24	0	-6	109	CHP3
605	2	14	0	200	60	0	0	104.50	Wind1
606	6	14	0	20	1	0	0	107	PV1

Table C.6: IEEE 14 Definition Node ID

Node ID	Voltage-Level	BUS-ID
1	69	409
2	69	407
3	69	408
4	69	411
5	69	410
6	13.80	412
7	13.80	419
8	18	420
9	13.80	417
10	13.80	416
11	13.80	415
12	13.80	414
13	13.80	413
14	13.80	418

C.3 IEEE 118 Network

Name	η	P_{max} MW	Curtail. costs /€MWh	Disp. costs /€MWh
Wind 4 & 8	1- 1	50	800	2.5-3.5
Wind 5-7	1	300	800	2.5-3.5
PV 1-7	1	20	200	1.3-3
Conv. 1-52	0.42	100-700	-	15-100
Feeder	1	1000	-	600
Storage 1-6	0.9/0.85	50	-	25

Table C.7: IEEE-118 scenario data

Table C.8: IEEE 118: bus data

Node ID	VLevel						
1	138	31	138	61	138	91	138
2	138	32	138	62	138	92	138
3	138	33	138	63	345	93	138
4	138	34	138	64	345	94	138
5	138	35	138	65	345	95	138
6	138	36	138	66	138	96	138
7	138	37	138	67	138	97	138
8	345	38	345	68	345	98	138
9	345	39	138	69	138	99	138
10	345	40	138	70	138	100	138
11	138	41	138	71	138	101	138
12	138	42	138	72	138	102	138
13	138	43	138	73	138	103	138
14	138	44	138	74	138	104	138
15	138	45	138	75	138	105	138
16	138	46	138	76	138	106	138
17	138	47	138	77	138	107	138
18	138	48	138	78	138	108	138
19	138	49	138	79	138	109	138
20	138	50	138	80	138	110	138
21	138	51	138	81	345	111	138
22	138	52	138	82	138	112	138
23	138	53	138	83	138	113	138
24	138	54	138	84	138	114	138
25	138	55	138	85	138	115	138
26	345	56	138	86	138	116	345
27	138	57	138	87	138	117	138
28	138	58	138	88	138	118	138
29	138	59	138	89	138		
30	345	60	138	90	138		

Table C.9: IEEE 118: Line data (1)

Line ID	Node1	Node2	Resistance	Reactance	Length	B
201	1	2	0.074698	0.246282	77.248512	0.005496
202	1	3	0.074829	0.245949	32.830618	0.005509
203	3	5	0.065260	0.292450	70.328333	0.006750
204	4	5	0.065084	0.295095	5.149901	0.006816
205	5	6	0.064893	0.294472	34.922765	0.006825
206	6	7	0.064661	0.293017	13.518490	0.006800
207	8	9	0.019940	0.249253	145.645632	0.021336
208	9	10	0.019960	0.249108	153.853286	0.021380
209	4	11	0.074718	0.245963	53.269286	0.005485
210	5	11	0.074141	0.249086	52.142746	0.005571
211	2	12	0.074758	0.246263	47.636582	0.005516
212	3	12	0.074575	0.246529	123.597619	0.005490
213	7	12	0.069390	0.273698	23.657357	0.006175
214	11	12	0.074903	0.246739	15.127834	0.005546
215	11	13	0.074799	0.245745	56.648909	0.005535
216	12	14	0.074829	0.246065	54.717696	0.005547
217	13	15	0.074737	0.245508	189.580723	0.005526
218	14	15	0.074823	0.245219	151.439270	0.005541
219	12	16	0.069301	0.272626	58.258253	0.006140
220	15	17	0.074381	0.246247	33.796224	0.021959
221	16	17	0.068965	0.273581	125.367898	0.006213
222	17	18	0.068014	0.279246	34.439962	0.006299
223	15	19	0.074737	0.245387	30.577536	0.005521
224	18	19	0.067701	0.280474	33.474355	0.005702
225	19	20	0.064129	0.297743	74.834496	0.006656
226	20	21	0.064068	0.297235	54.395827	0.006637
227	21	22	0.064072	0.297368	62.120678	0.006619
228	22	23	0.064035	0.297707	101.710541	0.006639
229	23	24	0.071637	0.261078	35.888371	0.023194
230	23	25	0.060924	0.312433	48.763123	0.029615
231	25	27	0.060989	0.312616	99.296525	0.029693
232	27	28	0.065237	0.291572	55.844237	0.006465
233	28	29	0.068907	0.274174	65.500301	0.006073
234	8	30	0.020659	0.241576	248.321779	0.005536
235	26	30	0.021551	0.231964	441.282125	0.005503
236	17	31	0.074588	0.245952	121.022669	0.005511
237	29	31	0.076988	0.235955	26.715110	0.005193
238	23	32	0.071724	0.260878	84.168691	0.023294

Table C.10: IEEE 118: Line data (2)

Line ID	Node1	Node2	Resistance	Reactance	Length	B
239	27	32	0.074651	0.246122	58.419187	0.005511
240	31	32	0.074553	0.246425	76.121971	0.005511
241	15	33	0.074820	0.244937	96.721574	0.005520
242	19	34	0.074779	0.245617	191.511936	0.005516
243	34	36	0.076917	0.236668	21.565210	0.004402
244	35	36	0.064651	0.294392	6.598310	0.006789
245	33	37	0.073516	0.251548	107.504179	0.005690
246	34	37	0.072127	0.264843	6.759245	0.024333
247	35	37	0.065084	0.294060	32.186880	0.006844
248	30	38	0.020710	0.241024	266.668301	0.004232
249	37	39	0.074627	0.246432	81.915610	0.005509
250	37	40	0.079112	0.224127	142.748813	0.004918
251	39	40	0.074823	0.246021	46.831910	0.005539
252	40	41	0.074602	0.245929	37.014912	0.005518
253	40	42	0.074631	0.246081	141.622272	0.005500
254	41	42	0.074641	0.245770	104.607360	0.005497
255	34	43	0.068162	0.277433	115.389965	0.006121
256	43	44	0.068456	0.276300	169.142054	0.005996
257	44	45	0.068493	0.275501	62.281613	0.006011
258	45	46	0.073843	0.250329	103.158950	0.005379
259	46	47	0.074203	0.247994	97.526246	0.005416
260	46	48	0.076063	0.239199	150.473664	0.005243
261	42	49	0.064934	0.293337	209.697523	0.006855
262	42	49	0.064934	0.293337	209.697523	0.006855
263	45	49	0.080298	0.218354	162.221875	0.004575
264	47	49	0.074840	0.244896	48.602189	0.005516
265	48	49	0.079332	0.223815	42.969485	0.004893
266	49	50	0.079385	0.223586	64.051891	0.004890
267	49	51	0.079325	0.223610	116.677440	0.004899
268	51	52	0.078503	0.227387	49.245926	0.004738
269	52	53	0.068465	0.276394	112.654080	0.006024
270	49	54	0.069052	0.273369	201.328934	0.006127
271	49	54	0.074193	0.248450	223.055078	0.005470
272	53	54	0.064169	0.297665	78.053184	0.004497
273	54	55	0.067335	0.281691	47.797517	0.007064
274	54	56	0.072315	0.251131	7.242048	0.016894
275	55	56	0.076996	0.238246	12.070080	0.005179
276	50	57	0.079224	0.223965	113.941555	0.004870

Table C.11: IEEE 118: Line data (3)

Line ID	Node1	Node2	Resistance	Reactance	Length	B
277	56	57	0.079274	0.223263	82.398413	0.004909
278	51	58	0.079200	0.223313	61.316006	0.004874
279	56	58	0.079274	0.223263	82.398413	0.004909
280	54	59	0.064698	0.294934	148.059648	0.006751
281	55	59	0.064681	0.294538	139.530125	0.006763
282	56	59	0.077052	0.234426	203.903885	0.004664
283	56	59	0.077696	0.231249	196.822771	0.004552
284	59	60	0.064564	0.295326	93.502886	0.006721
285	59	61	0.064582	0.295343	96.721574	0.006705
286	60	61	0.061255	0.313237	8.207654	0.029651
287	60	62	0.064689	0.295046	36.210240	0.006776
288	61	62	0.064574	0.294659	24.301094	0.006741
289	63	64	0.020718	0.240908	98.813722	0.005846
290	38	65	0.021372	0.233878	501.793459	0.005575
291	64	65	0.021097	0.236856	151.761139	0.006696
292	49	66	0.061207	0.312497	56.005171	0.007401
293	49	66	0.061207	0.312497	56.005171	0.007401
294	62	66	0.064888	0.293479	141.461338	0.007066
295	62	67	0.064820	0.293951	75.800102	0.006836
296	66	67	0.064809	0.293665	65.822170	0.006810
297	65	68	0.020745	0.240516	79.179725	0.021549
298	47	69	0.074700	0.245873	215.169293	0.005509
299	49	69	0.074717	0.245770	251.057664	0.005513
300	24	70	0.068526	0.275889	284.049216	0.006002
301	69	70	0.066981	0.283555	85.295232	0.023907
302	70	71	0.068665	0.276372	24.462029	0.006013
303	24	72	0.068583	0.275457	135.506765	0.006019
304	71	72	0.068453	0.276266	124.080422	0.005986
305	71	73	0.060281	0.316021	27.358848	0.007209
306	70	74	0.074610	0.246157	102.354278	0.005500
307	69	75	0.077299	0.232851	99.779328	0.020772
308	70	75	0.074700	0.246093	109.113523	0.005515
309	74	75	0.074641	0.246377	31.382208	0.005507
310	69	77	0.074929	0.244912	78.535987	0.022134
311	75	77	0.074392	0.247437	153.853286	0.005432
312	76	77	0.074314	0.247715	113.780621	0.005406
313	77	78	0.074156	0.244557	9.656064	0.021880
314	78	79	0.065263	0.291651	15.932506	0.006798

Table C.12: IEEE 118: Line data (4)

Line ID	Node1	Node2	Resistance	Reactance	Length	B
315	77	80	0.078889	0.225066	41.038272	0.019224
316	77	80	0.072179	0.257781	77.570381	0.004913
317	79	80	0.065000	0.293335	45.705370	0.006839
318	68	81	0.020808	0.240187	100.101197	0.021587
319	77	82	0.078889	0.225814	71.937677	0.019006
320	82	83	0.074878	0.245025	28.485389	0.022297
321	83	84	0.901935	1.904888	13.196621	0.032931
322	83	85	0.073319	0.252355	111.688474	0.005208
323	84	85	0.893421	1.896301	6.437376	0.032040
324	85	86	0.072661	0.255352	91.732608	0.005029
325	85	88	0.061154	0.311888	62.281613	0.007407
326	85	89	0.016725	0.121063	272.140070	0.002887
327	88	89	0.060920	0.312051	43.452288	0.007439
328	89	90	0.071692	0.260196	137.598912	0.006414
329	89	90	0.067377	0.282246	67.270579	0.026337
330	90	91	0.074768	0.246087	64.695629	0.005529
331	89	92	0.061016	0.311243	30.899405	0.029643
332	89	92	0.068592	0.275938	109.113523	0.006342
333	91	92	0.074707	0.245548	98.652787	0.005537
334	92	93	0.074646	0.245348	65.822170	0.005536
335	92	94	0.074795	0.245687	122.471078	0.005541
336	93	94	0.074755	0.245384	56.809843	0.005520
337	94	95	0.074737	0.245727	33.635290	0.005516
338	80	96	0.061053	0.312127	111.044736	0.007436
339	82	96	0.074883	0.244988	41.199206	0.022070
340	94	96	0.075253	0.243102	68.075251	0.005647
341	95	96	0.075504	0.241525	43.130419	0.005712
342	80	97	0.061173	0.312214	56.970778	0.007452
343	96	97	0.061110	0.312614	53.913024	0.007441
344	80	98	0.064744	0.293795	70.006464	0.006828
345	80	99	0.064805	0.294051	133.414618	0.006840
346	92	100	0.064709	0.294587	190.707264	0.006766
347	94	100	0.074959	0.244248	45.222566	0.022324
348	98	100	0.064977	0.292971	116.355571	0.006838
349	99	100	0.064939	0.293309	52.786483	0.006839
350	100	101	0.064652	0.294551	81.593741	0.006719
351	92	102	0.064689	0.293994	36.210240	0.006758
352	101	102	0.064689	0.294520	72.420480	0.006785

Table C.13: IEEE 118: Line data (5)

Line ID	Node1	Node2	Resistance	Reactance	Length	B
353	100	103	0.074836	0.245555	40.716403	0.022003
354	100	104	0.064925	0.293675	132.288077	0.006962
355	103	104	0.073721	0.250589	120.378931	0.005651
356	103	105	0.077112	0.234218	132.127142	0.005161
357	104	105	0.070433	0.267846	26.876045	0.006132
358	100	106	0.070465	0.266717	163.509350	0.006338
359	105	106	0.069317	0.270831	38.463322	0.006232
360	105	107	0.073268	0.252980	137.759846	0.005727
361	106	107	0.073268	0.252980	137.759846	0.005727
362	105	108	0.080640	0.217203	61.637875	0.005000
363	108	109	0.080162	0.219872	24.944832	0.005092
364	103	110	0.064107	0.297558	116.033702	0.006785
365	109	110	0.080041	0.219393	66.144038	0.005104
366	110	111	0.073334	0.251668	57.131712	0.005851
367	110	112	0.081644	0.211547	57.614515	0.017987
368	17	113	0.074510	0.245645	23.335488	0.005501
369	32	113	0.074641	0.246377	156.911040	0.005518
370	32	114	0.064939	0.294392	39.589862	0.006865
371	27	115	0.064906	0.293262	48.119386	0.006850
372	114	115	0.064802	0.293017	6.759245	0.006825
373	12	117	0.066778	0.284164	93.824755	0.006378
374	75	118	0.074602	0.247472	37.014912	0.005419
375	76	118	0.074355	0.246642	42.003878	0.005396
376	68	116	0.020444	0.243523	19.794931	0.022157
378	86	87	0.016608	0.121799	324.282816	0.002294

Table C.14: IEEE 118: Load data (4)

Load ID	Node1	Pload	Qload	Name
511	112	68	13	DanvilleV2
512	113	6	0	DeerCrkV2
513	114	8	3	WMedfordV2
514	115	22	7	MedfordV2
515	116	184	0	KygerCrkV2
516	117	20	8	CoreyV2
517	118	33	15	WHuntngdV2

Table C.15: IEEE 118: Load data (1)

Load ID	Node1	Pload	Qload	Name
401	1	51.00	27.00	RiversdeV2
402	2	20.00	9.00	PokagonV2
403	3	39.00	10.00	HickryCkV2
404	4	39.00	12.00	NwCarlsIV2
405	5	0.00	0	OliveV2
406	6	52.00	22.00	KankakeeV2
407	7	19.00	2.00	JacksnRdV2
408	8	28.00	0	OliveV1
409	9	0	0	BequineV1
410	10	0	0	BreedV1
411	11	70	23.00	SouthBndV2
412	12	47.00	10	TwinBrchV2
413	13	34.00	16.00	ConcordV2
414	14	14.00	1.00	GoshenJtV2
415	15	90	30	FtWayneV2
416	16	25.00	10	NEV2
417	17	11.00	3.00	SorensonV2
418	18	60	34.00	McKinleyV2
419	19	45.00	25.00	LincolnV2
420	20	18.00	3.00	AdamsV2
421	21	14.00	8.00	JayV2
422	22	10	5.00	RandolphV2
423	23	7.00	3.00	CollCnrV2
424	24	13.00	0	TrentonV2
425	25	0	0	TannrsCkV2
426	26	0	0	TannrsCkV1
427	27	71.00	13.00	MadisonV2
428	28	17.00	7.00	MullinV2
429	29	24.00	4.00	GrantV2
430	30	0	0	SorensonV1
431	31	43.00	27.00	DeerCrkV2
432	32	59.00	23.00	DelawareV2
433	33	23.00	9.00	HavilandV2
434	34	59.00	26.00	RockhillV2
435	35	33.00	9.00	WestLimaV2
436	36	31.00	17.00	SterlingV2
437	37	0	0	EastLimaV2
438	38	0	0	EastLimaV1

Table C.16: IEEE 118: Load data (2)

Load ID	Node1	Pload	Qload	Name
439	39	27.00	11.00	NwLibrtyV2
440	40	66.00	23.00	WestEndV2
441	41	37	10	STiffinV2
442	42	96	23	HowardV2
443	43	18	7	SKentonV2
444	44	16	8	WMVernonV2
445	45	53	22	NNewarkV2
446	46	28	10	WLancstV2
447	47	34	0	CrooksvlV2
448	48	20	11	ZanesvllV2
449	49	87	30	PhiloV2
450	50	17	4	WCambrdgV2
451	51	17	8	NewcmrstV2
452	52	18	5	SCoshoctV2
453	53	23	11	WoosterV2
454	54	113	32	TorreyV2
455	55	63	22	WagenhlsV2
456	56	84	18	SunnysdeV2
457	57	12	3	WNwPhil1V2
458	58	12	3	WNwPhil2V2
459	59	277	113	TiddV2
460	60	78	3	SWKammerV2
461	61	0	0	WKammerV2
462	62	77	14	NatriumV2
463	63	0	0	TiddV1
464	64	0	0	KammerV1
465	65	0	0	MuskngumV1
466	66	39	18	MuskngumV2
467	67	28	7	SummerflV2
468	68	0	0	SpornV1
469	70	66	20	PortsmthV2
470	71	0	0	NPortsmtV2
471	72	12	0	HillsbroV2
472	73	6	0	SargentsV2
473	74	68	27	BellefntV2
474	75	47	11	SthPointV2
475	76	68	36	DarrahV2
476	77	61	28	TurnerV2

Table C.17: IEEE 118: Load data (3)

Load ID	Node1	Pload	Qload	Name
477	78	71	26	ChemicalV2
478	79	39	32	CapitolHIV2
479	80	130	26	CabinCrkV2
480	81	0	0	KanawhaV1
481	82	54	27	LoganV2
482	83	20	10	SpriggV2
483	84	11	7	BetsyLneV2
484	85	24	15	BeaverCkV2
485	86	21	10	HazardV2
486	87	0	0	PinevilleV3
487	88	48	10	FremontV2
488	89	0	0	ClinchRvV2
489	90	163	42	HolstonV2
490	91	10	0	HolstonTV2
491	92	65	10	SaltvllV2
492	93	12	7	TazewellV2
493	94	30	16	SwitchbkV2
494	95	42	31	CaldwellV2
495	96	38	15	BaileysvV2
496	97	15	9	SundialV2
497	98	34	8	BradleyV2
498	99	42	0	HintonV2
499	100	37	18	GlenLynV2
500	101	22	15	WytheV2
501	102	5	3	SmytheV2
502	103	23	16	ClaytorV2
503	104	38	25	HancockV2
504	105	31	26	RoanokeV2
505	106	43	16	CloverdlV2
506	107	50	12	ReusensV2
507	108	2	1	BlaineV2
508	109	8	3	FranklinV2
509	110	39	30	FieldaleV2
510	111	0	0	DanRiverV2

Table C.18: IEEE 118: Generation data (1)

Gen-ID	Node1	Pgen	Pmax	Qmax	Pmin	Qmin	Uset	Name
601	1	0	100	15	0	-5	95.50	RiversdeV2
602	4	0	100	300	0	-300	99.80	NwCarlsV2
603	6	0	100	50	0	-13	99	KankakeeV2
604	8	0	100	300	0	-300	101.50	OliveV1
605	10	450	550	200	0	-147	105	BreedV1
606	12	85	185	120	0	-35	99	TwinBrchV2
607	15	0	100	30	0	-10	97	FtWayneV2
608	18	0	100	50	0	-16	97.30	McKinleyV2
609	19	0	100	24	0	-8	96.20	LincolnV2
610	24	0	100	300	0	-300	99.20	TrentonV2
611	25	220	320	140	0	-47	105	TannrsCkV2
612	26	314	414	1000	0	-1000	101.50	TannrsCkV1
613	27	0	100	300	0	-300	96.80	MadisonV2
614	31	7	107	300	0	-300	96.70	DeerCrkV2
615	32	0	100	42	0	-14	96.30	DelawareV2
616	34	0	100	24	0	-8	98.40	RockhillV2
617	36	0	100	24	0	-8	98	SterlingV2
618	40	0	100	300	0	-300	97	WestEndV2
619	42	0	100	300	0	-300	98.50	HowardV2
620	46	19	119	100	0	-100	100.50	WLancstV2
621	49	204	304	210	0	-85	102.50	PhiloV2
622	54	48	148	300	0	-300	95.50	TorreyV2
623	55	0	100	23	0	-8	95.20	WagenhlsV2
624	56	0	100	15	0	-8	95.40	SunnysdeV2
625	59	155	255	180	0	-60	98.50	TiddV2
626	61	160	260	300	0	-100	99.50	WKammerV2
627	62	0	100	20	0	-20	99.80	NatriumV2
628	65	391	491	200	0	-67	100.50	MuskgumV1
629	66	392	492	200	0	-67	105	MuskgumV2
630	70	0	100	32	0	-10	98.40	PortsmthV2
631	72	0	100	100	0	-100	98	HillsbroV2
632	73	0	100	100	0	-100	99.10	SargentsV2
633	74	0	100	9	0	-6	95.80	BellefntV2
634	76	0	100	23	0	-8	94.30	DarrahV2
635	77	0	100	70	0	-20	100.60	TurnerV2
636	80	477	577	280	0	-165	104	CabinCrkV2
637	85	0	100	23	0	-8	98.50	BeaverCkV2
638	87	4	104	1000	0	-100	101.50	PinevilleV3

Table C.19: IEEE 118: Generation data (2)

Gen-ID	Node1	Pgen	Pmax	Qmax	Pmin	Qmin	Uset	Name
639	89	607	707	300	0	-210	100.50	ClinchRvV2
640	90	0	100	300	0	-300	98.50	HolstonV2
641	91	0	100	100	0	-100	98	HolstonTV2
642	92	0	100	9	0	-3	99	SaltvllleV2
643	99	0	100	100	0	-100	101	HintonV2
644	100	252	352	155	0	-50	101.70	GlenLynV2
645	103	40	140	40	0	-15	100.10	ClaytorV2
646	104	0	100	23	0	-8	97.10	HancockV2
647	105	0	100	23	0	-8	96.50	RoanokeV2
648	107	0	100	200	0	-200	95.20	ReusensV2
649	110	0	100	23	0	-8	97.30	FieldaleV2
650	111	36	136	1000	0	-100	98	DanRiverV2
651	112	0	100	1000	0	-100	97.50	DanvilleV2
652	113	0	100	200	0	-100	99.30	DeerCrkV2
653	116	0	100	1000	0	-1000	100.50	KygerCrkV2
999001	10	0	50	15	0	-15	105	Wind1
999002	40	0	50	15	0	-15	97	Wind2
999003	42	0	50	15	0	-15	98.50	Wind3
999004	34	0	50	15	0	-15	98.40	Wind4
999005	55	0	50	15	0	-15	95.20	Wind5
999006	59	0	50	15	0	-15	98.50	Wind6
999007	61	0	50	15	0	-15	99.50	Wind7
999008	112	0	50	15	0	-15	97.50	Wind8
999011	12	0	20	1	0	-1	99	PV1
999012	32	0	20	1	0	-1	96.30	PV2
999013	25	0	20	1	0	-1	105	PV3
999014	70	0	20	1	0	-1	98.40	PV4
999015	62	0	20	1	0	-1	99.80	PV5
999016	65	0	20	1	0	-1	100.50	PV6
999017	90	0	20	1	0	-1	98.50	PV7

Table C.20: IEEE 118: Pumped Hydro

ID	Sammelschiene	Info	Name
999021	113	PSK1	PumpedHydro1
999022	19	PSK2	PumpedHydro2
999023	36	PSK3	PumpedHydro3
999024	24	PSK4	PumpedHydro4
999025	62	PSK5	PumpedHydro5
999026	89	PSK6	PumpedHydro6

Table C.21: IEEE 118: Transformer data

Trafo ID	Node1	Node2	VLevel1	VLevel2	Sr	Sr_max	U_k
701	8	5	339.83	138	100	0	2.67
702	26	25	331.20	138	100	0	3.82
703	30	17	331.20	138	100	0	3.88
704	38	37	322.58	138	100	0	3.75
705	63	59	331.20	138	100	0	3.86
706	64	61	339.83	138	100	0	2.68
707	65	66	322.58	138	100	0	3.70
708	68	69	322.58	138	100	0	3.70
709	81	80	322.58	138	100	0	3.70

Table C.22: IEEE 118: Feeder

Feeder ID	Node1	Uabs	Uphase	Name	Info
901	69	103.50	30	SpornV2	Feeder

Table C.23: IEEE 118: Shunt compensation

Shunt ID	Node1	Q
801	5	-40
802	17	0
803	34	14
804	37	-25
805	44	10
806	45	10
807	46	10
808	48	15
809	74	12
810	79	20
811	82	20
812	83	10
813	105	20
814	107	6
815	110	6

C.4 2 Area Network

Per unit **generator data** rated on 900 MVA and 20 kV

$$\begin{array}{llll} X_d = 1.8 & X_q = 1.7 & X_l = 0.2 & X'_d = 0.3 \\ X'_q = 0.55 & X''_d = 0.25 & X''_q = 0.25 & R_a = 0.0025 \\ T'_{d0} = 8s & T'_{q0} = 0.4s & T''_{d0} = 0.03s & T''_{q0} = 0.05s \end{array}$$

Per unit **line parameters** rated on 100 MVA and 230 kV

$$\begin{array}{ll} r = 0.0001 \text{ pu/km} & x_L = 0.001 \text{ pu/km} \\ b_C = 0.00175 \text{ pu/km} & \end{array}$$

Transformer

Impedance $j 0.15$ per unit on 900 MVA

Load

Bus7 :

$$P_L = 967 \text{ MW} \quad Q_L = 100 \text{ MVar} \quad Q_C = 200 \text{ MVar}$$

Bus9 :

$$P_L = 1767 \text{ MW} \quad Q_L = 100 \text{ MVar} \quad Q_C = 350 \text{ MVar}$$

C.5 5 Area Network

Table C.24: Generation conditions for two loadflow cases

	Case 1			Case 6		
	P MW	Q Mvar	No. Units	P MW	Q Mvar	No. Units
HPS1	75.2	77.9	4	0	-102	2
BPS2	600	95.6	6	560	-53	3
EPS2	500	132.7	5	490	-7	3
MPS2	491.7	122.4	6	488	-61	3
VPS2	375	132.8	4	490	3.7	3
LPS3	600	132.8	7	550	9.4	6
YPS3	313.3	51.5	3	393	-6.9	2
CPS4	279	59.3	3	270	4.7	3
GPS4	258.3	54.5	6	245	3.9	3
SPS4	350	52.3	4	380	25.2	2
TPS4	350	128.7	4	350	-32.6	3
NPS5	300	27.3	2	270	-42.2	1
PPS5	109	27.2	4	120	-11.2	2
TPS5	200	40.1	4	200	-9.7	4

Table C.25: Shunt Capacitor and Reactor Banks

	Case 1 Mvar	Case 6 Mvar
Capacitor		
212	400	400
216	300	300
409	60	60
411	30	30
Reactor		
414	30	30
415	60	60
416	60	90

Table C.26: Generator Parameters

Name	Node	Rating	H	Xa	Xd	Xq	Xd'	Td0'	Xd''	Td0''	Xq'	Tq0'	Xq''	Tq0''
		MVA	MWs/MVA	pu	pu	pu	pu	s	pu	s	pu	s	pu	s
HP51	101	333.3	2.9	0.14	1.1	0.65	0.25	8.5	0.24	0.05	0.6	0.4	0.25	0.2
BPS2	201	666.7	2.6	0.2	1.8	1.75	0.3	8.5	0.21	0.04	0.7	0.3	0.21	0.08
EPS2	202	555.6	2.2	0.17	2.2	2.1	0.3	4.5	0.2	0.04	0.5	1.5	0.21	0.06
MPS2	204	666.7	2.6	0.2	1.8	1.75	0.3	8.5	0.21	0.04	0.7	0.3	0.21	0.08
VP52	203	555.6	2.1	0.2	2.3	1.7	0.3	5	0.25	0.03	0.4	2	0.25	0.25
LP53	301	666.7	2.2	0.2	2.7	1.5	0.3	7.5	0.25	0.04	0.85	0.85	0.25	0.12
YP53	302	444.4	2.8	0.15	2	1.8	0.25	7.5	0.2	0.04	0.85	0.85	0.2	0.25
CP54	402	333.3	2.4	0.2	1.9	1.8	0.3	6.5	0.26	0.035	0.55	1.4	0.26	0.04
GP54	404	333.3	3.2	0.18	2.2	1.4	0.32	9	0.24	0.04	0.75	1.4	0.24	0.13
SP54	403	444.4	2.1	0.2	2.3	1.7	0.3	5	0.25	0.03	0.4	2	0.25	0.25
TP54	401	444.4	2.1	0.2	2.3	1.7	0.3	5	0.25	0.03	0.4	2	0.25	0.25
NPS5	501	333.3	2.8	0.15	2.2	1.7	0.3	7.5	0.24	0.025	0.8	1.5	0.24	0.1
TP55	502	250	3.2	0.2	2	1.5	0.3	7.5	0.22	0.04	0.8	3	0.22	0.2
PP55	503	166.7	6	0.15	2.3	2	0.25	5	0.17	0.022	0.35	1	0.17	0.035

Table C.27: Transformers: R and X in p.u. on 100MVA

	Node i	Node j	Rating	Uk in %	X	R
HPS1	101	102	333.3	12	0.036	0.00018
BPS2	201	206	666.7	16	0.024	0.00012
EPS2	202	209	555.6	16	0.0288	0.000144
VPS2	203	208	555.6	17	0.0306	0.000153
MPS2	204	215	666.7	16	0.024	0.00012
LPS3	301	303	666.7	16	0.024	0.00012
YPS3	302	312	444.4	15	0.0338	0.000169
TPS4	401	410	444.4	15	0.0338	0.000169
CPS4	402	408	333.3	17	0.051	0.000255
SPS4	403	407	444.4	15	0.0338	0.000169
GPS4	404	405	333.3	17	0.051	0.000255
NPS5	501	504	333.3	17	0.051	0.000255
TPS5	502	505	250	16	0.064	0.00032
PPS5	503	506	166.7	16	0.1	0.0005
	209	210	625	17	0.0272	0.000136
	213	214	625	17	0.0272	0.000136
	304	313	500	16	0.032	0.00016
	305	311	500	12	0.024	0.00012
	305	314	700	17	0.0243	0.0001215
	308	315	370	10	0.027	0.000135
	413	414	750	6	0.008	0.00004

Table C.28: SVC Data

Node	Case 1	Case 6
	Mvar	Mvar
205	-68.3	-29.4
313	71.4	54.2
412	58.2	0
507	22.6	-3.7
509	10.6	-109.3

Table C.29: Line data in p.u. on 100MVA

Node i	Node j	R	X	b
102	217	0.0042	0.0334	1.634
102	217	0.0039	0.031	1.52
102	309	0.0023	0.0178	0.874
102	309	0.0109	0.0868	0.76
205	206	0.0048	0.038	1.862
205	416	0.0019	0.023	1.46
206	207	0.0023	0.0178	0.874
206	212	0.0033	0.0264	1.292
206	215	0.0033	0.0264	1.292
207	208	0.0009	0.007	0.342
207	209	0.0008	0.0062	0.076
208	211	0.001	0.0083	0.912
209	212	0.0045	0.0356	0.437
210	213	0.0005	0.0073	3.08
211	212	0.0007	0.0054	0.266
211	214	0.0019	0.0155	0.19
212	217	0.007	0.0558	0.684
214	216	0.001	0.0077	0.095
214	217	0.0049	0.0388	0.475
215	216	0.0026	0.0202	0.988
215	217	0.0036	0.0287	1.406
216	217	0.0051	0.0403	0.494
303	304	0.001	0.014	1.48
303	305	0.0006	0.008	3.4
304	305	0.0003	0.004	0.424
305	306	0.0002	0.003	0.32
305	307	0.0002	0.0023	0.894
306	307	0.0001	0.0012	0.127
307	308	0.0012	0.0163	6.89
309	310	0.0045	0.0357	1.748
310	311	0	-0.0169	0
312	313	0.002	0.015	0.9
313	314	0.0005	0.005	0.52
315	509	0.0035	0.025	0.38
405	406	0.002	0.0238	0.762
405	408	0.0054	0.05	0.189
405	409	0.006	0.0407	2.37
406	407	0.0003	0.0038	0.124
407	408	0.0042	0.0513	0.412

Table C.30: Line data in p.u. on 100MVA

Node i	Node j	R	X	b
408	410	0.0055	0.064	2.02
409	411	0.0052	0.0355	0.92
410	411	0.0043	0.0532	0.427
410	412	0.0011	0.0133	1.708
410	413	0.002	0.0247	0.8
411	412	0.0006	0.0076	0.244
414	415	0.001	0.0125	0.78
415	416	0.0019	0.023	1.46
504	507	0.0115	0.075	1.12
504	508	0.013	0.0095	1.74
505	507	0.0008	0.0085	0.06
505	508	0.0025	0.028	0.17
506	507	0.0008	0.0085	0.06
506	508	0.003	0.028	0.14
507	508	0.002	0.019	0.09
507	509	0.015	0.11	1.8

Table C.31: Load case 1 and Load case 6

Node	Case 1		Case 6	
	MW	Mvar	MW	Mvar
102	450	45	270	30
205	390	39	235	25
206	130	13	80	10
207	1880	188	1110	120
208	210	21	125	15
211	1700	170	1035	110
212	1660	166	1000	110
215	480	48	290	30
216	1840	184	1105	120
217	1260	126	750	80
306	1230	123	900	90
307	650	65	470	50
308	655	66	620	100
309	195	20	140	15
312	115	12	92	10
313	2405	240	1625	165
314	250	25	180	20
405	990	99	730	75
406	740	74	540	55
408	150	15	110	10
409	260	26	190	20
410	530	53	390	40
411	575	58	420	45
412	1255	126	922	100
504	300	60	170	20
507	1000	200	565	65
508	800	160	450	50
509	200	40	117	15

Bibliography

- [1] K. Baker, G. Hug, and Xin Li. Inclusion of inter-temporal constraints into a distributed newton-raphson method. In *North American Power Symposium (NAPS), 2012*, pages 1–6. IEEE, 2012.
- [2] K. Baker, G. Hug, and Xin Li. Optimal integration of intermittent energy sources using distributed multi-step optimization. In *Power and Energy Society General Meeting, 2012 IEEE*, pages 1–8, 2012.
- [3] H. Behbehani, Z. Lubosny, and J.W. Bialek. Survey of supervisory power system stabilizers for enhancement of power system stability. In *Universities Power Engineering Conference, 2007. UPEC 2007. 42nd International*, pages 426–437, 2007.
- [4] P.N. Biskas and A.G. Bakirtzis. Decentralised opf of large multiarea power systems. *Generation, Transmission and Distribution, IEE Proceedings-*, 153(1):99–105, Jan 2006.
- [5] F. Borelli, A. Bemporad, and M. Morari. *Predictive Control for linear and hybrid systems*. ETH, 2011.
- [6] C. Breuer, D. Echternacht, C. Linnemann, and A. Moser. Technical and economic comparison of national and joint cross-border curative congestion management application. In *Energy Market (EEM), 2011 8th International Conference on the European*, pages 33–38, May 2011.
- [7] P. Brogan. The stability of multiple, high power, active front end voltage sourced converters when connected to wind farm collector systems. In *EPE Wind 2010*, 2010.
- [8] T. Demiray. *Simulation of Power System Dynamics using Dynamic Phasor Models*. PhD thesis, ETH Zurich, 2008.
- [9] Online Documentation. *PSS/E 25*. Siemens, December 1997.
- [10] K. Dong-Joon, M. Young-Hwan, and N. Hae-Kon. A practical approach to hvdc system control for damping subsynchronous oscillation using the novel eigenvalue analysis program. *Power Systems, IEEE Transactions on*, 22(4):1926–1934, Nov 2007.

- [11] K. Dong-Joon, M. Young-Hwan, and N. Hae-Kon. Ssr small-signal stability analysis program of power systems and its application to iee benchmark systems. In *Power Tech, 2007 IEEE Lausanne*, pages 161–166, July 2007.
- [12] D. Dotta, A.S. Silva, and I.C. Decker. Wide-area measurements-based two-level control design considering signal transmission delay. *IEEE Transactions on Power Systems*, 24(1):208–216, 2009.
- [13] Haesen E. *Multi-Objective Optimization of the Integration of Stochastic Distributed Energy Resources in Electricity Grids*. PhD thesis, Univerity Leuven, 2009.
- [14] Entso-E. Operation handbook. Technical report, Entso-E, 2004.
- [15] O. Föllinger. Regelungstechnik. hüthig. Technical report, ISBN 3–7785–2336–8, 1994.
- [16] P. Fortenbacher. Power flow modeling and grid constraint handling in power grids with high res in-feed, controllable loads, and storage devices. Master’s thesis, KIT and ETH, 2011.
- [17] Yong Fu, M. Shahidehpour, and Zuyi Li. Security-constrained unit commitment with ac constraints*. *Power Systems, IEEE Transactions on*, 20(3):1538–1550, 2005.
- [18] A. Fuchs, M. Imhof, T. Demiray, and M. Morari. Stabilization of large power systems using vsc–HVDC and model predictive control. *IEEE Transactions on Power Delivery*, 29(1):480–488, 2014.
- [19] O. Galland. The short-run security-constrained economic dispatch. Master’s thesis, KTH Stockholm, 2012.
- [20] M. Gibbard and D. Vowles. *Simplified 14-Generator Model of the SE Australian Power System*. <http://www.eleceng.adelaide.edu.au/groups/PCON/PowerSystems>, 2007.
- [21] M. Gibbard, D. Vowles, and P. Pourbeik. Interactions between, and effectiveness of, power system stabilizers and facts device stabilizers in multimachine systems. *Power Systems, IEEE Transactions on*, 15(2):748–755, 2000.
- [22] M.J. Gibbard. Co-ordinated design of multimachine power system stabilisers based on damping torque concepts. *Generation, Transmission and Distribution, IEE Proceedings C*, 135(4):276–284, Jul 1988.
- [23] M. Glavic and T. Van Cutsem. Investigating state reconstruction from scarce synchronized phasor measurements. In *IEEE PowerTech, Trondheim*, 2005.

- [24] S. Gomes, N. Martins, and C. Portela. Modal analysis applied to s-domain models of ac networks. In *Power Engineering Society Winter Meeting, 2001. IEEE*, volume 3, pages 1305–1310 vol.3, 2001.
- [25] S. Gomes, N. Martins, and C. Portela. Sequential computation of transfer function dominant poles of s-domain system models. *Power Systems, IEEE Transactions on*, 24(2):776–784, May 2009.
- [26] S. Gomes, N. Martins, and A. Stankovic. Improved controller design using new dynamic phasor models of svc’s suitable for high frequency analysis. In *Transmission and Distribution Conference and Exhibition, 2005/2006 IEEE PES*, pages 1436–1444, 2006.
- [27] G. Gross, C.F. Imparato, and P.M. Look. A tool for the comprehensive analysis of power system dynamic stability. *Power Apparatus and Systems, IEEE Transactions on*, PAS-101(1):226–234, Jan 1982.
- [28] R. M. Hamouda, M.R. Iravani, and R. Hackam. Torsional oscillations of series capacitor compensated ac/dc systems. *Power Systems, IEEE Transactions on*, 4(3):889–896, Aug 1989.
- [29] L. Harnefors. Analysis of subsynchronous torsional interaction with power electronic converters. *Power Systems, IEEE Transactions on*, 22(1):305–313, Feb 2007.
- [30] K. Heussen, S. Koch, A. Ulbig, and G. Andersson. Unified system-level modeling of intermittent renewable energy sources and energy storage for power system operation. *Systems Journal, IEEE*, 6(1):140–151, 2012.
- [31] G. Hirsch. *Semianalytische Simulation von systemimmanenten elektromechanischen Pendelschwingungen in Verbundnetzen*. PhD thesis, Universität der Bundeswehr Hamburg, 2003.
- [32] G. Hirsch. Undamped inherent inter-area oscillations in power grids. *Electrical Engineering*, 88(4):259–273, 2006.
- [33] G. Hug-Glanzmann and G. Andersson. N-1 security in optimal power flow control applied to limited areas. *Generation, Transmission Distribution, IET*, 3(2):206–215, 2009.
- [34] IEEE. Standard for Calculating the Current-Temperature of Bare Overhead Conductors. *IEEE Std 738-2006 (Revision of IEEE Std 738-1993)*, 1:c1–59, 2007.

- [35] M.R. Iravani, A.K.S. Chandhary, W.J. Giesbrecht, I.E. Hassan, A.J.F. Keri, K.C. Lee, J.A. Martinez, A.S. Morched, B.A. Mork, M. Parniani, A. Sarshar, D. Shirmohammadi, R.A. Walling, and D.A. Woodford. Modelling and analysis guidelines for slow transients. ii. controller interactions; harmonic interactions. *Power Delivery, IEEE Transactions on*, 11(3):1672–1677, Jul 1996.
- [36] E. Johansson. *Detailed description of Synchronous Machine Models used in Simpow*. ABB, December 2001.
- [37] D. Jovcic, N. Pahalawaththa, M. Zavahir, and H.A. Hassan. Svc dynamic analytical model. *Power Delivery, IEEE Transactions on*, 18(4):1455–1461, 2003.
- [38] I. Kamwa, R. Grondin, and Y. Hebert. Wide-area measurement based stabilizing control of large power systems—a decentralized/hierarchical approach. *IEEE Transactions on Power Systems*, 16(1):136–153, 2001.
- [39] R. Kankanamalage and G. Hug-Glanzmann. Usage of storage for optimal exploitation of transfer capacity: A predictive control approach. In *Power and Energy Society General Meeting, 2011 IEEE*, pages 1–8, 2011.
- [40] S. Kapoor and PM. Vaidya. Fast algorithms for convex quadratic programming and multicommodity flows. *Proceedings 18th Annual ACM Symposium on Theory of Computing*, 1:147 – 159, 1986.
- [41] C. Karawita and U.D. Annakkage. Multi-infeed hvdc interaction studies using small-signal stability assessment. *Power Delivery, IEEE Transactions on*, 24(2):910–918, April 2009.
- [42] C. Karawita and U.D. Annakkage. A hybrid network model for small signal stability analysis of power systems. *Power Systems, IEEE Transactions on*, 25(1):443–451, Feb 2010.
- [43] B.H. Kim and R. Baldick. A comparison of distributed optimal power flow algorithms. *Power Systems, IEEE Transactions on*, 15(2):599–604, May 2000.
- [44] H. Kocewiak, J. Hjerrild, and C.L. Bak. Wind turbine converter control interaction with complex wind farm systems. *Renewable Power Generation, IET*, 7(4):380–389, July 2013.
- [45] Y. Kokai, C. Fukui, and T. Kawahara. Power systems stability solutions for a low-carbon society. In *Hitachi Review Vol. 60, No. 3*, 2011.
- [46] P. Krause. *Analysis of electric machinery and drive systems*. IEEE Press, 2002.

- [47] E.S. Kuh and R.A. Rohrer. The state-variable approach to network analysis. *Proceedings of the IEEE*, 53(7):672–686, July 1965.
- [48] A. Kumar, S.C. Srivastava, and S.N. Singh. Congestion management in competitive power market: A bibliographical survey. *Electric Power Systems Research*, 76(13):153 – 164, 2005.
- [49] P. Kundur. *Power system stability and control*. McGraw, 1994.
- [50] P. Kundur, G.J. Rogers, D.Y. Wong, L. Wang, and M.G. Lauby. A comprehensive computer program package for small signal stability analysis of power systems. *Power Systems, IEEE Transactions on*, 5(4):1076 –1083, nov 1990.
- [51] F. Kunz and A. Zerrahn. The benefit of coordinating congestion management in germany. In *DIW Berlin - German Institute for Economic Research*, 2013.
- [52] Yong Li, C. Rehtanz, S. Ruberg, Longfu Luo, and Yijia Cao. Wide-area robust coordination approach of HVDC and facts controllers for damping multiple interarea oscillations. *IEEE Transactions on Power Delivery*, 27(3):1096–1105, 2012.
- [53] L. Lima, N. Martins, and S. Carneiro Jr. Augmented state-space formulations for the study of electric network including distributed-parameter transmission line models. In *International Conference on Power Systems Transients*, 1999.
- [54] M. Liserre, R. Teodorescu, and F. Blaabjerg. Stability of photovoltaic and wind turbine grid-connected inverters for a large set of grid impedance values. *Power Electronics, IEEE Transactions on*, 21(1):263–272, Jan 2006.
- [55] J. Lofberg. Yalmip : a toolbox for modeling and optimization in matlab. In *Computer Aided Control Systems Design, 2004 IEEE International Symposium on*, pages 284–289, 2004.
- [56] O. Lotter. Natural minimal set of state equations of linear power grid. *Electrical Engineering, Springer*, 5:405–409, 2007.
- [57] J. Maciejowski. *Predictive control: with constraints*. Pearson education, 2002.
- [58] B. Marinescu, J-M Coulondre, P. Tsamasphyrou, and J.-Y. Bourmaud. Improving tso’s coordination for cross-border redispatch: a discussion of possible approaches in the european context. In *CIGRE/IEEE PES, 2005. International Symposium*, pages 378–385, Oct 2005.
- [59] Hui Ni, G.T. Heydt, and L. Mili. Power system stability agents using robust wide area control. *IEEE Transactions on Power Systems*, 17(4):1123–1131, 2002.

- [60] G. Oggioni, Y. Smeers, E. Allevi, and S. Schaible. A generalized nash equilibrium model of market coupling in the european power system. *Networks and Spatial Economics*, 12(4):503–560, 2012.
- [61] F. Okou, L.-A. Dessaint, and O. Akhrif. Power systems stability enhancement using a wide-area signals based hierarchical controller. *IEEE Transactions on Power Systems*, 20(3):1465–1477, 2005.
- [62] B. Pal and B. Chaudhuri. *Robust Control in Power Systems*. Springer, 2005.
- [63] M. Parniani and M.R. Irvani. Computer analysis of small-signal stability of power systems including network dynamics. *Generation, Transmission and Distribution, IEE Proceedings-*, 142(6):613–617, Nov 1995.
- [64] R.A. Ramos, L.F.C. Alberto, and N.G. Bretas. A new methodology for the coordinated design of robust decentralized power system damping controllers. *IEEE Transactions on Power Systems*, 19(1):444–454, 2004.
- [65] J. Rawlings and D. Mayne. *Model predictive Control: Theory and design*. Nob Hill Publishing, 2009.
- [66] M.G. Safonov and R.Y. Chiang. A schur method for balanced-truncation model reduction. *IEEE Transactions on Automatic Control*, 34(7):729–733, 1989.
- [67] O. Samuelsson, H. Johannsdottir, N. Gustavsson, T. Hrafnsson, D. Karlsson, D. Novosel, J. Sälj, and A. Sollie. Power system damping in iceland based on phasor measurements. In *Power Systems and Communication Systems Infrastructures for the Future, Beijing, China*, 2002.
- [68] D. Shirmohammadi, B. Wollenberg, A. Vojdani, P. Sandrin, M. Pereira, F. Rahimi, T. Schneider, and B. Stott. Transmission dispatch and congestion management in the emerging energy market structures. *Power Systems, IEEE Transactions on*, 13(4):1466–1474, Nov 1998.
- [69] J.G. Slootweg, J. Perssonand, A.M. van Voordenand, G.C. Paapand, and W.L. Kling. A study of the eigenvalue analysis capabilities of power system dynamics simulation software. In *14th Power Systems Computation Conference Sevilla Spain*, 2002.
- [70] A. Ulbig and G. Andersson. On operational flexibility in power systems. In *Power and Energy Society General Meeting, 2012 IEEE*, pages 1–8, 2012.
- [71] A. Ulbig, S. Koch, and G. Andersson. The power nodes modeling framework modeling and assessing the operational flexibility of hydro power units. In *XII SEPOPE, Rio de Janeiro, Brazil*, 2012.

- [72] S.L. Varricchio, S. Gomes, and N. Martins. s-domain approach to reduce harmonic voltage distortions using sensitivity analysis. In *Power Engineering Society Winter Meeting, 2001. IEEE*, volume 2, pages 809–814 vol.2, 2001.
- [73] A. Venkat. *Distributed Model Predictive Control: Theory and Application*. PhD thesis, University of Wisconsin-Madison, 2006.
- [74] A.N. Venkat, I.A. Hiskens, J.B. Rawlings, and S.J. Wright. Distributed MPC strategies with application to power system automatic generation control. *IEEE Transactions on Control Systems Technology*, 16(6):1192–1206, 2008.
- [75] D.J. Vowles and M.J. Gibbard. *Mudpack - a software package for the analysis of the small-signal dynamic performance and control of large electric power systems*. School of Electrical & Electronic Engineering, The University of Adelaide, South Australia, 12 2007.
- [76] D.J. Vowles and M.J. Gibbard. Power systems dynamics group contribution to the ieeec benchmark systems for stability controls task force, 2014.
- [77] LZ Yao, G Strbac, XP Zhang, R Allan, M Bradley, HB Wan, and P Turner. A concurrent optimal power flow for enforcement of system solvability, voltage and thermal constraints. *13th PSCC, Trondheim, Norway*, 1:351–357, 1999.
- [78] R. Zarate-Mihano, A.J. Conejo, and F. Milano. Opf-based security redispatching including facts devices. *Generation, Transmission Distribution, IET*, 2(6):821–833, November 2008.
- [79] Lidong Zhang, L. Harnefors, and H-P. Nee. Modeling and control of vsc-hvdc links connected to island systems. *Power Systems, IEEE Transactions on*, 26(2):783–793, May 2011.

Author's Publications

- [80] M. Kahl, C. Freye, and T. Leibfried. A cooperative multi-area optimization with renewable generation and storage devices. *Power Systems, IEEE Transactions on*, 2014. (Accepted for future publication).
- [81] M. Kahl and T. Leibfried. Modellbasierte Regelungsalgorithmen für das Energienetz der Zukunft. In *Lecture Notes in Informatics (LNI) Berlin*, 2011.
- [82] M. Kahl and T. Leibfried. Decentralized model predictive control of electrical power systems. In *International Conference on Power Systems Transients (IPST2013) Vancouver*, 2013.
- [83] M. Kahl, D. Uber, and T. Leibfried. Dynamic state estimator for voltage stability and low frequency oscillation detection. In *IEEE Innovative Smart Grid Technologies Conference- Asia*, 2014.
- [84] M. Kahl, S. Wenig, and T. Leibfried. Dezentrale modellprädiktive Optimierungsstrategien zur Einbindung erneuerbarer Erzeugungskapazität und Speichersysteme. In *Konferenz für Nachhaltige Energieversorgung und Integration von Speichern-NEIS Hamburg*, 2013.
- [85] U. Reiner, M. Kahl, T. Leibfried, F. Allering, and H. Schmeck. Mergeomobil-labor - entwicklungsumgebung für zukünftige smart-homes. In *ETG Kongress Leipzig*, 2010.

Supervised Theses

- [86] A. Benazza. Verfahren zur Modellierung von Energieübertragungsnetzen. Studienarbeit, KIT, 2010.
- [87] M. Bergner. Modellierung einer Synchronmaschine und deren Interaktion mit einem dynamischen Netzmodell. Studienarbeit, KIT, 2012.
- [88] W. Biener. Synthese von dezentralen Zustandsreglern mittels linearer Matrixgleichungen für Elektroenergiesysteme. Studienarbeit, KIT, 2012.
- [89] J. Chang. Dezentrale Regelung eines Netzverbundes. Masterarbeit, KIT, 2014.
- [90] A. Engelmann. Zustandsschätzung für transiente Betriebsfälle in einem Energieübertragungsnetz. Bachelorarbeit, KIT, 2013.
- [91] E. Fastanz. Simulation von Pendelschwingungen im Verbundnetz. Studienarbeit, KIT, 2014.
- [92] C. Freye. Verfahren zur Modellbasierte Betriebsführung eines BHKWs. Bachelorarbeit, KIT, 2010.
- [93] C. Freye. Kooperationsbasierte modellprädiktive Optimierung von Elektroenergiesystemen unter Berücksichtigung von Netzrestriktionen. Masterarbeit, KIT, 2013.
- [94] F. Götz. Auslegung von Power Systems Stabilisern mittels Modal-Analyse von Energieübertragungsnetzen. Bachelorarbeit, KIT, 2010.
- [95] S. Knauff. Implementierung einer Modellprädiktiven Regelung in DigSilent PowerFactory. Bachelorarbeit, KIT, 2013.
- [96] M. Lang. Modellierung von Selbstgeführten Stromrichtern. Bachelorarbeit, KIT, 2011.
- [97] S. Löffler. Automatisierte Leistungsdatenerfassung in einem Smart-home. Bachelorarbeit, KIT, 2011.
- [98] M. Ling. Entwicklung eines generischen Modells für netzgeführte Stromrichter. Technical report, KIT, 2010.

- [99] T. Lommel. Erweiterte optimale Einbindung von konventionellen und dezentralen Kraftwerken unter Berücksichtigung von Netzrestriktionen. Diplomarbeit, KIT, 2012.
- [100] L. Merkert. Modellprädiktive Regelung eines Energieübertragungsnetzes. Diplomarbeit, KIT, 2011.
- [101] N. Meyer-Hübner. Modellierung von stromrichterbetriebenen Anlagen und deren Regelung in einem realen Verteilnetz. Studienarbeit, KIT, 2012.
- [102] P. Müller. Beschreibung von unsymmetrischen Netzzuständen mittels eines dynamischen Modells. Studienarbeit, KIT, 2012.
- [103] J. Noteisen. Modellierung und Regelung eines TCSC im Verbundnetz. Bachelorarbeit, KIT, 2012.
- [104] S. Schneider. Optimale Einbindung von konventionellen und dezentralen Kraftwerken unter Berücksichtigung von Netzrestriktionen. Bachelorarbeit, KIT, 2011.
- [105] T. Strobel. Entwicklung eines generischen Windkraftanlagen Modells. Bachelorarbeit, KIT, 2011.
- [106] A. Trumpf. Auslegung von Power System Stabilisern mittels Eigenwertanalyse. Bachelorarbeit, KIT, 2013.
- [107] D. Uber. Entwicklung eines Zustandschätzers für dynamische Betriebszustände von Elektroenergiesystemen. Diplomarbeit, KIT, 2012.
- [108] A. Wöber. Stabilitätsuntersuchungen von stromrichtergespeisten Anlagen im Verteilnetz. Bachelorarbeit, KIT, 2012.
- [109] C. Wegner. Hierarchische Regelung von Energieübertragungsnetzen im Zustandsraum. Diplomarbeit, KIT, 2011.
- [110] S. Wenig. Dezentrale modellprädiktive Optimierungsstrategien zur Einbindung erneuerbarer Erzeugungskapazitäten und Speichersysteme. Diplomarbeit, KIT, 2013.